

**A Hybrid Brain-Computer Interface Based on Electroencephalography and Functional  
Transcranial Doppler Ultrasound**

by

**Aya Khalaf**

B.S. in Biomedical Engineering, Cairo University, 2012

M.S. in Biomedical Engineering, Cairo University, 2015

Submitted to the Graduate Faculty of  
Swanson School of Engineering in partial fulfillment  
of the requirements for the degree of  
Doctor of Philosophy

University of Pittsburgh

2019

UNIVERSITY OF PITTSBURGH  
SWANSON SCHOOL OF ENGINEERING

This dissertation was presented

by

**Aya Khalaf**

It was defended on

May 30, 2019

and approved by

Murat Akcakaya, Ph.D., Assistant Professor,  
Department of Electrical and Computer Engineering

Amro El-Jaroudi, Ph.D., Associate Professor,  
Department of Electrical and Computer Engineering

Zhi-Hong Mao, Ph.D., Professor,  
Department of Electrical and Computer Engineering

Ervin Sejdic, Ph.D., Associate Professor,  
Department of Electrical and Computer Engineering

Elizabeth Skidmore, Ph.D., Professor,  
Department of Occupational Therapy

Dissertation Director: Murat Akcakaya, Ph.D., Assistant Professor

Copyright © by Aya Khalaf

2019

# **A Hybrid Brain-Computer Interface Based on Electroencephalography and Functional Transcranial Doppler Ultrasound**

Aya Khalaf, Ph.D.

University of Pittsburgh, 2019

Hybrid brain computer interfaces (BCIs) combining multiple brain imaging modalities have been proposed recently to boost the performance of single modality BCIs. We advance the state of hybrid BCIs by introducing a novel system that measures electrical brain activity as well as cerebral blood flow velocity using Electroencephalography (EEG) and functional transcranial Doppler ultrasound (fTCD), respectively. The system we developed employs two different paradigms to induce changes simultaneously in EEG and fTCD and to infer user intent. One of these paradigms includes visual stimuli to simultaneously induce steady state visually evoked potentials (SSVEPs) and instructs users to perform word generation (WG) and mental rotation (MR) tasks, while the other paradigm instructs users to perform left and right arm motor imagery (MI) tasks through visual stimuli.

To improve accuracy and information transfer rate (ITR) of the proposed system compared to those obtained through our preliminary analysis, using classical feature extraction approaches, we mainly contribute to multi-modal fusion of EEG and fTCD features. Specifically, we proposed a probabilistic fusion of EEG and fTCD evidences instead of simple concatenation of EEG and fTCD feature vectors that we performed in our preliminary analysis. Experimental results showed that the MI paradigm outperformed the MR/WG one in terms of both accuracy and ITR. In particular, 93.85%, 93.71%, and 100% average accuracies and 19.89, 26.55, and 40.83 bits/min

average ITRs were achieved for right MI vs baseline, left MI versus baseline, and right MI versus left MI, respectively. Moreover, for both paradigms, the EEG-fTCD BCI with the proposed analysis techniques outperformed all EEG- fNIRS BCIs in terms of accuracy and ITR.

In addition, to investigate the feasibility of increasing the possible number of BCI commands, we extended our approaches to solve the 3-class problems for both paradigms. It was found that the MI paradigm outperformed the MR/WG paradigm and achieved 96.58% average accuracy and 45 bits/min average ITR. Finally, we introduced a transfer learning approach to reduce the calibration requirements of the proposed BCI. This approach was found to be very efficient especially with the MI paradigm as it reduced the calibration requirements by at least 60.43%.

# Table of Contents

<b>Acknowledgement</b> .....	<b>xviii</b>
<b>1.0 Introduction</b> .....	<b>1</b>
<b>1.1 EEG-based BCIs</b> .....	<b>3</b>
<b>1.1.1 Steady-state visual evoked potentials (SSVEPs) BCIs</b> .....	<b>3</b>
<b>1.1.2 Event-related desynchronization/synchronization (ERD/ERS) BCIs</b> .....	<b>5</b>
<b>1.1.3 P300 BCIs</b> .....	<b>5</b>
<b>1.1.4 Slow cortical potentials (SCPs) BCIs</b> .....	<b>6</b>
<b>1.2 Multi-modal BCIs</b> .....	<b>6</b>
<b>1.3 Contributions</b> .....	<b>8</b>
<b>2.0 Literature Review</b> .....	<b>10</b>
<b>2.1 Preprocessing</b> .....	<b>11</b>
<b>2.2 Feature Extraction</b> .....	<b>13</b>
<b>2.3 Feature Selection and Reduction</b> .....	<b>17</b>
<b>2.4 Information Fusion</b> .....	<b>17</b>
<b>2.5 Classification</b> .....	<b>19</b>
<b>3.0 A Brain-Computer Interface Based on Functional Transcranial Doppler Ultrasound Using Wavelet Transform and Support Vector Machines</b> .....	<b>21</b>
<b>3.1 Materials and Methods</b> .....	<b>22</b>
<b>3.1.1 Participants</b> .....	<b>22</b>
<b>3.1.2 Experimental Procedure</b> .....	<b>23</b>
<b>3.1.2.1 Mental Rotation Task</b> .....	<b>23</b>
<b>3.1.2.2 Word Generation Task</b> .....	<b>24</b>
<b>3.1.3 Data Analysis</b> .....	<b>24</b>

3.1.3.1	Preprocessing .....	25
3.1.3.2	Feature Extraction.....	26
3.1.3.3	Feature Selection.....	28
3.1.3.4	Classification .....	29
3.2	Results.....	30
3.2.1	2-Class Problems .....	31
3.2.2	3-Class Problem.....	35
3.2.3	Transmission Rate.....	37
3.3	Discussion .....	38
3.4	Conclusion .....	41
4.0	A Novel Motor Imagery Hybrid Brain Computer Interface Using EEG and Functional Transcranial Doppler Ultrasound .....	43
4.1	Materials and Methods .....	44
4.1.1	Simultaneous Data Acquisition.....	44
4.1.2	Visual Presentation Design.....	44
4.1.3	Participants.....	45
4.1.4	Feature Extraction and Fusion .....	46
4.1.5	Feature Selection .....	46
4.1.6	Classification.....	48
4.1.7	Evaluation of the Effectiveness of the Hybrid System.....	48
4.2	Results.....	49
4.2.1	Right/Left arm MI vs Baseline.....	50
4.2.2	Right arm MI vs left arm MI .....	54
4.3	Discussion .....	59
4.4	Conclusion .....	64

<b>5.0 Towards Optimal Visual Presentation Design for Hybrid EEG-ftCD Brain-Computer Interfaces .....</b>	<b>65</b>
<b>5.1 Materials and Methods .....</b>	<b>68</b>
<b>5.1.1 Simultaneous Data Acquisition.....</b>	<b>68</b>
<b>5.1.2 Visual Presentation Design.....</b>	<b>68</b>
<b>5.1.3 Participants.....</b>	<b>70</b>
<b>5.1.4 Feature Extraction and Fusion .....</b>	<b>70</b>
<b>5.1.5 Feature Selection .....</b>	<b>71</b>
<b>5.1.6 Classification.....</b>	<b>71</b>
<b>5.1.7 Evaluation of the Effectiveness of the Hybrid System.....</b>	<b>72</b>
<b>5.1.8 Incremental Analysis .....</b>	<b>72</b>
<b>5.2 Results.....</b>	<b>73</b>
<b>5.2.1 MR/WG versus Baseline.....</b>	<b>74</b>
<b>5.2.2 MR versus WG .....</b>	<b>79</b>
<b>5.3 Discussion .....</b>	<b>84</b>
<b>5.4 Conclusion .....</b>	<b>88</b>
<b>6.0 Common Spatial Pattern and Wavelet Decomposition for Motor Imagery EEG-ftCD Brain-Computer Interface .....</b>	<b>89</b>
<b>6.1 Materials and Methods .....</b>	<b>90</b>
<b>6.1.1 Preprocessing.....</b>	<b>90</b>
<b>6.1.2 Common Spatial Pattern (CSP).....</b>	<b>90</b>
<b>6.1.3 Wavelet Decomposition .....</b>	<b>93</b>
<b>6.1.4 Feature Reduction and Classification .....</b>	<b>93</b>
<b>6.1.5 Bayesian Fusion and Decision Making.....</b>	<b>94</b>
<b>6.1.5.1 Assumption 1: Joint Distribution.....</b>	<b>95</b>
<b>6.1.5.2 Assumption 2: Independent Distributions .....</b>	<b>96</b>

6.1.5.3 Assumption 3: Weighted Independent Distributions .....	97
6.1.6 EEG-ftCD Analysis Across Time .....	98
6.2 Results.....	98
6.3 Discussion .....	105
6.4 Conclusion.....	111
<b>7.0 EEG-ftCD Hybrid Brain-Computer Interface Using Template Matching and Wavelet Decomposition .....</b>	<b>112</b>
7.1 Materials and Methods .....	113
7.1.1 Preprocessing.....	114
7.1.2 Feature Extraction .....	114
7.1.2.1 Template Matching.....	114
7.1.2.2 Wavelet Decomposition .....	116
7.1.3 Feature Selection and Reduction .....	116
7.1.4 Feature Fusion and Decision Making.....	117
7.1.5 Temporal Analysis .....	117
7.2 Results.....	119
7.3 Discussion .....	125
7.4 Conclusion .....	131
<b>8.0 3-Class EEG-ftCD Brain-Computer Interfaces.....</b>	<b>132</b>
8.1 Materials and Methods .....	132
8.1.1 EEG Feature Extraction.....	132
8.1.1.1 MI Paradigm .....	132
8.1.1.2 Flickering MR/WG Paradigm .....	133
8.1.2 ftCD Feature Extraction .....	134
8.1.3 Feature Selection and Reduction .....	134
8.1.4 Feature Fusion and Decision Making.....	135

8.2 Results.....	136
8.3 Discussion .....	140
8.4 Conclusion .....	141
<b>9.0 A Probabilistic Transfer Learning Approach for Calibration Time Reduction in Hybrid EEG-ftCD Brain-Computer Interfaces .....</b>	<b>142</b>
9.1 Introduction .....	142
9.2 Materials and Methods .....	144
9.2.1 Similarity Measure.....	145
9.2.2 Proposed Transfer Learning Algorithm .....	146
9.2.3 Performance Evaluation.....	149
9.3 Results.....	150
9.3.1 MI Paradigm .....	151
9.3.2 Flickering MR/WG paradigm.....	154
9.4 Discussion .....	156
9.5 Conclusion .....	158
<b>10.0 Conclusions.....</b>	<b>159</b>
<b>Appendix.....</b>	<b>162</b>
<b>Bibliography .....</b>	<b>168</b>

## List of Tables

Table 1	Average maximum accuracy and the corresponding sensitivity, specificity, and time at different state durations for the word generation task versus resting state using MW and IW methods. ....	32
Table 2	Average maximum accuracy and the corresponding sensitivity, specificity, and time at different state durations for the mental rotation task versus resting state using MW and IW methods. ....	33
Table 3	Average maximum accuracy and the corresponding sensitivity, specificity, and time at different state durations for the mental rotation versus word generation using MW and IW methods. ....	34
Table 4	Average maximum accuracy and the corresponding sensitivity, specificity, and time at different state durations for the 3-class (mental rotation (MR), word generation (WG), and resting state problem using MW and IW methods. ....	36
Table 5	Comparison between the proposed MW method and the state of the art methods for binary BCIs. ....	40
Table 6	Maximum accuracy (Acc) and the corresponding time for each subject using hybrid system, EEG only, and fTCD only. These measures were obtained for right arm MI vs baseline problem. ....	52
Table 7	Maximum accuracy (Acc) and the corresponding time for each subject using hybrid system, EEG only, and fTCD only. These measures were obtained for left arm MI vs baseline problem. ....	53
Table 8	Maximum accuracy (Acc) and the corresponding time for each subject using hybrid system, EEG only, and fTCD only. These measures were obtained for left arm MI vs right arm MI. ....	54
Table 9	P-values representing significance of the EEG-fTCD system in terms of accuracy for the binary problems using subject-independent and subject-specific CDF thresholds. ....	55
Table 10	P-values representing significance of the EEG-fTCD system in terms of bit rates for the binary problems using subject-independent and subject-specific CDF thresholds. ...	55
Table 11	Comparison between the proposed hybrid system and the state of the art hybrid EEG-fNIRS BCIs employing motor imagery tasks. ....	63

Table 12	Maximum accuracy (Acc) and the corresponding and time for each subject using hybrid system, EEG only, and fTCD only. These measures were obtained for MR vs baseline problem using subject-independent and subject-specific thresholds. ....	75
Table 13	Maximum accuracy (Acc) and the corresponding and time for each subject using hybrid system, EEG only, and fTCD only. These measures were obtained for WG vs baseline problem using subject-independent and subject-specific thresholds. ....	76
Table 14	Maximum accuracy (Acc) and the corresponding and time for each subject using hybrid system, EEG only, and fTCD only. These measures were obtained for MR vs WG problem using subject-independent and subject-specific thresholds. ....	77
Table 15	P-values representing significance of the EEG-fTCD system for the binary problems using subject-independent and subject-specific CDF thresholds. ....	78
Table 16	Comparison between the proposed hybrid system and the state of the art hybrid BCIs.	86
Table 17	Maximum accuracy achieved for each subject using hybrid combinations (A1, A2, A3), EEG only, and fTCD only for right MI vs baseline problem. ....	100
Table 18	Maximum accuracy achieved for each subject using hybrid combinations (A1, A2, A3), EEG only, and fTCD only for left MI vs baseline problem. ....	100
Table 19	Maximum accuracy achieved for each subject using hybrid combinations (A1, A2, A3), EEG only, and fTCD only for right MI vs left MI problem. ....	102
Table 20	P-values showing accuracy significance of A1, A2, and A3 compared to EEG only for the 3 binary problems. ....	102
Table 21	P-values showing ITR significance of A1, A2, and A3 compared to EEG only for the 3 binary problems. ....	103
Table 22	Comparison between the proposed hybrid system and the state-of-the-art hybrid BCIs.	110
Table 23	Maximum accuracy achieved for each subject using hybrid combinations (A1, A2, A3), EEG only, and fTCD only for MR vs baseline problem. ....	121
Table 24	Maximum accuracy achieved for each subject using hybrid combinations (A1, A2, A3), EEG only, and fTCD only for WG vs baseline problem. ....	122
Table 25	Maximum accuracy achieved for each subject using hybrid combinations (A1, A2, A3), EEG only, and fTCD only for MR vs WG problem. ....	123
Table 26	P-values showing \significance of A1, A2, and A3 compared to EEG only and fTCD only for the 3 binary problems. ....	124

Table 27	Comparison between the proposed hybrid system and the state-of-the-art hybrid BCIs. 130
Table 28	Maximum accuracy achieved for each subject using A3, EEG only, and fTCD only for MI paradigm..... 137
Table 29	Maximum accuracy achieved for each subject using A2, EEG only, and fTCD only for flickering MR/WG paradigm..... 138
Table 30	Maximum accuracy (Acc) and the corresponding sensitivity (Se), specificity (Sp), and time for each subject using hybrid system, EEG only, and fTCD only. These measures were obtained for right arm MI vs baseline problem using subject-independent threshold..... 162
Table 31	Maximum accuracy (Acc) and the corresponding sensitivity (Se), specificity (Sp), and time for each subject using hybrid system, EEG only, and fTCD only. These measures were obtained for right arm MI vs baseline problem using subject-specific thresholds. 163
Table 32	Maximum accuracy (Acc) and the corresponding sensitivity (Se), specificity (Sp), and time for each subject using hybrid system, EEG only, and fTCD only. These measures were obtained for left arm MI vs baseline problem using subject-independent threshold. 164
Table 33	Maximum accuracy (Acc) and the corresponding sensitivity (Se), specificity (Sp), and time for each subject using hybrid system, EEG only, and fTCD only. These measures were obtained for left arm MI vs baseline problem using subject-specific thresholds. 165
Table 34	Maximum accuracy (Acc) and the corresponding right arm and left arm sensitivities (SeR, and SeL), and time for each subject using hybrid system, EEG only, and fTCD only. These measures were obtained for right arm MI vs left arm MI problem using subject-independent threshold. .... 166
Table 35	Maximum accuracy (Acc) and the corresponding right arm and left arm sensitivities (SeR, and SeL), and time for each subject using hybrid system, EEG only, and fTCD only. These measures were obtained for right arm MI vs left arm MI problem using subject-specific thresholds..... 167

## List of Figures

Figure 1	The main building blocks of a BCI system. ....	1
Figure 2	a) EEG cap with electrodes connected b) sample of the EEG signals recorded from 8 different channels.....	4
Figure 3	Power spectral density for EEG responses due to stimuli flickering with frequencies 5 and 15 Hz. It can be noted that there are spikes at the harmonics of each stimulus frequency [149]......	4
Figure 4	a) top view for the skull with the transcranial Doppler probe fixed on the left transtemporal window b) sample Doppler ultrasound signal showing the change in cerebral blood velocity across time [150]......	7
Figure 5	Sample of the mental rotation task. Each participant was asked to decide if the pair of images are identical or mirrored by mentally rotating one of the two images. ....	24
Figure 6	A flowchart for the algorithm used for data analysis using moving window (MW) and incremental window (IW) methods. ....	27
Figure 7	Transmission rate in bits/min for binary and 3-class problems using a) IW method b) MW method. ....	37
Figure 8	Stimulus presentation for the hybrid BCI system.....	45
Figure 9	Transmission rates for each participant (p) calculated using both EEG and fTCD, EEG only, and fTCD only for right arm MI vs baseline problem with a) subject-independent threshold b) subject-specific thresholds.....	56
Figure 10	Transmission rates for each participant (p) calculated using both EEG and fTCD, EEG only, and fTCD only for left arm MI vs baseline problem with a) subject-independent threshold b) subject-specific thresholds.....	56
Figure 11	Transmission rates for each participant (p) calculated using both EEG and fTCD, EEG only, and fTCD only for right arm MI vs left arm MI problem with a) subject-independent threshold b) subject-specific thresholds. ....	57
Figure 12	Average transmission rates calculated using EEG-fTCD combination for the 3 binary problems with subject-independent and subject-specific thresholds. ....	58
Figure 13	2D histogram of the significant features during right arm versus left arm MI at each channel and each frequency window of width 2Hz for EEG and 50 Hz for fTCD. The heat maps demonstrate, across all participants, how many times any of the features within .....	58

Figure 14	Difference between left fTCD channel (channel 2) and right fTCD channel (channel 1) during right arm and left arm MI for a) fTCD normalized envelope signals in time domain b) power spectrum features in frequency domain.....	60
Figure 15	Stimulus presentation for our motor imagery EEG-fTCD BCI (a) and the proposed flickering MR/WG hybrid BCI (b) as well as the hybrid system setup captured during one of the data collection sessions (c).....	67
Figure 16	Diagram showing feature extraction, selection, and classification stages applied on EEG and fTCD signals. ....	71
Figure 17	Sensitivities (mean and standard deviation) calculated using both EEG and fTCD, EEG only, and fTCD only for flickering MR vs baseline problem (a), flickering WG vs baseline problem (b), and flickering MR vs flickering WG (c).....	79
Figure 18	Specificities (mean and standard deviation) calculated using both EEG and fTCD, EEG only, and fTCD only for flickering MR vs baseline problem (a), flickering WG vs baseline problem (b), and flickering MR vs flickering WG (c).....	80
Figure 19	Transmission rates for each participant (p) calculated using both EEG and fTCD, EEG only, and fTCD only for flickering MR vs baseline problem with subject-independent threshold (a) and subject-specific thresholds (b).....	81
Figure 20	Transmission rates for each participant (p) calculated using both EEG and fTCD, EEG only, and fTCD only for flickering WG vs baseline problem with subject-independent threshold (a) and subject-specific thresholds (b). ....	82
Figure 21	Transmission rates for each participant (p) calculated using both EEG and fTCD, EEG only, and fTCD only for flickering MR vs flickering WG problem with subject-independent threshold (a) and subject-specific thresholds (b).....	82
Figure 22	Average transmission rates calculated using EEG-fTCD combination for the 3 binary problems with subject-independent and subject-specific thresholds. ....	83
Figure 23	2D histogram of the fTCD significant features appearing at right fTCD channel (CH1) and left fTCD channel (CH2) among the 11 individuals participated in the study. ...	83
Figure 24	Probabilistic graphical model illustrating the state and measurement relationships assuming EEG and fTCD evidences are jointly distributed (a) and independent (b). 96	96
Figure 25	Sensitivities and specificities (mean and standard deviation) calculated using A1, A2, A3, EEG only, and fTCD only for right MI vs baseline problem (a), left MI vs baseline problem (b), and right MI vs left MI (c). ....	101
Figure 26	Average ITRs calculated using EEG only, fTCD only, and the 3 hybrid combinations (A1, A2, and A3) for right MI vs baseline problem (a), left MI vs baseline problem (b), and right MI vs left MI problem (c).....	104

Figure 27	For each task, wavelet coefficients of each wavelet band were averaged across trials corresponding to that task. The figure shows average approximation and level 4 detail wavelet coefficients for right MI vs baseline problem (a, c) and left MI vs baseline problem (b, d). It can be noted that, for each fTCD channel, the difference between right MI coefficients and baseline coefficients (Fig.4. a and Fig.4. c) is higher than the difference between left MI coefficients and baseline coefficients (Fig.4. b and Fig.4. d). .....	107
Figure 28	Sensitivities and specificities (mean and standard deviation) calculated using A1, A2, A3, EEG only, and fTCD only for flickering MR vs baseline problem (a), flickering WG vs baseline problem (b), and flickering MR vs flickering WG (c). .....	123
Figure 29	Information transfer rates (ITRs) for each participant (P) calculated using EEG only, fTCD only, and the 3 hybrid combinations (A1, A2, and A3) for MR vs baseline problem (a), WG vs baseline problem (b), and MR vs WG problem (c). Average ITRs for the 3 classifications problems. ....	124
Figure 30	(a) Right fTCD channel (channel 1) and left fTCD channel (channel 2) normalized envelope signals during MR and WG tasks, (b) Difference between right fTCD channel (channel 1) and left fTCD channel (channel 2) envelope signals shown in (a) for MR and WG tasks, (c) power spectrum of EEG signals collected from electrodes P1, P2, P5, and P6 during MR task (flickering frequency= 7 Hz) (d) power spectrum of EEG signals collected from electrodes P1, P2, P5, and P6 during WG task (flickering frequency= 17 Hz). .....	127
Figure 31	Sensitivities and specificities (mean and standard deviation) calculated using EEG-fTCD, EEG only, and fTCD only for the MI paradigm (a), and the flickering MR/WG paradigm (b). .....	138
Figure 32	Information transfer rates (ITRs) for each participant (P) calculated using EEG only, fTCD only, and the EEG-fTCD combination for the MI paradigm (a), and the flickering MR/WG paradigm (b). .....	139
Figure 33	Average ITRs calculated using EEG only, fTCD only, and the hybrid combination for the MI paradigm (a), and the flickering MR/WG paradigm (b). .....	139
Figure 34	Identifying the top similar datasets using the proposed transfer learning approach. ....	147
Figure 35	Testing phase of the proposed transfer learning approach. ....	148
Figure 36	Average accuracy (a) and average ITR (b) as a function of the number of training trials for right MI versus baseline problem. ....	152
Figure 37	Average accuracy (a) and average ITR (b) as a function of the number of training trials for left MI versus baseline problem. ....	153
Figure 38	Average accuracy (a) and average ITR (b) as a function of the number of training trials for right MI versus left MI problem. ....	153

Figure 39	Average accuracy (a) and average ITR (b) as a function of the number of training trials for MR versus baseline problem. ....	155
Figure 40	Average accuracy (a) and average ITR (b) as a function of the number of training trials for WG versus baseline problem. ....	155
Figure 41	Average accuracy (a) and average ITR (b) as a function of the number of training trials MR versus WG problem. ....	156

## Acknowledgement

I would like to thank Dr. Murat Akcakaya for his endless support, motivation, and encouragement. Without his persistent help, this dissertation would not have been possible. His insight, enthusiasm, and invaluable advice had great impact on both my academic and personal life.

I would like also to thank the members of my dissertation committee, Dr. Amro El-Jaroudi, Dr. Zhi-Hong Mao, Dr. Ervin Sejdic, and Dr. Elizabeth Skidmore for their valuable time and constructive feedback that helped me to improve the quality of this dissertation. I am also grateful to Dr. Mahmoud El-Nokali and Dr. Amro El-Jaroudi for their continuous help and invaluable support.

Also, I would like to express my very great appreciation to all my friends who have always been a significant source of support and encouragement. Specifically, I would like to thank Khaled Sayed for his support and for the fruitful research discussions we had. Warmest thanks to my dear sister Busra Susam for her care and for always being there for me. Special thanks also to my friends, Hoda, Randa, Safaa, Yasmine, Yassin, and Amr.

Last but not least, my deepest gratitude to my family for their endless love and support.

*To the memory of my beloved mother and father*

## 1.0 Introduction

Brain computer interfaces (BCIs) translate brain activity into control signals that can be used to command external devices as shown in Fig.1. The main objective of BCIs is to either bypass or restore neuromuscular activity for individuals experiencing neurological deficits that cause motor impairment such as stroke, Parkinson's disease, and amyotrophic lateral sclerosis [1]. Therefore, developing BCIs is essential for those individuals to communicate with the surrounding environment using only their brain signals. Prosthetic limbs and wheelchairs are common BCI applications targeting patients with neurological deficits [2], [3]. BCIs are also used to design rehabilitation programs for disabled individuals to restore the lost functionalities [4]. Such programs are cost-effective as they can be administered in clinics or at home without requiring additional supervision from a rehabilitation therapist. In addition, BCIs have other diverse applications such as control of humanoid robots [5] and aircrafts [6] as well as controlling virtual reality environments [7].

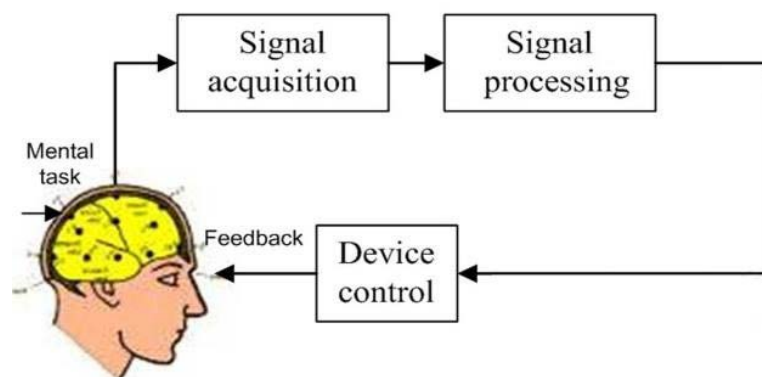


**Figure 1 The main building blocks of a BCI system.**

Current BCI systems can be categorized into active, reactive and passive BCIs [8]. The first category relies on the active performance by the BCI user of cognitive tasks such as mental calculation and motor imagery [9]. In such systems, training should be provided to the subjects in order to be able to perform these mental tasks so that the BCI system can identify the recorded brain activity with sufficient accuracy. The second category, reactive BCIs, are event driven which means that they employ external stimuli to generate certain brain activity. In such systems, brain response to visual, auditory or tactile stimuli is measured and analyzed [10]. The main advantage of this BCI category is that the user does not have to be trained to be able to use the BCI. Passive BCIs use brain signals that are generated by the BCI user unintentionally such as signals generated due to drowsiness and vigilance [11].

BCIs record mental activity either invasively or non-invasively and translate the recorded brain activity into signals needed for controlling external devices or providing neurofeedback for patients during rehabilitation [12]. Non-invasive BCIs are usually used to avoid risks of surgical procedures needed for invasive BCIs [1]. To design noninvasive BCI systems, different modalities have been investigated including functional near-infrared spectroscopy (fNIRS) [13], functional magnetic resonance imaging (fMRI) [14], and magnetoencephalography (MEG) [15]. However, these modalities have limitations that hamper BCI usage outside the laboratory-controlled environment. For instance, fMRI and MEG are expensive nonportable equipment that can be used efficiently only in a controlled environment [16]. On the other hand, fNIRS does not require highly controlled environment, but it lacks the speed needed for real-time BCIs [17].

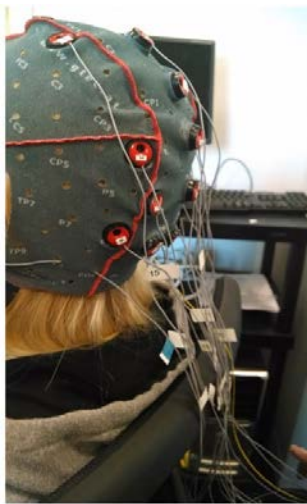
Given the limitations of the previously mentioned modalities, Electroencephalography (EEG) is widely used to design non-invasive BCIs due to its portability and low cost [18], [19]. Moreover, it has high temporal resolution, therefore, it can be used for developing real-time BCIs.

EEG measures brain electrical activity using electrodes connected to a cap that is placed on the scalp as seen in Fig.2. Different EEG signals have been investigated by researchers in a vast number of studies to be used for controlling BCI systems. Depending on the brain signal/pattern employed for BCI design, EEG-based BCIs can be categorized into event-related desynchronization/synchronization (ERD/ERS) BCIs, steady-state visual evoked potentials (SSVEPs) BCIs, P300 BCIs, and slow cortical potentials (SCPs) BCIs [20].

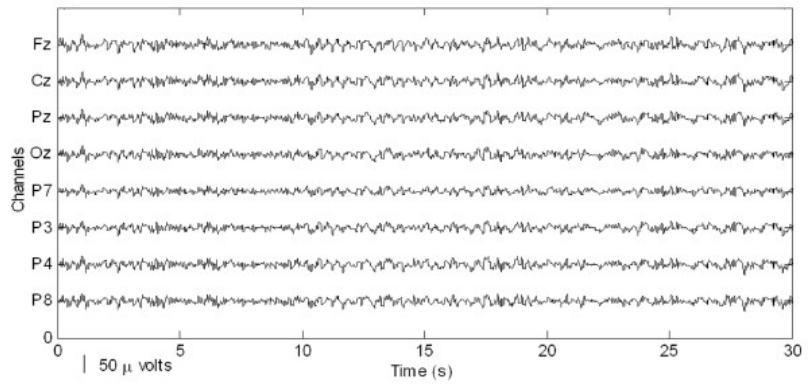
## **1.1 EEG-based BCIs**

### **1.1.1 Steady-state visual evoked potentials (SSVEPs) BCIs**

Among several categories of EEG-based BCIs, SSVEP BCIs have been extensively investigated for communication and control purposes [21]–[23]. In such SSVEP systems, visual stimuli with different flickering frequencies are used to elicit temporally matching electrical oscillation in the visual cortex [24]. For instance, in a binary BCI system in which the user observes two visual stimuli flickering with frequencies 5 and 15 *Hz*, considering the EEG power spectrum due to each stimulus, it is expected that peaks will appear at the flickering frequency of that stimulus and its harmonics as seen in Fig.3. Therefore, to issue a command using SSVEP BCI, the user has to focus his/her attention on one of the visual stimuli shown on the screen.



a)



b)

**Figure 2 a) EEG cap with electrodes connected b) sample of the EEG signals recorded from 8 different channels.**

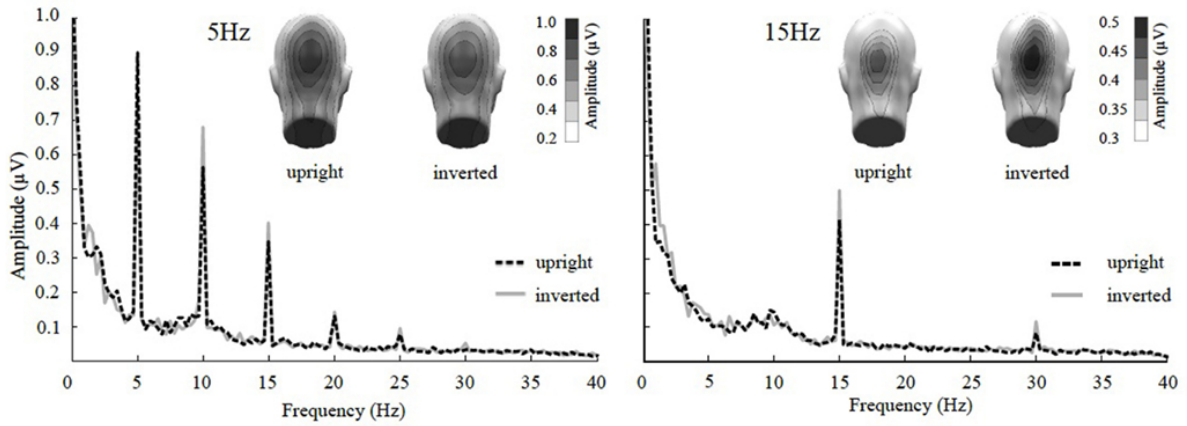


**Figure 3 Power spectral density for EEG responses due to stimuli flickering with frequencies 5 and 15 Hz. It can be noted that there are spikes at the harmonics of each stimulus frequency [149].**

### **1.1.2 Event-related desynchronization/synchronization (ERD/ERS) BCIs**

ERD reflects neural activity enhancement and it occurs during movement planning, actual movement, or motor imagery (MI). ERD is represented by a reduction in EEG frequency power in alpha (8-12 Hz) and beta (12-30 Hz) bands on the motor area. In contrast to ERD, ERS is represented by an increase in EEG frequency power in alpha and beta bands [25]. MI is known to induce ERD in the ipsilateral hemisphere and ERS in the contralateral hemisphere.

BCIs based on MI have been intensively used in rehabilitation applications that seek assisting disabled individuals as well as restoring an individual's physical and cognitive functions lost due to neural disorders [26]. It was found that the MI process activates the same brain regions activated during the actual physical movement [27]. Therefore, during the rehabilitation process, patients with motor impairments practice the MI process to activate the injured brain motor regions [28]. Several studies were performed on both healthy and nonhealthy participants to examine the feasibility of motor imagery for BCI applications [27], [29], [30]. With the goal of motor recovery after a stroke, several motor imagery BCIs with robotic feedback were developed [28], [4]. Such systems decode the motor imagery signals into robot assisted movements and it was shown that such systems yielded motor improvements.

### **1.1.3 P300 BCIs**

The P300 evoked potentials are positive waves in EEG signal that are mainly elicited by infrequent occurrence of visual, auditory or tactile stimuli. P300 appears in around 300 *ms* after presenting an infrequent stimulus among many frequent stimuli [31]. A number of research studies have shown that decreasing frequency of occurrence of the target stimulus will lead to a higher

P300 amplitude. Nevertheless, the user may get used to the infrequent presence of the target stimuli which may decrease the P300 amplitude and consequently decreases the performance [31], [32]. One advantage of using P300-based BCIs is that they do not require training.

#### **1.1.4 Slow cortical potentials (SCPs) BCIs**

Slow cortical potentials (SCPs) are slow voltage shifts that appear in EEG signals and last for few seconds. The frequency of SCPs is usually below 1 Hz [33]. Such brain activities are mainly associated with changes in the level of cortical activity. In particular, an increase in the neural activity will elicit negative SCPs and a decrease in the neural activity will induce positive SCPs [33]. These shifts in SCPs can be used to control a BCI. For instance, patients can move a cursor or select tasks on computer by self-regulating these brain activities [34].

### **1.2 Multi-modal BCIs**

Although EEG is the most common modality used for BCI design due to its high temporal resolution, cost effectiveness, and portability [18], it suffers from low signal-to-noise ratio and it encounters non-stationarities due to brain background activities [35]. Moreover, although the performance of EEG-based BCIs is stable in laboratory environment, such performance decreases significantly when the system is used in complex environments or for long periods [36], [37]. BCI performance also decreases when it is controlled by severely motor-impaired patients [38].

To boost the performance of EEG-based BCI, many studies suggested using fNIRS as a second modality to be simultaneously acquired with the EEG [39], [40] since it is less sensitive to

electrical noise as well as electromyography artifacts [41]. However, as mentioned earlier, fNIRS has a relatively slow response [42] and is difficult to setup as it requires at least 20 sensors for data acquisition [43], [44]. Therefore, to avoid fNIRS disadvantages, we suggest functional transcranial Doppler ultrasound (fTCD) to be simultaneously recorded with EEG. Compared to fNIRS, fTCD has a faster response time. In addition, it is easier to setup and requires fewer sensors. fTCD assesses cerebral blood velocity using two ultrasound sensors placed on the left-side and right-side transtemporal window located above the zygomatic arch [45] as shown in Fig.4. It was observed that signals recorded using fTCD change with different cognitive tasks. Based on this observation, a study suggested that it is possible to develop a BCI that is based on fTCD modality using mental rotation and word generation cognitive tasks [46]. However, an observation period of 45 seconds was required to achieve acceptable accuracy which is not practical for a real-time BCI. Towards more efficient fTCD-based BCIs, shorter observation periods (15-20 seconds) were achieved [47], [48]. In a recent study, detailed in chapter 3, we examined fTCD as an approach for real-time BCI [49] and achieved approximately 80% accuracy within 5 seconds of the task onset. Therefore, it is expected that EEG and fTCD, when combined, can produce an efficient multi-modal hybrid BCI.

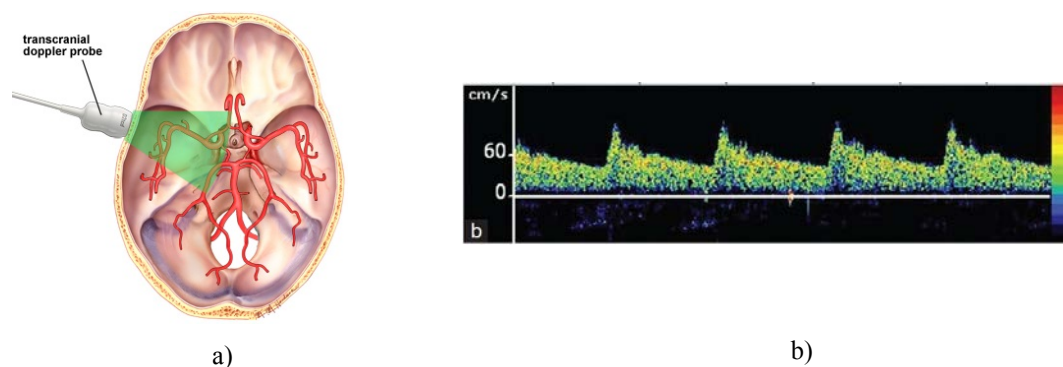


**Figure 4 a) top view for the skull with the transcranial Doppler probe fixed on the left transtemporal window  
b) sample Doppler ultrasound signal showing the change in cerebral blood velocity across time [150].**

### 1.3 Contributions

Initially, as explained in chapter 3, we investigate the possibility of designing a real-time BCI based on fTCD. Inspired by the results achieved using the fTCD-based BCI, we propose a novel multi-modal hybrid EGG-fTCD system that simultaneously measures brain electrical activity as well as cerebral blood flow velocity. The cognitive tasks to be presented to the users of such a system have to be differentiable using both EEG and fTCD in order for the hybrid BCI to be efficient. Based on a study that proved that the cerebral blood velocity in left and right middle cerebral arteries (MCAs) changes depending on whether the moving arm is the left or the right one [50], we suggested designing MI-based EGG-fTCD hybrid BCI. However, it was found that there are slight differences between the recorded fTCD signals in response to right and left MI tasks which indeed affected the overall performance accuracy of the hybrid system. To boost the performance of the system, we introduce a presentation paradigm for the EEG-fTCD hybrid system that is claimed to provide higher overall performance compared to those obtained using MI paradigm. Specifically, instead of using 2 imagery tasks (right and left MI), we designed mental rotation (imagery) and word generation (analytical) tasks since, these tasks were proved to be separable for the fTCD-based BCI as described in chapter 3. However, such tasks cannot be distinguished using the EEG. To develop an efficient hybrid BCI in which cognitive tasks can be differentiated using both neuroimaging modalities, we propose altering the word generation (WG) and mental rotation (MR) tasks into flickering checkerboard-textured WG and MR tasks with each task flickering with a different frequency. Consequently, EEG will differentiate MR and WG tasks because they will elicit different SSVEPs while fTCD will distinguish the same tasks due to differences in cerebral blood flow velocity. The coming chapters are organized as follows:

- Chapter 2 introduces a literature review about the existing multi-modal BCIs.
- Chapter 3 shows a study we performed to examine the feasibility of fTCD for real-time BCIs.
- Chapter 4 explains the hybrid EEG-fTCD system implementation using MI paradigm. In addition, it shows the performance measures obtained using this paradigm.
- Chapter 5 illustrates the design of flickering MR/WG paradigm to be presented to the hybrid users as well as the performance measures we obtained.
- Chapter 6 shows feature extraction and fusion techniques that we present to improve the performance of the hybrid system utilizing MI paradigm.
- Chapter 7 shows feature extraction and fusion techniques that we present to improve the performance of flickering MR/WG paradigm.
- Chapter 8 explains extension of our feature extraction and fusion techniques to solve 3-class problems of both MI and flickering MR/WG paradigms.
- Chapter 9 introduces a transfer learning approach that we suggest to reduce calibration requirements of the hybrid system utilizing both MI and flickering MR/WG paradigms.
- Chapter 10 presents remarks and conclusions about the performance of both MI and flickering MR/WG paradigms.

## 2.0 Literature Review

Recently, hybrid BCIs have been extensively studied so that the process of identifying user intent can be performed with a minimal amount of error in a reasonable amount of time [51]. Hybrid BCIs can be categorized into 2 main classes including BCIs exploiting multimodal signals (multi-modal BCIs) and BCIs using single modality to sense different patterns of the same brain activity due to mental tasks with different nature (multi-paradigm BCIs) [52]. For the design of BCIs that belong to the first class, signals from modalities such as EEG, fTCD, fNIRS, fMRI, EOG, EMG, etc., are recorded simultaneously [53]. Multimodal BCIs can be further divided into 2 subcategories including BCIs sensing brain signals only such as EEG-fNIRS and EEG-fMRI systems and BCIs sensing brain and non-brain signals such as EEG-EMG and EEG-EOG systems [54]. The other hybrid BCI category includes BCIs based on different brain patterns. In these systems, different patterns (SSVEP, MI, P300, etc.) of the same physiological signal (EEG) are used to design the hybrid BCI [55]. Both hybrid BCI categories can exploit multisensory stimulation (visual, auditory, and tactile) depending on the employed recording modalities [52].

In general, BCI research focuses on developing direct connection between the human brain and a device by converting a user's expressed intention into a meaningful control signal that drives an application. This process requires several processing steps following acquisition of the BCI input signals. These steps include: a) preprocessing, b) feature extraction, c) feature selection and reduction, d) information fusion, and f) classification. In this chapter, we focus on reviewing these processing steps for both categories of multi-modal BCIs exploiting brain and non-brain signals. More specifically, we review each of the processing steps mentioned above for each modality employed for multi-modal BCI design separately as detailed below.

## 2.1 Preprocessing

Artifacts are undesired electrical signals that originate from different sources than those used to control BCIs. Such signals can interfere with the signals employed as source of control and can alter the characteristics of physiological phenomena of interest or even be mistakenly used to control a BCI system [56]. Therefore, it is essential to efficiently remove such artifacts to avoid degradation of BCI system performance especially when used by patients in a real-life environment. The performance of BCI systems could be affected by several physiological and non-physiological artifacts. Physiological artifacts are usually caused by muscular, ocular, respiratory, and heart activities while non-physiological artifacts include artifacts due to equipment and artifacts due to surrounding environment such as power line interference [57].

**EEG:** EEG signals are known to be highly contaminated with physiological activities due to eye blinking, eye movements, muscle contractions, respiration, and heart electrical activity [56]. The most significant physiological artifacts are eye movements and blinking since they generate high-magnitude artifacts compared to EEG amplitude [58].

To eliminate high frequency EEG artifacts, classical temporal filtering methods such as IIR low-pass filters have been employed [59], [60]. In addition, band-pass filters were extensively used to remove both low and high frequency artifacts [61]–[79]. Alternatively, subject-dependent filtering methods have been introduced to account for variations in ranges of various physiological artifacts across subjects and to improve signal to noise ratio (SNR). For instance, a subject-dependent band-pass filtering method was designed using point-biserial correlation coefficient to filter EEG signals [80]. Moreover, in another study, a temporal FIR filter for all channels was developed using a regularization method that favors a sparse solution for the coefficients as an alternative to common sparse spectral spatial pattern (CSSSP) which optimizes a filter per channel

[81], [82]. Other preprocessing techniques have been used to eliminate noise such as linear detrending to remove low frequency drift [83] and independent component analysis (ICA) to remove nonbrain artifacts [64], [77].

On the other hand, in addition to temporal filtering, EEG data can be also filtered in the spatial domain. For instance, the Laplacian filter was employed in various studies to improve the spatial resolution of EEG data [59], [66], [71], [73], [81]. In other studies, EEG data were spatially filtered using common average reference (CAR) to achieve the same purpose [61], [80].

**fNIRS:** fNIRS signals are mainly contaminated with physiological and instrumental noise. To remove high frequency artifacts due to breathing and heart electrical activity, IIR low-pass filters [59], [81], [84], exponential moving average filters [60], median filtering [64], Gaussian low-pass filters, and wavelet denoising [79] have been used. In addition, slow Baseline drifts were removed using high-pass filters [77], [83] and linear detrending [59]. Several studies employed band-pass filters to remove both low and high frequency artifacts [78], [80]. On the other hand, similar to EEG signals, fNIRS signals were also be spatially filtered using common average reference (CAR) [64].

**fTCD:** High frequency noise present in fTCD signals is usually removed using low-pass FIR filters [85] [86] or using moving average [84]. Moreover, high-pass filters can be used to remove Doppler shifts caused by reflections off the vessel walls [84].

**EOG:** To eliminate baseline drift as well as high frequency noise, band-pass filters [61], [62], [69], [74], [87], high-pass and low-pass filters [70] have been used. Moving average has been also employed to remove high frequency noise [74]. As a preprocessing step before feature extraction, some studies rectify EOG signals [74].

**EMG:** An important preprocessing step for EMG signals is to obtain the signal envelope which can be calculated using mean filtering [88], band-pass filtering [73], [74], [89], low-pass and high-pass filtering [72] [71]. To attenuate effect of crosstalk [90], ICA can be applied to EMG signals [72]. In some studies, the EMG signal is rectified before feature extraction [72].

**ECG:** ECG signals are mainly preprocessed using band-pass filtering [75]–[77] and detrending to remove baseline drift [77].

## 2.2 Feature Extraction

BCI systems rely mainly on the variations between the brain activity patterns due to target and non-target stimuli. The distinctive differences between these patterns can be captured using efficient pattern recognition techniques that aim at classifying mental activity into a certain class according to the extracted features. One of the main steps of pattern recognition process is feature extraction which aims at representing signal characteristics in a compact form that can be interpreted by a classification algorithm.

**EEG:** Several feature extraction techniques have been employed to extract EEG features in both the time and frequency domains. One of the most efficient feature extraction methods especially for MI BCIs is common spatial pattern [60], [62], [63], [80], [81] and its variations such as generic learning regularized common spatial patterns [78] and one-versus-rest common spatial pattern designed for multi-class classification [61]. Another efficient feature extraction technique known to be successful with SSVEP BCIs is canonical correlation analysis [88] [72] [91].

To reduce the number of extracted features especially in case of using a high number of electrodes, average amplitudes [65], [69], [79], [92] or downsampled signal amplitudes [64], [70] [93] are considered. However, some studies employ signal amplitudes without downsampling or averaging [87]. Moreover, thresholding signal amplitudes was performed to identify user intent [66], [67]. Differential entropy was also considered as a feature to extract discriminative information from EEG signals [68]. Various other techniques have been employed to extract features from EEG data such as Hilbert Transform [59] and autoregressive modeling [66], [67], [71], [73].

EEG data have been analyzed in the frequency domain using features extracted from the Fourier Transform [72] and the EEG bi-spectrum [75]. Moreover, many studies have exploited power spectrum density estimation [66], [67], [71], [73], [76], [77] while other studies used the power spectrum to calculate band power spectral features [64], [78], [81], [83], [94]. Features extracted using wavelet analysis were also considered through applying fuzzy mutual information based wavelet packet decomposition to EEG data [95].

**fNIRS:** In fNIRS systems, optical intensity signals are translated into concentration changes according to the modified Beer–Lambert law [96]. Mainly 4 concentration signals including deoxygenated hemoglobin (HbR), oxygenated hemoglobin (HbO), HbR + HbO, and HbO - HbR are used for feature extraction. In some studies, amplitudes of these signals [59], [77], [83], average of peak amplitudes of HbO and HbR [79], or average of HbO and HbR time courses [80], [81] are used as features. Moreover, slopes which identify the changes in the signal amplitudes across time are extracted as features [78], [80], [84]. In one study, the difference between the HbO current value and the previous value was considered as a feature [60]. In another

study, to capture the decrease or increase in HbO and HbR , the mean of first few samples was subtracted from the mean of the following samples [64].

Although the features extracted from fNIRS signals are usually simple features, in one study generic learning regularized common spatial patterns was applied to fNIRS signals to extract spatial patterns characteristic to the mental tasks performed by the users [78].

**fTCD:** Most common time domain features extracted from fTCD signals include hemodynamic laterality, slope, mean, range, and change in signal value measured from the beginning to the end of each trial [84]. In the frequency domain, features derived from power spectrum and wavelet decomposition of fTCD signals were extracted [85], [86], [97], [98].

**EOG:** Analyzing EOG signals is usually performed either to recognize different eye movements or to identify gaze direction. Such aims can be achieved through calculating certain features or through thresholding EOG amplitudes. EOG features may include temporal features such as minimum, mean, maximum, and variance of EOG amplitude [68] or frequency domain features such as wavelet coefficients extracted using fuzzy mutual information based wavelet packet decomposition [95].

For instance, eye movements including saccades, blinks, and winks were identified using an algorithm that employs sets of fuzzy logic rules [70], [99]. Moreover, using such sets of fuzzy logic rules, the algorithm computed the area at which the user gazes [12]. To distinguish different eye movements, canonical correlation analysis (CCA) [61], multithresholding [87] have been applied to EOG signals. Binary thresholding was also used to identify right and left eye movements [66], [67]. To detect saccades and blinks, thresholding was applied to wavelet coefficients resulting from wavelet decomposition [68]. In another study, average EOG amplitude was thresholded using subject-specific threshold for winking detection [69]. Rapid repeated eye

movements were detected through thresholding the EOG amplitude and the number of crossings of a certain threshold with a specific time window as well as maximum and minimum EOG amplitude while single eye blink was detected through negative derivative and thresholding EOG amplitude [74].

To determine gaze direction, difference of EOG signals from right and left electrodes (right and left eye) was thresholded based on the receiver operating characteristics curve [62]. In another study, the maximum positive potential from the right eye and the minimum negative potential from the left eye were thresholded to determine the gaze direction [94].

In certain studies, EOG is used to enhance the performance of EEG BCIs. In particular, EOG was used to identify the EEG intervals with the minimum EOG artifacts [92]. In another study, ICA and minus rule were used to obtain an approximation for vertical and horizontal EEG from forehead EOG [68].

**EMG:** The common EMG features in the literature are usually extracted in the time domain such as waveform length [71], [73], mean of EMG absolute value, EMG variance, and EMG log variance [73]. Alternatively, many studies threshold the envelope of EMG signal to infer user intent. Such envelope can be calculated using mean filtering [88], rectification and low-pass filtering [93], and the Hilbert transform [74]. Thresholding can be also applied to envelope of the Integrated EMG (iEMG) [91].

Recently, researchers have investigated features representing corticomuscular coupling. These features either measure the correlation between band-limited power time-courses (CBPT) associated with EMG and EEG or the coherence between EEG and EMG such as corticomuscular coherence (CMC) [89].

**ECG:** ECG features of interest for BCI community are either signal-specific or signal-independent features. Common signal specific features include R-R interval [77] and transient heart rate changes based on instantaneous heart rate [76] while signal independent features include absolute log of ECG bi-spectrum [75] and coefficients resulting from fuzzy mutual information based wavelet packet decomposition [95].

### **2.3 Feature Selection and Reduction**

Feature selection or reduction has been shown to be essential for BCI systems since the feature vectors from multiple modalities can be high dimensional vectors depending on the number of channels from each modality and the sampling rate of each modality. Several techniques have been employed to reduce the dimensionality of feature vectors such as signal downsampling performed especially when the signal amplitudes are intended to be used as features [59], [62], [64], [68], [69], [70], [73], [79], [81], [83], [87], [93]. Feature selection methods such as mutual information [59], exhaustive search [84], Fisher criterion [84], and spectral regression-based kernel discriminant analysis [95] have been also employed.

### **2.4 Information Fusion**

One of the simplest approaches to fuse information from multiple modalities is to concatenate the feature vectors corresponding to the signals collected from all modalities [59], [68], [71], [75], [78], [84], [95], [97], [98]. However, in certain multi-modal systems, information

fusion is not needed since each modality is used to identify different set of commands. Such an approach has been employed in several EEG-EOG [61], [87], [94], EEG-fNIRS [79], and EEG-EOG-EMG systems [74]. Alternatively, another group of multi-modal BCIs uses different modalities to take decisions sequentially. For instance, in an EEG-fNIRS system, detection of MI was performed using fNIRS while classification of MI was achieved using EEG [60].

Certain studies investigating hybrid BCIs aim to infer the user intent through a 2- step hierarchical process. In particular, all the possible commands that can be issued through the BCI are categorized into fewer groups. One of the modalities identifies the group to which the command reflecting user intent belongs, while the second modality recognizes the exact command from the selected group [70], [72], [73], [76], [91].

In certain multi-modal BCI systems, information fusion is performed through exploiting features that can only be calculated using signals from multiple modalities. For instance, features representing corticomuscular coupling were used to infer user intent in an EEG-EMG BCI. These features consider the correlation between band-limited power time-courses (CBPT) associated with EMG and EEG or the coherence between EEG and EMG such as corticomuscular coherence (CMC) [89].

Logic decision rules have been investigated to infer user intent. For instance, in an EEG-EMG system, ‘AND’ fusion rules of classification output were developed based on which modality gives higher accuracy [88]. In another study utilizing an EEG-EOG system, a decision rule was developed based on combinations of all possible classifiers’ outputs [65]. To improve the performance of multi-modal systems, one modality can be used to confirm the decision of the other modality [69]. For instance, in an EEG-EOG speller system, subjects were instructed to actively wink once if the EEG classifier denoted the target letter as the top candidate.

Fusion of information from multiple modalities can also be performed on the classifier level. For instance, the outputs of an EEG classifier and 3 fNIRS classifiers were combined using a naïve Bayesian approach [83]. In another study, user intent inferred from EEG and gaze information provided by an eye-tracker were fused under Bayes rule assuming independence [63]. In an EEG- fNIRS system, optimal classifiers of single features were constructed and probabilistically fused under a feature independence assumption [61].

Projected scores of two EEG and fNIRS sLDA classifiers were combined as input for a meta sLDA [80]. In another study, Meta LDA classifier was constructed by optimally combining outputs of and EEG LDA classifier and 2 fNIRS LDA classifiers [81]. Alternatively, a meta classifier was designed with a fusion rule based on the weighted sum of class probabilities of 4 different classifiers including 2 EEG classifiers and 2 fNIRS classifiers where the input observation is assigned to the class with the highest probability sum [64]. In an EEG-fTCD system, projected EEG and fTCD SVM scores were combined using a probabilistic fusion approach under 3 different assumptions [85], [86].

## **2.5 Classification**

The main aim of BCI systems is to translate brain activity into control commands to derive certain applications. This goal can be achieved either using regression or classification algorithms [100]. However, in BCI systems, classification algorithms are more popular than regression algorithms. Classification techniques are used to recognize the user intent based on the characterization of the brain activity in response to certain tasks/stimuli.

Various classification algorithms have been used in BCI applications to infer user intent such as Linear discriminant analysis (LDA) [62], [64], [69]–[71], [73], [75], [77]–[79], [84], [87], [92], [93], [95] and shrinkage linear discriminant analysis (sLDA) [80]. Support vector machines with linear [60], [61], [64], [89] and radial basis function (RBF) kernels [72] were also employed to identify user intent. In addition, some studies utilized neural networks with different architectures such as extreme learning machines (ELMs) [59] and feedforward neural networks [63]. Researchers also investigated  $L_2$ -regularized linear logistic regression classifiers [83] and minimum distance classifiers [65].

Moreover, regression models have also been investigated in certain passive BCI applications. For instance, support vector regression (SVR) with RBF kernel was employed to estimate vigilance levels [68].

### **3.0 A Brain-Computer Interface Based on Functional Transcranial Doppler Ultrasound Using Wavelet Transform and Support Vector Machines <sup>1</sup>**

In this chapter, we propose feature selection techniques to build an fTCD-based BCI system that overcomes the speed limitations of previous fTCD-BCIs. Given the fact that fTCD detects different velocities of cerebral blood flow in response to different cognitive tasks, these tasks can be used as the selections in the development of the fTCD-based BCI if such cognitive tasks could be differentiated with sufficient accuracy and speed. Here, cognitive tasks including word generation and mental rotation as well as the resting state are considered for the development of the BCI. These cognitive tasks have already been explored in BCI design and it was shown that both mental rotation and word generation cause significant increase in cerebral blood flow velocity in right and left middle cerebral arteries [101]. However, the word generation task resulted in significantly stronger activation in the left middle cerebral arteries while the mental rotation task shows bilateral activation [102] so it is expected that these tasks can be differentiated with a high accuracy if employed in a BCI application.

Four subject-specific classification schemes are formulated to study the feasibility of 2-class and 3-class real-time fTCD- based BCIs. The first and second classification schemes are formulated to distinguish each cognitive task from the resting state. The third scheme aims at classification of the word generation and mental rotation tasks against each other. Finally, in the fourth scheme, a 3-class classification problem combining mental rotation, word generation and

---

<sup>1</sup> Based on Aya Khalaf, Ervin Sejdic, Murat Akcakaya, "A Brain-computer Interface Based on Functional Transcranial Doppler Ultrasound Using Wavelet Transform and Support Vector Machines," *Journal of Neuroscience Methods*, vol. 293, pp. 174-182, 2018 © [2018] ELSEVIER.

the resting state is studied with the aim of increasing the number of possible selections for the BCI. For all these classification schemes, features derived from a five-level wavelet transform are used in a support vector machines (SVM) classifier that employs a linear kernel. To determine the classification accuracy as a function of data rate (speed), two methods for feature vector formulation are employed: (1) moving window (MW), and (2) incremental window (IW) methods. These feature vector formulation methods are presented in section 3.1.3. Finally, we show that with the proposed techniques we can achieve significant improvements in the data rate and hence the speed of operation, without compromising the accuracy.

### **3.1 Materials and Methods**

This section includes a description of the recruited participants, experimental procedure, and the proposed preprocessing, feature extraction, selection and classification methods.

#### **3.1.1 Participants**

All research procedures were approved by the local institutional review board at the University of Pittsburgh and all participants provided informed consent. Data was collected from 20 healthy participants including 10 males and 10 females with mean age of  $21.5 \pm 1.86$  years, mean weight of  $67.9 \pm 14.2$  kg and mean height of  $174 \pm 9.69$  cm [103]. None of the participants had a history of migraines, concussions, strokes, heart murmurs, or other brain related injuries. Participants were also subjected to the Edinburgh handedness tests [104] which showed 16

participants were right-handed, with a mean score of 64% , 3 participants were left-handed, with a mean score of 80%, and one was ambidextrous.

### **3.1.2 Experimental Procedure**

Two 2 MHz transducers were fixed on the left-side and right-side transtemporal window located above the zygomatic arch [45] . The depth of the TCD was set to 50 mm to approximate the depth of the mid-point of the middle cerebral arteries segment [105]. Since a previous TCD study [106] reported that the maximum safe continuous exposure time to TCD is 30 minutes to avoid thermal damage to brain tissues, the data collection session was divided into 3 parts. In the first section, each participant was asked to take a rest so that the cerebral blood flow is stabilized while recording a 20-min baseline period. The next two sections were each 15-min trials with a 5-min break in between. Each of these trials included five-word generation tasks and five mental rotation tasks, in a random order. Within each trial, every task lasted 45 seconds (which we denote as an activation period for each task) with a 45-second resting period between consecutive tasks. In total, each participant underwent 20 cognitive tasks divided evenly into word generation and mental rotation.

#### **3.1.2.1 Mental Rotation Task**

Randomly selected pairs of images from a database of 3D shapes constructed from cubes [107] were displayed on the screen for a duration of 9 seconds. This means that for an activation period of 45 seconds, 5 different pairs of images were displayed. Each pair of images were displayed as either identical or symmetrically mirrored images. Participants were asked to decide

if the displayed image pairs were identical or mirrored by mentally rotating these images as seen in Fig.5.

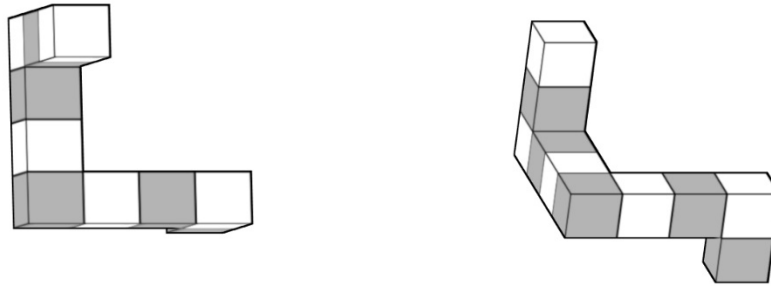


**Figure 5** Sample of the mental rotation task. Each participant was asked to decide if the pair of images are identical or mirrored by mentally rotating one of the two images.

### **3.1.2.2 Word Generation Task**

During the 45-second activation periods, a randomly chosen letter was displayed on the screen. The participants were asked to think of words starting with that displayed letter. This nonverbal action was chosen to avoid artifacts due to speech or intrathoracic pressure changes [108].

### **3.1.3 Data Analysis**

Two methods for classifying the cognitive tasks were tested; a moving window (MW) and an incremental window (IW). In the MW method, a window containing the first 0.5 seconds of the fTCD data was used for feature extraction. After taking the classification decision based on the data from that window, the window was shifted by 0.25 seconds and features were recalculated for that new window of data and a new classification decision was made. This procedure was

repeated until the window reached 45 seconds, the length of a task. Note that in this approach the classification decision at a specific time was independent of all past windows.

As a second method, an incremental window was employed in which all the samples up to the time of classification were included. Initially, features were extracted from the first 0.5 seconds of data and a classification decision was made. Then, the size of the window was increased by 0.5 seconds, features were recalculated and a new decision was made. This incremental increase was then repeated until the length of the task was reached. One drawback of this method is that when the window size increases, fine changes in the signal, that might correspond to a specific task, might be dominated by the trend of the majority of the samples. The choice of the window size and the amount of shift or increment for both methods was performed empirically. It was found that the smaller the window size, the better the performance accuracy.

Fig.6 shows a flowchart for the main algorithm steps as well as the differences between these two windowing methods. Data transmission rate for both windowing methods was calculated according to (1).

$$B = \log_2(N) + P\log_2(P) + (1 - P)\log_2\left(\frac{1 - P}{N - 1}\right) \quad (1)$$

where  $N$  is the number of classes,  $P$  is the classification accuracy and  $B$  is the data transmission rate per trial.

### 3.1.3.1 Preprocessing

The data was approximately bandlimited to under 4 kHz. A 150th order low pass filter of 5 kHz corner frequency was applied for antialiasing purposes. The original data was sampled at 44.1 kHz, and it was downsampled by a factor of 5 to reduce computation requirements.

### 3.1.3.2 Feature Extraction

Five level wavelet decomposition [109] was performed for each window defined by the IW, and MW methods using the Daubechies 4 mother wavelet. The choice of the number of decomposition levels was determined using visual inspection. First, approximate coefficients of the last level of each task were plotted to check if they show any difference between the 3 tasks. The number of decomposition levels was increased and approximate coefficients of the last level were plotted until no difference could be seen.

After performing the wavelet decomposition over each window of data, simple statistical features including mean, variance, skewness, and kurtosis were calculated for the wavelet coefficients. For each TCD channel, these 4 features were calculated for 6 wavelet bands resulting in a total of 24 statistical features for each channel (i.e., a total of 48 features), and these features were considered for feature selection. Both the skewness and kurtosis measure deviations from Gaussianity. Kurtosis [110] measures the peak of the curve compared to the Gaussian curve. The skewness also measures the asymmetry of a given probability distribution. A probability distribution with a heavier tail and higher peak than the Gaussian has a positive kurtosis while lighter tails with flatter peaks give a negative kurtosis. A positive skewness value reflects a distribution with the right side tail longer than the left side and with a mean that is greater than the mode; whereas, a distribution with a left side tail that is longer than the right side and a mean value less than the mode has a negative skewness [111].

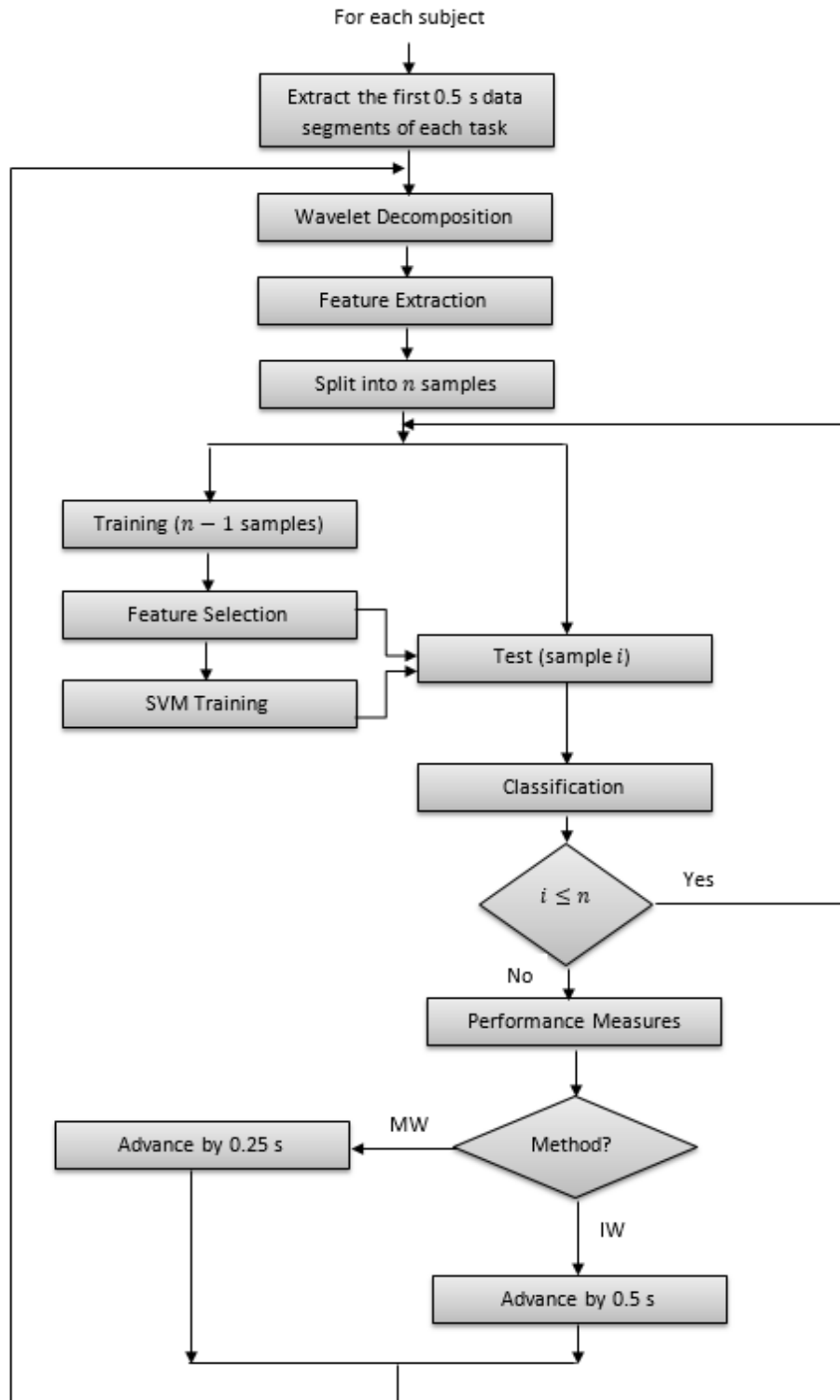


**Figure 6 A flowchart for the algorithm used for data analysis using moving window (MW) and incremental window (IW) methods.**

### 3.1.3.3 Feature Selection

Features were statistically assessed using the Wilcoxon test [112], which is a nonparametric hypothesis test used to evaluate differences between two populations. One advantage of this test is that it does not restrict the data to follow any specific parametric distribution such as the Gaussianity assumption imposed by the Student-t test [113]. Briefly, for each feature, the difference between the two groups per sample is calculated. The higher the difference magnitude, the higher the rank assigned to that sample. Only ranks of positive differences are considered to estimate the Wilcoxon test statistic  $w$  while negative differences and zero-magnitude differences are excluded. The Wilcoxon test statistic  $w$  given by (2) is the sum of all the positive ranks.

$$W = \sum_{i=1}^{n'} R_i^{(+)} \quad (2)$$

where  $R_i^{(+)}$  is the rank of the  $i$ th positive difference and  $n'$  is the number of samples with positive rank. This means that  $n' \leq n$ ; that is, the number of positive differences is at most equal to the total number of available samples  $n$ .

When applying the Wilcoxon test, we chose a  $p$ -value of 0.05 to be used for the test and the features that satisfy such criteria were selected independently of each other. Therefore, the number of features can vary from person to person depending on the significance of each feature whether it satisfies the chosen  $p$ -value or not. For example, during cross-validation to predict the system performance, at each validation step, the number of features changes based on the Wilcoxon test. As for the 3-class problem, considering the fact that the Wilcoxon test is a binary feature selection method, a one versus one approach [114] was used to decompose the 3-class problem into 3 binary problems with a  $p$ -value of 0.05. The resulting 3 sets of selected features were used separately as inputs for 3 binary SVM classifiers as indicated in the next subsection.

### 3.1.3.4 Classification

Support vector machines (SVM) were used to perform the classification task [114]. Basic SVM is a linear classifier that formulates an optimization problem aimed at finding an optimal hyper plane that has the largest possible distance to the nearest data point in the training set regardless of the class that such point belongs to. Consequently, SVM achieves better generalization compared to the other linear classifiers such as linear discriminant analysis. Given the fact that the classes are not typically linearly separable, a kernel can be used to transform each observation into higher dimensional feature space in which the classes are linearly separable. Common kernels include linear, polynomial, and radial basis function kernels.

In order to reduce the computational complexity, a linear kernel was employed in this work. Four different classification schemes were formulated. In the first two schemes, two 2-class classifiers were developed to distinguish the word generation task from the resting state and mental rotation task from the resting state. In the third scheme, a 2-class classifier was developed to distinguish between the features corresponding to mental rotation and word generation. Finally, a 3-class classifier was developed to jointly distinguish among the mental rotation, word generation and resting state. A one versus one approach was used to convert the 3-class problem into 3 binary problems since the SVM is basically a binary classifier [114]. The majority vote obtained from the 3 classifiers was considered for the final decision.

To evaluate the robustness of the proposed system, for each participant, leave-one-out cross validation was used to assess the performance measures. MATLAB (R2015b) was used to run the experiments on a HP Z840 Workstation with Intel®, and Xeon® CPU, 2.2 GHz processor speed, and 128 GB RAM.

### 3.2 Results

The proposed methodology was tested using fTCD data recorded from 20 participants. Three types of problems were analyzed including: 1) cognitive tasks versus resting state (two 2-class problems i.e., mental rotation task vs resting state and word generation task vs. resting state), 2) mental rotation task versus word generation task (one 2-class problem) and 3) mental rotation versus word generation versus resting state (one 3-class problem). For each classification problem, MW and IW methods, as described in Section 3.1.3, were applied for feature extraction and performance measures (speed, sensitivity, specificity and accuracy of classification) were analyzed.

Tables 1 through 4 show the average of the maximum classification accuracy and corresponding sensitivity and specificity values achieved by each participant using IW and MW data analysis and feature extraction methods at different state durations. A state duration is defined as the period in which a mental activity takes place before it is assigned to a specific class. In other words, it is the time since the task onset till the time point at which a decision has to be made. In case of both MW and IW methods, for each state duration, all possible windows that are within that period (i.e. state duration) were considered, and the window achieving the maximum accuracy was selected to compute the average accuracy, sensitivity, specificity and time across participants. For example, in the MW method, a 5-s state duration means that the windows 0-0.5s, 0.25-0.75s, 0.5-1s, ....., and 4.5-5s are used for the analysis and the performance measures (accuracy, sensitivity, specificity and time) for the window that obtains the maximum accuracy are considered to calculate average performance measures across participants, while for the IW method, windows 0-0.5s, 0-1s, 0-1.5s,....., and 0-5s are analyzed and the average performance measures are

computed in the same way described above for the MW method. Time column shown in these tables represents the average time at which the maximum accuracy was achieved for each participant within the corresponding state duration.

### **3.2.1 2-Class Problems**

As seen in Tables 1-2, the MW method achieved higher average accuracies, compared to the IW method, in a relatively short time of approximately 3 s, an average accuracy, sensitivity and specificity of 80.29%, 81.18%, and 79.41%, for the resting state versus mental rotation and 82.35%, 82.94%, and 81.76% for the resting state versus word generation. In addition, according to Tables 1 and 2, within approximately 3 s of the cognitive activity onset, an average accuracy, sensitivity, and specificity of 74.41%, 72.94%, and 75.88% was achieved for the resting state versus mental rotation classification compared to 77.94%, 77.65%, and 78.24% for the resting state versus word generation problems using the IW method. Moreover, as seen in Table 3, using the MW method for the task versus task classification achieved 79.72%, 80.56%, and 78.89% average accuracy, sensitivity and specificity while IW method obtained average accuracy, sensitivity and specificity of 74.64%, 72.86%, and 76.43%. Both methods achieved such accuracies within approximately 3 s of the task onset.

Considering the maximum performance accuracy that could be achieved by each of the three binary classification problems, the MW method obtained the best possible accuracy compared to the IW method at each state duration. Using the MW method an average accuracy, sensitivity, and specificity of 94.41%, 95.29%, and 93.53% was achieved for the mental rotation versus resting state problem after 15.57 s from the task onset while the IW method obtained an average accuracy, sensitivity, and specificity of 89.41%, 89.41%, and 89.41% respectively in

**Table 1 Average maximum accuracy and the corresponding sensitivity, specificity, and time at different state durations for the word generation task versus resting state using MW and IW methods.**

	State Duration (S)	Time(s)	Sensitivity (%)	Specificity (%)	Accuracy (%)
MW Method	5.0	2.84	82.94%±09.19%	81.76%±09.51%	82.35%±06.87%
	7.5	4.41	88.82%±09.28%	85.88%±07.12%	87.35%±05.89%
	10.0	4.93	90.00%±08.66%	86.47%±07.02%	88.24%±05.29%
	12.5	4.93	90.00%±08.66%	86.47%±07.02%	88.24%±05.29%
	15.0	6.10	90.59%±08.99%	87.65%±06.64%	89.12%±05.07%
	17.5	6.63	91.18%±09.27%	87.65%±06.64%	89.41%±05.29%
	20.0	8.62	91.76%±08.09%	88.24%±06.36%	90.00%±05.00%
	22.5	8.62	91.76%±08.09%	88.24%±06.36%	90.00%±05.00%
	45	21.22	94.70%±07.17%	91.76%±07.28%	93.24%±04.31%
IW Method	5.0	2.50	77.65%±13.93%	78.24%±13.80%	77.94%±11.73%
	7.5	3.17	80.00%±12.25%	80.59%±13.91%	80.29%±10.96%
	10.0	3.65	80.59%±11.97%	81.76%±12.37%	81.18%±09.93%
	12.5	4.79	82.94%±07.72%	82.35%±12.51%	82.65%±08.31%
	15.0	5.82	83.53%±08.62%	83.53%±11.69%	83.53%±08.06%
	17.5	6.65	83.53%±08.62%	84.12%±12.28%	83.82%±08.39%
	20.0	7.32	84.12%±09.39%	84.12%±12.28%	84.12%±08.88%
	22.5	7.88	84.71%±09.43%	84.12%±12.28%	84.41%±08.82%
	45	13.88	86.47%±09.31%	90.59%±12.49%	88.53%±08.62%

**Table 2 Average maximum accuracy and the corresponding sensitivity, specificity, and time at different state durations for the mental rotation task versus resting state using MW and IW methods.**

	State Duration (S)	Time(s)	Sensitivity (%)	Specificity (%)	Accuracy (%)
MW Method	5.0	2.04	81.18%±09.28%	79.41%±13.45%	80.29%±09.27%
	7.5	4.19	84.12%±12.28%	84.12%±10.64%	84.12%±08.52%
	10.0	5.78	87.65%±09.03%	86.47%±10.57%	87.06%±06.86%
	12.5	5.96	88.82%±09.28%	87.06%±10.47%	87.94%±06.86%
	15.0	7.82	90.59%±08.27%	88.82%±09.93%	89.71%±05.44%
	17.5	10.34	90.59%±09.66%	93.53%±07.02%	92.06%±04.70%
	20.0	11.19	92.35%±08.31%	93.53%±07.02%	92.94%±04.70%
	22.5	11.19	92.35%±08.31%	93.53%±07.02%	92.94%±04.70%
	45	15.57	95.29%±06.24%	93.53%±07.02%	94.41%±03.91%
IW Method	5.0	2.59	72.94%±17.95%	75.88%±16.61%	74.41%±14.35%
	7.5	3.47	77.06%±14.04%	78.24%±17.04%	77.65%±13.36%
	10.0	4.59	81.18%±13.17%	77.65%±17.51%	79.41%±12.36%
	12.5	4.88	82.94%±12.13%	79.41%±14.78%	81.18%±09.77%
	15.0	6.06	83.53%±11.15%	81.76%±15.09%	82.65%±10.33%
	17.5	7.29	83.53%±11.15%	83.53%±13.67%	83.53%±09.81%
	20.0	8.41	84.71%±11.79%	83.53%±13.67%	84.12%±10.19%
	22.5	9.97	85.29%±12.31%	84.12%±12.78%	84.71%±09.60%
	45	20.38	89.41%±09.66%	89.41%±11.44%	89.41%±07.05%

**Table 3 Average maximum accuracy and the corresponding sensitivity, specificity, and time at different state durations for the mental rotation versus word generation using MW and IW methods.**

	State Duration (S)	Time(s)	Sensitivity (%)	Specificity (%)	Accuracy (%)
MW Method	5.0	2.24	80.56%±11.62%	78.89%±10.23%	79.72%±06.75%
	7.5	3.18	83.33%±12.37%	81.11%±11.32%	82.22%±07.90%
	10.0	3.87	85.00%±11.50%	81.11%±11.32%	83.06%±07.89%
	12.5	5.93	87.78%±08.78%	84.44%±09.84%	86.11%±07.58%
	15.0	7.22	91.11%±08.32%	86.11%±09.16%	88.61%±06.14%
	17.5	9.01	92.78%±08.26%	87.22%±09.58%	90.00%±05.94%
	20.0	10.78	92.22%±09.43%	89.44%±08.73%	90.83%±04.62%
	22.5	11.28	91.67%±09.24%	91.11%±07.58%	91.39%±04.47%
	45	15.41	93.89%±07.78%	91.67%±07.86%	92.78%±03.52%
IW Method	5.0	2.50	72.86%±13.26%	76.43%±11.51%	74.64%±07.71%
	7.5	3.73	78.57%±09.49%	79.29%±13.28%	78.93%±05.94%
	10.0	4.80	79.29%±09.97%	82.14%±11.88%	80.71%±07.03%
	12.5	6.87	80.71%±09.97%	85.00%±10.92%	82.86%±06.99%
	15.0	6.87	80.71%±09.97%	85.00%±10.92%	82.86%±06.99%
	17.5	7.17	82.14%±11.21%	85.00%±10.92%	83.57%±07.70%
	20.0	7.17	82.14%±11.21%	85.00%±10.92%	83.57%±07.70%
	22.5	10.93	83.57%±10.08%	86.43%±11.51%	85.00%±07.34%
	45	19.00	90.00%±09.61%	87.86%±11.88%	88.93%±07.12%

20.38 s. On the other hand, word generation versus resting state problem obtained an average accuracy, sensitivity, and specificity 93.24%, 94.70%, and 91.76% respectively after 21.22 s from task onset using MW method while IW method achieved 88.53%, 86.47%, and 90.59% average accuracy, sensitivity, and specificity in 13.88 s. Considering the task versus task problem, the IW method achieved an average accuracy, sensitivity, and specificity of 88.93% , 90.00%, and 87.86% in 19 s while the MW method obtained 92.78%, 93.89%, and 91.67% accuracy, sensitivity, and specificity in 15.41 s.

### **3.2.2 3-Class Problem**

As shown in Table 4, the MW method shows better performance when compared to the IW method. Average accuracies of 66.12%, 68.26%, and 61.32% were achieved for mental rotation, word generation and resting state respectively with overall accuracy of 65.27% using the MW method within 5 s from the onset of the cognitive task (chance level is 33%). Using the IW method achieved accuracies of 57.70%, 69.71%, and 63.20% for mental rotation, word generation and resting state respectively with overall accuracy of 63.80% at the same 5-second period. Utilizing the whole observation period with the MW method, average accuracies of 72.19%, 75.93%, and 70.88% for mental rotation, word generation and resting state respectively with overall accuracy of 72.91% were obtained at average time of 11.27 s. Mental rotation, word generation and resting state accuracies of 70.10%, 77.86%, and, 67.04% were achieved in average time of 14.29 s with an overall accuracy of 71.57% using IW method.

**Table 4 Average maximum accuracy and the corresponding sensitivity, specificity, and time at different state durations for the 3-class (mental rotation (MR), word generation (WG), and resting state problem using MW and IW methods.**

	State Duration (S)	Time(s)	MR Sensitivity (%)	WG Sensitivity (%)	Specificity (%)	Accuracy (%)
MW Method	5.0	3.35	59.20%±11.97%	70.43%±06.67%	51.90%±22.34%	60.23%±08.89%
	7.5	4.05	63.02%±04.83%	69.10%±07.37%	55.76%±22.73%	62.33%±08.47%
	10.0	4.68	66.12%±09.66%	68.26%±09.19%	61.32%±16.63%	65.27%±09.06%
	12.5	5.75	68.00%±10.33%	71.00%±11.01%	65.00%±18.41%	68.00%±10.80%
	15.0	6.13	70.20%±10.54%	73.65%±08.23%	62.15%±25.73%	68.36%±10.09%
	17.5	7.63	68.78%±12.29%	76.92%±06.99%	67.76%±14.18%	70.83%±08.08%
	20.0	9.45	68.17%±12.29%	76.20%±06.99%	68.91%±13.98%	70.67%±07.98%
	22.5	9.45	68.17%±12.29%	76.20%±06.99%	68.91%±13.98%	70.67%±07.98%
	45	11.27	72.19%±11.01%	75.93%±07.07%	70.88%±14.14%	72.91%±07.73%
IW Method	5.0	2.53	50.00%±18.26%	65.00%±10.80%	47.00%±29.46%	54.00%±11.84%
	7.5	3.41	58.23%±13.17%	68.01%±12.29%	48.42%±30.47%	58.21%±11.35%
	10.0	3.97	54.07%±23.19%	69.23%±12.87%	58.70%±17.29%	60.67%±08.86%
	12.5	4.59	55.00%±22.73%	69.33%±12.87%	63.67%±10.59%	62.33%±06.49%
	15.0	4.94	57.70%±23.12%	69.71%±12.87%	63.20%±10.59%	63.80%±07.28%
	17.5	4.94	57.70%±23.12%	69.71%±12.87%	63.20%±10.59%	63.80%±07.28%
	20.0	5.94	65.00%±10.80%	68.96%±14.49%	57.04%±22.63%	63.67%±06.37%
	22.5	9.59	68.00%±13.17%	70.48%±12.87%	61.52%±25.58%	66.64%±08.46%
	45	14.29	70.10%±15.63%	77.86%±13.17%	67.04%±29.08%	71.57%±12.59%

### 3.2.3 Transmission Rate

The bit rate was calculated in bits/trial using (1) then divided by state duration in minutes to give bit rate in bits/min. Among the 3 binary problems described above, the bit rate calculated for the word generation versus resting state was the highest compared to the other binary problems. As seen in Fig. 7 using the IW method, a maximum bit rate of 3.95 and 2.28 bits per minute was achieved for the word generation vs resting state and the 3-class problem respectively. The MW method obtained a maximum bit rate of 3.83 and 3.09 bits per minute for the same problems. Moreover, maximum bit rates of 3.3, and 2.04 bits per min were achieved for mental rotation versus resting state and mental rotation versus word generation respectively using the MW method while IW method obtained bit rates of 1.30, and 1.63 bits per min for the same problems.

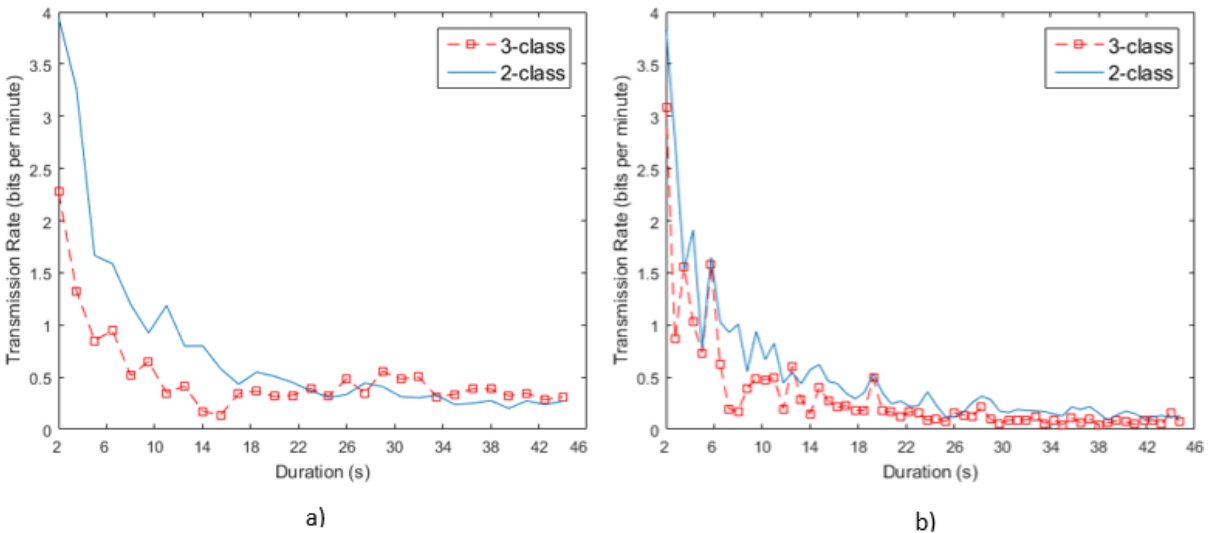


Figure 7 Transmission rate in bits/min for binary and 3-class problems using a) IW method b) MW method.

### 3.3 Discussion

Considering the performance measures shown in Tables 1-3, among the 3 binary classification problems we addressed, the word generation versus baseline problem offered the highest accuracy within 3 s of the onset of the cognitive activity compared to the other binary problems. Therefore, it can be considered as the best candidate to build binary selection based BCIs. Additionally, according to Tables 1-3, it is clear that the MW method achieved the best accuracy. The main difference between the MW method and the IW method is that the MW method just accounts for the information belonging to the current window while the IW method considers all the fTCD data up to the moment at which the decision is taken. One disadvantage of the IW method is that the performance measures would be significantly degraded if the participant lost concentration at some point during the task; this means that nonstationarities in the data would affect the future classification process.

Table 5 compares our method with the existing methods based on fTCD and NIRS. During comparison, both speed (observation period) and accuracy have been considered. For the proposed system, we include the accuracies for two different observation periods (3 s and 45 s). Although an observation period of 45 s is not practical for a real-time BCI, we computed the performance measures of the system with such observation period to ensure a fair comparison with the work proposed by Myrden et al. (2011) who used the same dataset employed in this work and achieved the reported accuracies for 45 s observation time. As seen in Table 5, the proposed MW method outperformed the other fTCD-based methods in the literature in terms of both accuracy and observation period. We achieved comparable accuracies to the Myrden et al. (2011) system with only 3 s observation period. On the other hand, NIRS is a portable and hemodynamic-based

modality that, like fTCD, is a promising tool to develop BCI applications. Recent NIRS-based BCIs proposed by Fazli et al., 2012, and Shin et al., 2016 showed promising results, shown in Table 5, that lead to development of a BCI that combines both fTCD and fNIRS [84]. However, the approach proposed in this chapter outperformed these studies as it obtained average accuracies of 80.29% and 82.35% within approximately 3 s of the onset of the mental task for mental rotation vs resting state and word generation vs resting state classification problems respectively. Therefore, we believe that the presented results are promising and can be used to develop a real-time fTCD-based BCI application.

The proposed 3-class fTCD-based BCI achieved an average accuracy of 65.27% using the MW method within 5 s of the task onset as seen in Table 4. The studies suggested in [116], [117] reported accuracies of 62.40% within 15 s [116] and 40% within 5 s [117] of the onset of the cognitive task. Moreover, the maximum classification accuracy over the whole observation period obtained by our approach was 72.91% achieved in 11.27 s compared to the previously reported 73.11% obtained in 24.90 s [117].

A maximum bit rate of 3.83 and 3.09 bits per minute were achieved for the binary and the 3-class problems respectively using the moving window method, while the incremental window achieved maximum bit rates of 3.95 and 2.28 bits per minute. This is compared to 0.3 and 1.2 bits per minute previously reported for 2 and 3-class fTCD-based BCIs [102], [117]. Being able to obtain reasonable classification accuracies within relatively short time period for the binary problems as well as the 3-class problem introduces the possibility of developing a real time fTCD-based BCI with acceptable data transmission rates. Applications of the proposed BCI include controlling assistive devices that can be used for communication and movement control through which the users can control prosthetic limbs or wheel chairs [118]. Another application of this

**Table 5** Comparison between the proposed MW method and the state of the art methods for binary BCIs.

Method	BCI Type	Accuracy	Observation Period (s)
Myrden et al., 2011	fTCD	82.90%	45
Myrden et al., 2011	fTCD	85.70%	45
Aleem and Chau, 2013	fTCD	80.00%	20
Lu et al., 2015	fTCD	79.69%	15
Fazli et al., 2012	fNIRS	73.30%	7
Shin et al., 2016	fNIRS	77.00%	10
Faress and Chau, 2013	fTCD-fNIRS	76.10%	20
Proposed method (MR/rest)	fTCD	80.29%	3
Proposed method (WG/rest)	fTCD	82.35%	3
Proposed method (MR/rest)	fTCD	93.24%	45
Proposed method (WG/rest)	fTCD	94.41%	45

technology is the environmental control such that the BCI users can adjust lights and temperature in their houses or control the TV, etc. [119]. The BCI systems have the potential to enhance the quality of life for individuals with disabilities specially those who experience locked-in syndrome. Specifically, it would decrease their level of dependency to their caretakers and improve the individual's contact with society [120]. In addition, BCI has been recently shown to be a promising neurorehabilitation tool that can help individuals with disabilities to restore neuromuscular functions [121].

### 3.4 Conclusion

In this chapter, we investigated the possibility of developing 2-class and 3-class BCI systems using data acquired through bilateral fTCD measurements. To construct the BCI system, two different methodologies, incremental window (IW) and moving window (MW), were proposed. The main differences between these methods are the windowing and feature vector formulation. For each method, the raw data was analyzed using wavelet transform. Statistical features were calculated from the wavelet transform coefficients. These features were subjected to Wilcoxon test for feature selection followed by classification with SVM with linear kernel. With the proposed approach, we showed that within 3 s of the onset of the cognitive task, an accuracy of 80.29% was obtained for the mental rotation versus resting state problem while the word generation versus resting state achieved an accuracy of 82.35% using the MW. The MW method used for the task versus task problem achieved a mean classification accuracy of 79.72% within 3 s of the onset of cognitive activity. In addition, the MW method used for the 3-class problem obtained an average accuracy of 65.72% within 5 s of the onset of mental tasks. The presented results show significant improvement in the data rate without a compromise in the accuracy of cognitive task classification. Compared to the previous fTCD studies, the proposed method showed an increase of 12% and 9% accuracy for the 2-class and the 3-class BCIs respectively. In terms of speed, the proposed BCIs are at least 12 and 2.5 times faster than the 2-class and the 3-class systems proposed in previous fTCD studies. Such promising results support the real-time implementation of a 2-class and 3-class fTCD-based BCIs. Moreover, the improvements in the data transmission rate reported in this chapter imply that it would be feasible to utilize the fTCD in a multi-modal hybrid BCI. Such an approach to fuse information from multiple modalities to achieve a certain task simultaneously will likely improve the system performance compared to a

single modality BCI. For example, a hybrid system that employs both EEG and fTCD may be able to achieve higher performance by utilizing both sources of information simultaneously. Such a hybrid BCI will be the subject of our future research.

## 4.0 A Novel Motor Imagery Hybrid Brain Computer Interface Using EEG and Functional Transcranial Doppler Ultrasound <sup>2</sup>

It was found that the cerebral blood velocity in left and right middle cerebral arteries (MCAs) changes depending on whether the moving arm is the left or the right one [50]. Such findings suggest that fTCD might be promising for MI-based BCIs. Inspired by these findings as well as the results we achieved previously with fTCD as a candidate for real-time BCIs, we propose MI-based hybrid BCI that uses both EEG and fTCD modalities. Such system will acquire the electrical activity of the brain using the EEG and the vascular response of the brain using the fTCD. We claim that combining these modalities will result in a system with higher performance accuracy, faster response time, and less setup complexity. In this chapter, cognitive tasks including left arm MI and right arm MI are considered for the BCI design. Three different binary selection problems were formulated to study the feasibility of 2-class BCI. The first two classification problems are formulated to differentiate between each cognitive task and the baseline while the third problem aims at classification of the left arm and right arm MI tasks against each other. For the 3 binary selection problems, features derived from the power spectrum for both EEG and fTCD signals were calculated. In addition, mutual information and linear SVM were used for feature selection and classification.

---

<sup>2</sup> Based on Aya Khalaf, Ervin Sejdic, Murat Akcakaya, "A Novel Motor Imagery Hybrid Brain Computer Interface using EEG and Functional Transcranial Doppler Ultrasound," *Journal of Neuroscience Methods*, vol. 313, pp. 44-53, 2019 © [2019] ELSEVIER.

## 4.1 Materials and Methods

### 4.1.1 Simultaneous Data Acquisition

EEG was collected using 16 electrodes placed according to the 10-10 system over frontal, central, and parietal lobes at positions Fp1, Fp2, F3, F4, Fz, Fc1, Fc2, Cz, P1, P2, C1, C2, Cp3, Cp4, P5, and P6. The left mastoid was used as the reference for all participants. A g.tec EEG system with g. USBamp, a bio-signal amplifier, was used in this study. It included 16 24-bit simultaneously sampled channels with an internal digital signal filtering and processing unit and sampling rate up to 38.4 kHz. The data were digitized with a sampling rate of 256 samples/sec and filtered by the amplifier's 8th order bandpass filter with corner frequencies 2, 62 Hz in addition to 4th order notch filters with corner frequencies 58, 62 Hz. Through the band-pass filter, our aim was to remove possible DC drift and high frequency noise. Processed data were transferred from the amplifiers to a laptop via USB 2.0.

The fTCD data was collected with two 2 MHz transducers using SONARA TCD system of 145 Mw ultrasonic power. These transducers were placed on the left and right sides of the transtemporal window located above the zygomatic arch. Since the middle cerebral arteries (MCAs) provide approximately 80% of the brain with blood [122], the fTCD depth was set to 50 mm which is the depth of the mid-point of the MCAs [105].

### 4.1.2 Visual Presentation Design

In this presentation scheme, a basic motor imagery task is visualized while acquiring EEG and fTCD simultaneously. As seen in Fig. 8, the screen shows a horizontal arrow pointing to the

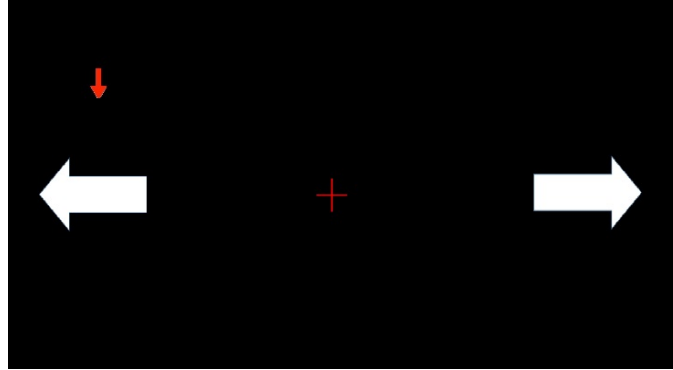


**Figure 8 Stimulus presentation for the hybrid BCI system.**

right representing right arm MI and another horizontal arrow pointing to the left representing left arm MI as well as a fixation cross that represents the baseline. Each trial lasts for 10 s. During each trial, a vertical small arrow, shown in Fig. 8, points randomly to one of the 3 tasks for duration of 10 s and the user has to take a rest if the vertical arrow points to the fixation cross or to imagine moving either left or right arm depending on which MI task is specified by the vertical arrow. A total of 150 trials are presented per session.

### **4.1.3 Participants**

10 healthy right-handed subjects including 4 males and 6 females participated in the experiment with ages ranging from 23 to 32 years old (mean and standard deviation:  $26.7 \pm 2.3$ ). The experiment lasted for approximately 1 hour and 15 min including the time required for the setup. All research procedures were approved by local Institutional Review Board (IRB) under the University of Pittsburgh IRB number of PRO16080475. Participants signed a written informed consent before starting the experiment. During the experiment, subjects were seated in a comfortable chair approximately 1 m away from the screen. Each participant attended one session.

#### **4.1.4 Feature Extraction and Fusion**

The 16-channel EEG data as well as the two-channel fTCD data corresponding to each task were segmented and extracted. For each segment, the power spectrum was estimated using Welch's method [123]. The features corresponding to each segment included the raw power spectrum for that segment. The number of features obtained from each power spectrum was reduced by considering the average power over a narrow range of frequencies instead of using all the power spectrum values at all frequency bins as features. The average power over each consecutive 2 Hz for the EEG data was obtained. Since the fTCD signal has much higher bandwidth ( $\approx 2.5$  KHz) compared to the EEG signals ( $\approx 60$  Hz) and considering the need to reduce the number of features, the average power over each consecutive 50 Hz for the fTCD data was obtained to form reduced power spectrums. For each observation, the EEG feature vector was formed by concatenating reduced power spectrums corresponding to the 16 EEG segments while fTCD feature vector was formed by concatenating reduced power spectrums corresponding to the 2 fTCD segments. For each observation, the overall feature vector was formed by concatenating the EEG feature vector and the fTCD feature vector. The feature vector representing each trial contained 420 features including 320 EEG features as well as 100 fTCD features. Specifically, 20 features were extracted from each EEG electrode giving a total of 320 features whereas each fTCD sensor contributed 50 features giving a total of 100 fTCD features.

#### **4.1.5 Feature Selection**

Feature selection methods are divided into two main categories including filter and wrapper/embedded methods [124]. The main advantage of the filter methods compared to wrapper

and embedded methods is the low computational complexity. However, filter methods assume feature independence and can select redundant features. Due to the high dimensionality of the EEG-fTCD feature vector (420 features), we decided to apply a filter method for feature selection. Mutual information [125] was used to select the significant features out of concatenated EEG-fTCD feature vector. Mutual information measures the information provided by a variable to reduce the uncertainty about another variable. In the feature extraction context, mutual information measures contribution of each feature towards taking a correct decision by assigning each feature a score based on its contribution. The higher the score is, the higher the contribution is of that feature towards correct classification. To calculate the mutual information score, each feature is quantized adaptively such that the number of data samples is almost the same in each quantization bin so that quantization levels are equiprobable [126]. Mutual information score between the discretized feature value  $x$  and the class label  $y$  is given by (3). In this chapter, to determine the number of features to be used for each binary selection problem, the cumulative distribution function (CDF) was calculated for the mutual information scores. We calculated CDF thresholds corresponding to probabilities ranging from 0.5 to 0.95 with 0.05 step in addition CDF thresholds corresponding to probabilities 0.98 and 0.99. For each CDF threshold, the features obtaining scores greater than or equal that threshold were selected. The performance measures including accuracy, sensitivity, and specificity corresponding to each CDF threshold were computed.

$$MI = \sum_{x \in X} \sum_{y \in Y} p(x, y) \log \left( \frac{p(x, y)}{p(x)p(y)} \right) \quad (3)$$

#### **4.1.6 Classification**

Since the BCI is intended to be used for real-time applications, we used linear SVM to reduce computational expenses. To investigate the feasibility of 2-class BCI, three binary classification problems were formulated including right arm MI versus baseline, left arm MI versus baseline, and right arm MI versus left arm MI. Based on the classification results, we calculated some performance measures to evaluate the hybrid system. These measures included accuracy, sensitivity, specificity, and information transfer rate (ITR), known also as the bit rate, given by (1). The objective behind calculating sensitivity and specificity is to test if the classifier recognizes both classes with similar accuracies or it is biased towards one of the classes. Specifically, sensitivity is the accuracy of detecting right/left MI while specificity reflects the accuracy of detecting the baseline.

#### **4.1.7 Evaluation of the Effectiveness of the Hybrid System**

To evaluate the significance of the EEG-ftCD combination compared to the system using EEG only, Wilcoxon signed-rank test was used to statistically compare the accuracies and bit rates obtained using the combination to those obtained using EEG only. In particular, EEG-ftCD accuracy vector as well as EEG only accuracy vector containing the accuracies of the 10 participants represented the two groups to be compared. Moreover, same comparison was performed between EEG-ftCD bit rate vector and the bit rate vector obtained using EEG only.

## 4.2 Results

Subject-specific classification was performed on each participant using leave-one-out cross validation. For each participant, we analyzed the accuracy profile across time using an incremental window the width of which increases by 1 s. The maximum width for the incremental window is 10 s which represents the trial length. The accuracy analysis was performed using 12 different CDF thresholds corresponding to probabilities ranging from 0.5 to 0.95 with 0.05 step as well as the thresholds corresponding to probabilities of 0.98, and 0.99. Therefore, 12 different accuracy profiles across time were obtained per participant. Average performance measures over all participants were obtained using subject-independent and subject-specific CDF thresholds. For subject-independent threshold, the maximum accuracy at each CDF threshold was obtained for each participant yielding 12 different accuracies for each participant corresponding to the 12 CDF thresholds. For each threshold, the average accuracy over all the 10 participants was obtained. The threshold at which the maximum accuracy was achieved was selected as the general CDF threshold that can be used with all participants. For subject-specific thresholds, the maximum accuracy across all the CDF thresholds for each subject was obtained and considered as the subject's performance accuracy. Therefore, in subject-specific analysis, each subject might have different CDF threshold that corresponds to his/her maximum performance accuracy.

Tables 6 through 8 show the maximum accuracy achieved by each participant and the corresponding time calculated using the EEG-ftCD combination. Corresponding sensitivity and specificity values are reported in detail in Tables 30-35 in the appendix section of this chapter. Here, in the results section, we report only the average sensitivities and specificities. To reveal the significance of the hybrid system, the same performance measures were calculated using EEG only and ftCD only with the same time interval at which the EEG-ftCD combination gives the

maximum accuracy as seen in Tables 6-8. Transmission rates corresponding to the accuracies and times listed in Tables 6 through 8 were also calculated for each binary problem using EEG data, fTCD data, and EEG-fTCD combination as seen in Fig. 9, 10, and 11. Fig. 12 compares average bit rates obtained using subject-independent and subject-specific thresholds for the 3 binary problems. Tables 9 and 10 list the p-values representing the significance of the EEG-fTCD hybrid system. These p-values are calculated by statistically comparing the EEG-fTCD accuracy/bit rate vector with the EEG only accuracy/bit rate vector for all the binary selection problems when subject-independent and subject-specific CDF thresholds are used for feature selection.

#### **4.2.1 Right/Left arm MI vs Baseline**

Table 6 shows the maximum accuracies and corresponding times for right arm MI versus baseline problem using subject-independent and subject-specific thresholds while appendix Tables 30 through 33 show details about sensitivity and specificity values for each individual. For subject-independent threshold analysis, average accuracy, sensitivity and specificity of 85.73%, 87.31%, and 83.86% were achieved using both EEG and fTCD within 7.2 s of the cognitive activity onset. In the meantime, using EEG only, we obtained 81.56%, 85.19%, and 77.27% average accuracy, sensitivity and specificity respectively.

Despite the low fTCD accuracy of 58.65%, when combined with EEG, fTCD data boosted the overall performance of the hybrid system with average accuracy increase of 4.17% compared to the accuracy obtained with the EEG only. As shown in Table 6 and Fig. 9. (a), the EEG-fTCD combination scored higher accuracy and bit rate for 8 out of the 10 participants. In terms of statistical comparison, as seen in Tables 9 and 10 the differences between hybrid and EEG only performance measures were shown to be significant as they correspond to a p-value of 0.012 in terms of accuracy comparison and p-value of 0.0078 in terms of bit rate comparison.

On the other hand, same performance measures were calculated for right arm MI versus baseline problem using subject-specific thresholds as shown in Table 6. It was found that the EEG-ftCD combination achieved 88.33%, 90.96%, and 85.23% average accuracy, sensitivity, and specificity respectively within 7.7s compared to 83.85%, 86.92%, and 80.23% obtained by EEG only and 58.23%, 61.92%, and 53.86% obtained by ftCD only. The average accuracy difference between the hybrid combination and the EEG only was 4.48%. As seen in Fig. 9. (b), the EEG-ftCD combination achieved higher bit rates compared to EEG only for all of the participants using subject-specific thresholds. However, Fig. 12 shows that subject-independent threshold obtained slightly higher average transmission rate 4.19 bits/min of compared to 3.87 bits/min for subject-specific threshold. In terms of statistical comparison, the EEG-ftCD combination achieved higher accuracy and bit rate compared to EEG only for all the participants with a p-value of 0.002 for both accuracy and bit rate (Tables 9, and 10).

Table 7 shows the performance measures for left arm MI versus baseline problem using subject-independent and subject-specific thresholds. Using subject-independent threshold, average accuracy, sensitivity and specificity of 86.49%, 87.55%, and 85.23% were obtained using EEG-ftCD combination within 6.3s. EEG only scored 83.61% accuracy, 85.09% and 81.82% specificity. A difference of 2.89% was achieved with 0.0098 p-value of as seen in Table 9. In terms of bit rates, a p-value of 0.0059 was achieved as shown in Table 10. The hybrid system obtained higher accuracies and bit rates compared to EEG for 9 out of 10 subjects. In contrast, using subject-specific threshold, an average accuracy difference of 5.36% was achieved with a p-value of 0.0078. In terms of bit rates, also, a p-value of 0.0078 was achieved as seen in Table 10. For 8 out of 10 participants, EEG-ftCD scored higher accuracy and bit rate compared to EEG only. EEG-ftCD scored 89.48% accuracy, 91.89% sensitivity, and 86.59% specificity within 6.1s while EEG only

scored 84.12% accuracy, 86.42% sensitivity, and 81.36% specificity. Considering Fig. 10, we obtained higher bit rates using the EEG-ftCD combination compared to bit rates generated using EEG only and ftCD only. In addition, as seen in Fig. 12, subject-specific thresholds achieved 6.02 bits/min average bit rate compared to 5.45 bits/min for subject-independent threshold.

**Table 6 Maximum accuracy (Acc) and the corresponding time for each subject using hybrid system, EEG only, and ftCD only. These measures were obtained for right arm MI vs baseline problem.**

Sub_ID	Subject-independent threshold			Subject- specific threshold				
	Time(s)	Acc_EEG	Acc_ftCD	Acc_Hybrid	Time(s)	Acc_EEG	Acc_ftCD	Acc_Hybrid
1	10	91.67%	57.29%	<b>93.75%</b>	10	91.67%	59.38%	<b>94.79%</b>
2	10	83.33%	56.26%	83.33%	7	91.67%	61.46%	<b>92.71%</b>
3	2	79.17%	45.83%	<b>84.38%</b>	7	81.25%	51.04%	<b>86.46%</b>
4	9	81.25%	55.21%	<b>87.50%</b>	9	81.25%	55.21%	<b>87.50%</b>
5	9	87.50%	61.46%	<b>90.63%</b>	9	87.50%	61.46%	<b>90.63%</b>
6	4	72.92%	56.25%	<b>82.29%</b>	7	85.42%	56.25%	<b>86.46%</b>
7	6	79.17%	56.25%	<b>83.33%</b>	6	80.21%	47.92%	<b>86.46%</b>
8	7	80.21%	66.67%	<b>89.58%</b>	7	81.25%	69.79%	<b>91.67%</b>
9	5	73.96%	61.46%	71.88%	5	71.88%	50.00%	<b>76.04%</b>
10	10	86.46%	69.79%	<b>90.63%</b>	10	86.46%	69.79%	<b>90.63%</b>
<b>Mean</b>	<b>7.2</b>	<b>81.56%</b>	<b>58.65%</b>	<b>85.73%</b>	<b>7.7</b>	<b>83.85%</b>	<b>58.23%</b>	<b>88.33%</b>

**Table 7 Maximum accuracy (Acc) and the corresponding time for each subject using hybrid system, EEG only, and fTCD only. These measures were obtained for left arm MI vs baseline problem.**

Sub_ID	Subject-independent threshold			Subject- specific threshold				
	Time(s)	Acc_EEG	Acc_fTCD	Acc_Hybrid	Time(s)	Acc_EEG	Acc_fTCD	Acc_Hybrid
1	10	88.66%	74.23%	<b>93.81%</b>	10	87.63%	65.98%	<b>97.94%</b>
2	7	93.81%	58.76%	92.78%	7	91.75%	65.98%	<b>93.81%</b>
3	8	80.41%	46.39%	<b>89.69%</b>	4	81.44%	51.55%	<b>93.81%</b>
4	2	73.32%	50.52%	<b>74.23%</b>	5	78.35%	61.86%	<b>81.44%</b>
5	8	77.32%	43.30%	<b>80.41%</b>	9	87.63%	53.61%	87.63%
6	2	85.57%	52.58%	<b>86.60%</b>	3	74.23%	53.61%	<b>86.60%</b>
7	3	88.66%	54.64%	<b>90.72%</b>	3	88.66%	54.64%	<b>90.72%</b>
8	9	86.60%	55.67%	<b>88.66%</b>	9	85.57%	50.52%	<b>92.78%</b>
9	5	74.23%	48.45%	<b>79.38%</b>	5	74.23%	48.45%	<b>79.38%</b>
10	9	87.63%	55.67%	<b>88.66%</b>	6	91.75%	47.42%	90.72%
<b>Mean</b>	<b>6.3</b>	<b>83.61%</b>	<b>54.02%</b>	<b>86.49%</b>	<b>6.1</b>	<b>84.12%</b>	<b>55.36%</b>	<b>89.48%</b>

**Table 8 Maximum accuracy (Acc) and the corresponding time for each subject using hybrid system, EEG only, and fTCD only. These measures were obtained for left arm MI vs right arm MI.**

Sub_ID	Subject-independent threshold				Subject- specific threshold			
	Time(s)	Acc_EEG	Acc_fTCD	Acc_Hybrid	Time(s)	Acc_EEG	Acc_fTCD	Acc_Hybrid
1	1	86.67%	44.76%	86.67%	1	82.86%	51.43%	<b>93.33%</b>
2	5	75.24%	38.10%	75.24%	5	75.24%	38.10%	75.24%
3	10	73.33%	46.67%	<b>75.24%</b>	6	71.43%	69.52%	<b>81.90%</b>
4	1	82.86%	45.71%	<b>83.81%</b>	2	81.90%	53.33%	<b>85.71%</b>
5	1	78.10%	50.48%	<b>81.90%</b>	1	78.10%	50.48%	<b>81.90%</b>
6	3	85.71%	42.86%	83.81%	3	85.71%	42.86%	83.81%
7	4	75.24%	44.76%	71.43%	4	71.43%	43.81%	<b>79.05%</b>
8	7	89.52%	45.71%	<b>92.38%</b>	9	96.19%	50.00%	<b>97.14%</b>
9	1	70.48%	44.76%	<b>71.43%</b>	1	70.48%	44.76%	<b>71.43%</b>
10	1	65.71%	62.86%	<b>68.57%</b>	2	62.86%	66.67%	<b>74.29%</b>
<b>Mean</b>	<b>3.4</b>	<b>78.29%</b>	<b>46.67%</b>	<b>79.05%</b>	<b>3.4</b>	<b>77.62%</b>	<b>51.10%</b>	<b>82.38%</b>

#### 4.2.2 Right arm MI vs left arm MI

The maximum accuracies and corresponding times for right arm MI versus left arm MI are shown in Table 8 for subject-independent and subject-specific threshold respectively. See also appendix Tables 34, and 35 for details about sensitivity and specificity values for each individual. Right arm MI versus left arm MI classification achieved 79.05%, 79.04%, and 79.06% average accuracy, sensitivity and specificity respectively using the EEG-fTCD combination within 3.4 s while EEG data only obtained average accuracy, sensitivity and specificity of 79.29%, 78.08%,

and 78.49% respectively. The average accuracy difference was low and insignificant (p-value=0.3828) according to Table 9. However, subject-specific thresholds obtained higher performance measures as, within 3.4 s, it achieved 82.38% average accuracy, 82.12% sensitivity and 82.64% specificity using the EEG-ftCD combination and 77.62%, 78.65%, and 76.60% using EEG only leading to a significant average accuracy difference of 4.76 % with 0.0195 p-value as seen in Table 9. The EEG-ftCD combination scored higher accuracy for 8 out of 10 participants. On the other hand, bit rates for each participant were calculated and visualized as seen in Fig. 11. It can be noted that the bit rate difference between EEG-ftCD combination and EEG only based on subject-specific threshold is much higher compared to the same difference obtained using subject-independent threshold (p-value of 0.25 compared to p-value of 0.0195). On average, from Fig. 12, 10.57 bits/min and 9.91 bits/min were achieved using subject-specific and subject-independent thresholds respectively.

**Table 9 P-values representing significance of the EEG-ftCD system in terms of accuracy for the binary problems using subject-independent and subject-specific CDF thresholds.**

Threshold	Right MI vs Baseline	Left MI vs Baseline	Right MI vs Left MI
Subject-independent	0.0117	0.0098	0.3828
Subject-specific	0.002	0.0078	0.0195

**Table 10 P-values representing significance of the EEG-ftCD system in terms of bit rates for the binary problems using subject-independent and subject-specific CDF thresholds.**

Threshold	Right MI vs Baseline	Left MI vs Baseline	Right MI vs Left MI
Subject-independent	0.0078	0.0059	0.2500
Subject-specific	0.0020	0.0078	0.0195

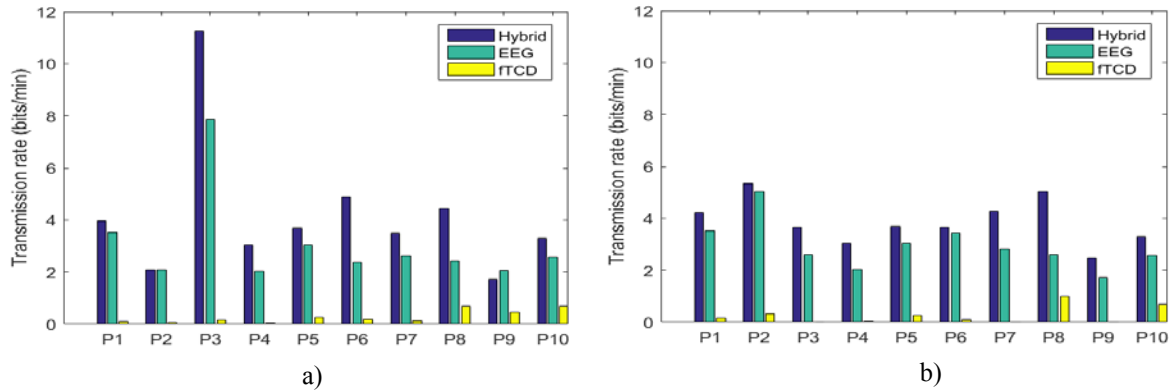


**Figure 9** Transmission rates for each participant (p) calculated using both EEG and fTCD, EEG only, and fTCD only for right arm MI vs baseline problem with a) subject-independent threshold b) subject-specific thresholds.

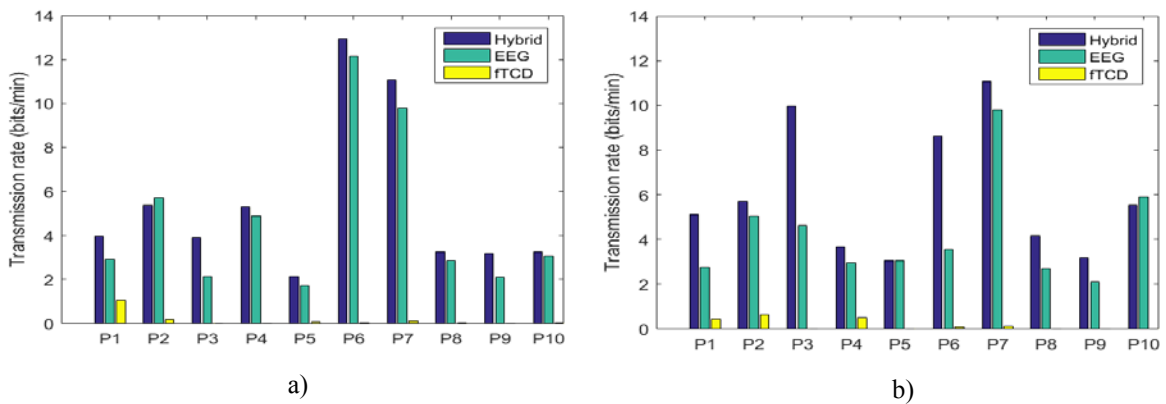


**Figure 10** Transmission rates for each participant (p) calculated using both EEG and fTCD, EEG only, and fTCD only for left arm MI vs baseline problem with a) subject-independent threshold b) subject-specific thresholds.

By Inspecting the selected significant features across all participants for the right arm MI versus left arm MI problem, it was found that, as seen in Fig. 13, across all electrodes, the EEG average power spectrum values at frequencies up to 2 Hz (delta frequency band) are the most common selected features across participants. Moreover, it was found that the common selected

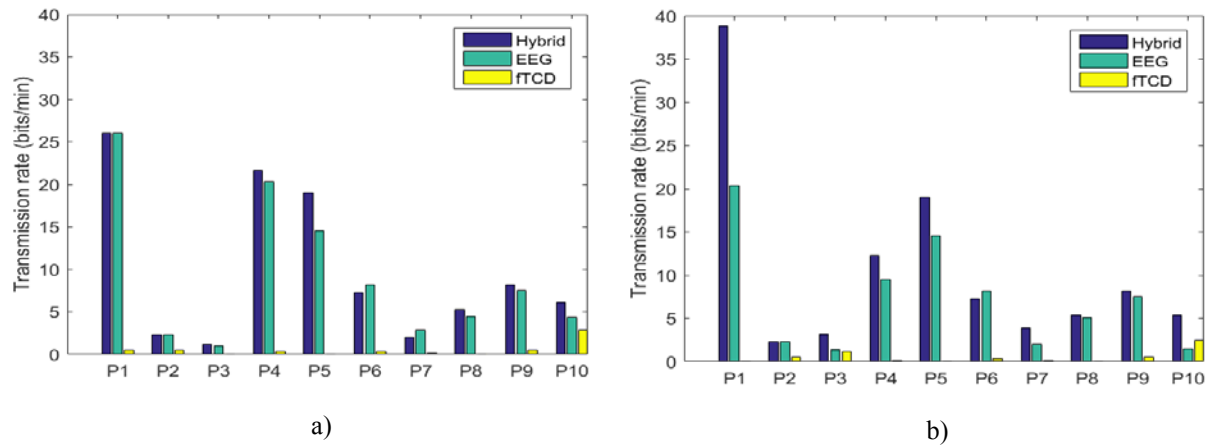


**Figure 11 Transmission rates for each participant (p) calculated using both EEG and fTCD, EEG only, and fTCD only for right arm MI vs left arm MI problem with a) subject-independent threshold b) subject-specific thresholds.**

features belonging to theta (5-8 Hz) and mu (8–13 Hz) bands are coming from electrodes Fp1, Fp2, F3, and F4 while the common features belonging to beta (16–28 Hz) band are associated with electrodes C1, C2, Cp3, Cp4, P5, and P6. As for the fTCD, the common significant features were found at frequency bands 550-600, 2000-2050 and 2150-2200 Hz for the right fTCD channel and at frequency band 2050-2100 Hz for the left fTCD channel.

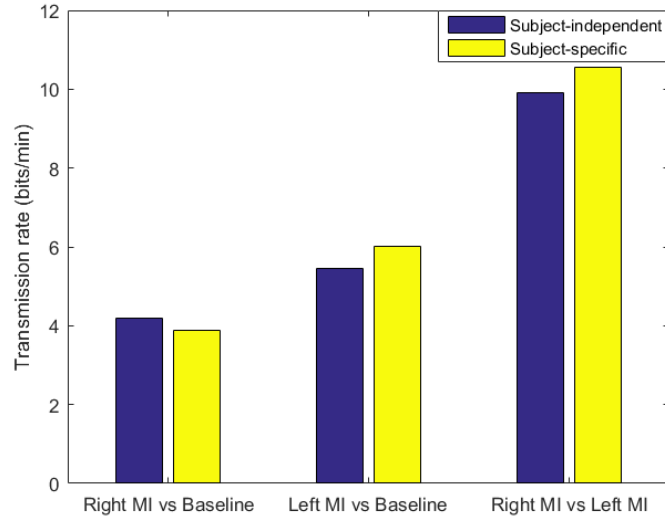


**Figure 12 Average transmission rates calculated using EEG-ftCD combination for the 3 binary problems with subject-independent and subject-specific thresholds.**

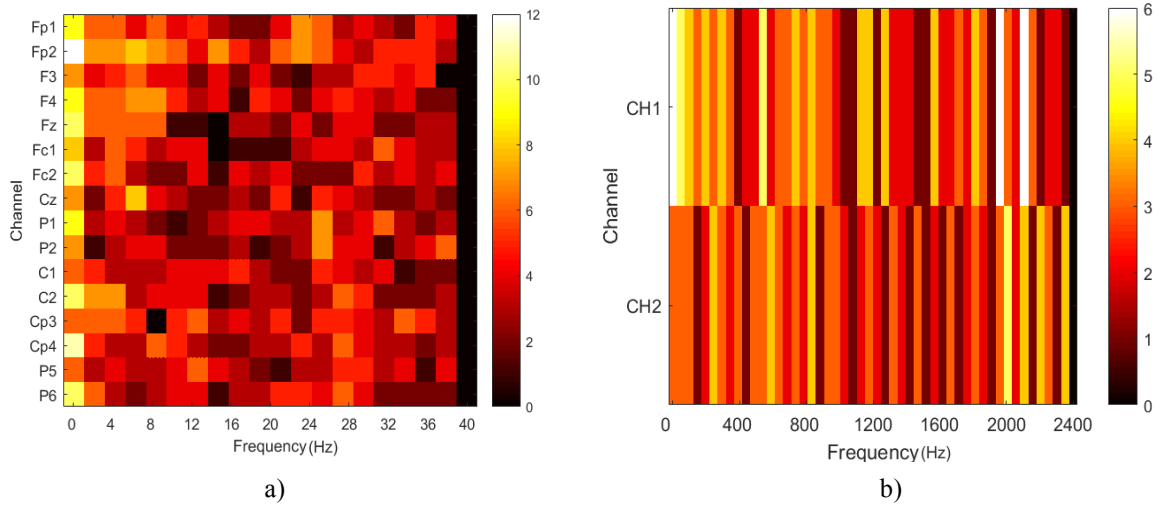


**Figure 13 2D histogram of the significant features during right arm versus left arm MI at each channel and each frequency window of width 2Hz for EEG and 50 Hz for ftCD. The heat maps demonstrate, across all participants, how many times any of the features within**

### 4.3 Discussion

Considering the performance measures reported for the 3 binary classification problems we studied, it is noted that subject-specific thresholds achieved higher performance measures compared to subject-independent threshold. However, the EEG-fTCD combination for right/left MI versus baseline problems was proven to be significant compared to EEG only using also subject-independent thresholds as seen in Tables 9, and 10. Thus, it is possible to use subject-independent thresholds for right/left MI versus baseline problems. In this case, the same analysis can be performed for all participants and no parameter selection (CDF threshold) needs to be performed for each participant. In contrast, the EEG-fTCD combination was shown to be significant for right arm MI versus left arm MI problem using only subject-specific thresholds. Thus, the CDF threshold has to be optimized for each participant separately. In terms of accuracy, right/left arm MI versus baseline problems achieved higher accuracy compared to right arm MI versus left arm MI. In contrast, it took approximately 7s on average for right/left MI versus baseline problems to achieve maximum accuracy while right arm MI versus left arm MI problem obtained maximum accuracy within approximately 3 s. Consequently, right arm MI versus left arm MI achieved the highest transmission rate of 10.57 bits/min.

Despite the high accuracies obtained in a previous study with the fTCD data only (see chapter 3.0), in this chapter, we obtained low accuracy with fTCD data only due to several reasons. It is well known that fTCD can differentiate imagery and analytical tasks since analytical tasks induce higher blood velocity in left MCAs while imagery tasks induce bilateral activation. However, in this chapter, both tasks are imagery tasks which makes the classification problem harder to solve. In addition, in the previous study, a 15-min baseline period was recorded before starting the tasks to stabilize the cerebral blood flow. Moreover, a resting period of 45 s was

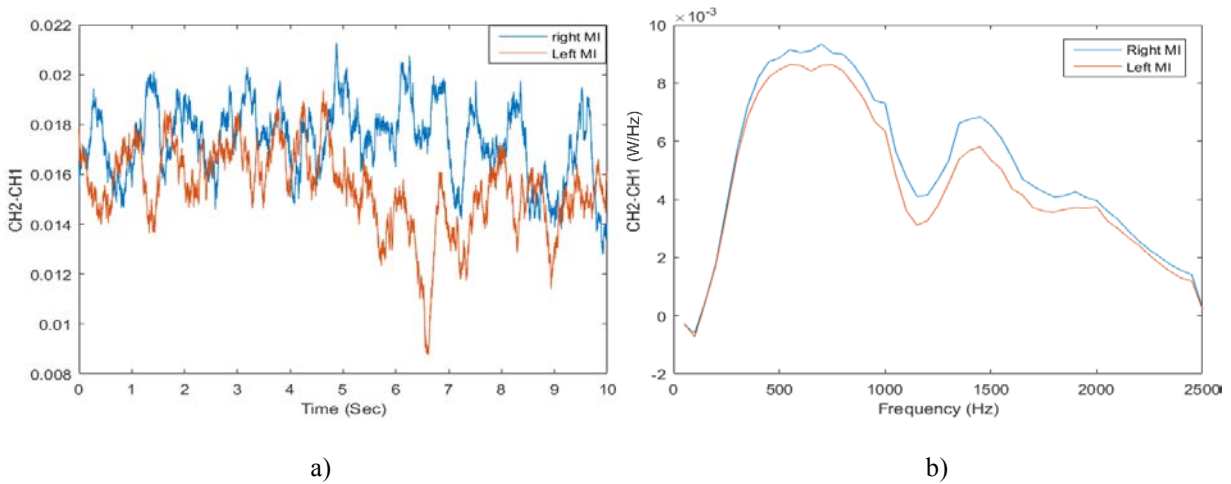


**Figure 14 Difference between left fTCD channel (channel 2) and right fTCD channel (channel 1) during right arm and left arm MI for a) fTCD normalized envelope signals in time domain b) power spectrum features in frequency domain.**

inserted between consecutive tasks. In this chapter, no baseline/rest periods were added to stabilize the cerebral blood flow since such periods will reduce the communication speed. In fact, the baseline was shown at random times since it was designed as a task that resembles the condition in which the BCI user does not intend to produce a command. Moreover, the baseline will be used later to normalize data across all participants such that all the data can be employed in one machine learning problem to infer user intent based on data from other users. This concept is known as transfer learning.

The study presented in [50] proved that the cerebral blood velocity during right arm movement increases significantly in the contralateral MCAs than the ipsilateral MCAs while left arm movement induces bilateral activation. One of the objectives behind this chapter was to confirm if the same phenomenon happens during motor imagery. To achieve this aim, we calculated the difference between left and right fTCD channels in both time and frequency domains during left and right motor imagery tasks. In the time domain, we calculated the difference between

average envelope signals of left and right fTCD channels during left and right motor imagery tasks as shown in Fig. 14. (a). Moreover, in the frequency domain, we calculated the difference between average values of the fTCD power spectrum features, described in section 4.1.4, of left and right fTCD channels during left and right motor imagery tasks as seen in Fig. 14 (b). It was found that the difference between the left and right channels is much higher for the right arm motor imagery with the left channel giving higher feature values while a smaller difference between the 2 channels was observed during left arm motor imagery as seen in Fig. 14 (a). This difference (CH2-CH1) during left arm motor imagery was much smaller than the difference during right arm motor imagery in the frequency ranges from 500 Hz to 750 Hz and from 1100Hz to 1800 Hz as shown in Fig. 14 (b). The reported results conform with the findings obtained using actual physical right arm movement [50] as the contralateral MCAs showed higher activation compared to the ipsilateral MCAs. In contrast, left arm motor imagery did not produce bilateral activation as expected. However, the difference in feature values between left and right fTCD channels during left arm motor imagery was smaller at specific frequency ranges.

In summary, as described above, through our time and frequency domain analyses to compare our work with [50], we showed that motor imagery induces differences in fTCD that could enable the separation among right arm MI vs left arm MI vs baseline.

Table 11 shows comparison between our method and the existing EEG-fNIRS BCIs that employ motor imagery tasks [127], [83], [59], [60], [78]. Comparisons were performed in terms of trial length and accuracy. In Table 11, we included the accuracies for the three binary problems achieved using subject-specific thresholds. The proposed hybrid BCI outperformed all methods in comparison in terms of trial length since it does not require baseline/rest periods before/after each task. Therefore, we claim that the proposed hybrid BCI is faster than EEG-fNIRS BCIs and it can

be used to design real-time BCI applications especially that, after the presentation of 10-s trial, the user intent can be identified within milliseconds. In terms of accuracy, we achieved similar or higher accuracies with shorter task duration. However, the system suggested by Buccino et al. [78] obtained 94.20% accuracy which is higher than the best accuracy achieved by our system, but that system is slower than ours since it requires 6 s baseline before starting each trial.

To improve the accuracy for right arm MI versus left arm MI since it is significantly lower than the accuracies obtained for right/left MI versus baseline problems, our future directions include using common spatial pattern (CSP) for EEG analysis instead of power spectrum since CSP was proved to be successful with motor imagery BCIs [60], [78], [127]. Moreover, given that the most efficient fTCD-based BCI in literature employed wavelet analysis, we plan to use wavelet decomposition for analyzing fTCD data. Both the number of decomposition levels and the mother wavelet to be used will be optimized to achieve the best possible accuracy.

Recently, ultrasound was considered as a potential brain stimulation modality. It was found that focused ultrasound energy transmitted through human brain can change EEG oscillatory dynamics. In particular, it was proved that the ultrasonic energy targeted to somatosensory cortex affect the phase of beta frequency band found in brain electrical activity [128]. However, in this study, we are interested in proving the significance of the hybrid system compared to EEG only in terms of accuracy and information transfer rate even if such improvement occurred due to ultrasound stimulation.

**Table 11 Comparison between the proposed hybrid system and the state of the art hybrid EEG-fNIRS BCIs employing motor imagery tasks.**

Method	BCI Type	Task Type	Accuracy	Trial length (s)	
				Task	Baseline/rest
[127] Fazli et al., 2012	EEG+fNIRS	Right/left hand gripping MI	83.20%	15	6/0
[83] Blokland et al., 2014	EEG+fNIRS	Finger & thumb tapping MI /Rest	79.00%	15	0/30±3
[59] Yin et al., 2015	EEG+fNIRS	Right hand clenching force/ speed MI	89.00%	10	0/21±1
[60] Koo et al. 2015	fTCD+NIRS	Right/left hand grasp MI	88.00%	15	0/60
[78] Buccino et al., 2016	EEG+fNIRS	Right/left arm raising & hand gripping MI	72.20%	6	6/0
[78] Buccino et al., 2016	EEG+fNIRS	Arm raising & hand gripping MI /Rest	94.20%	6	6/0
Proposed method	EEG+fTCD	Right MI/baseline	<b>88.33%</b>	10	NA
Proposed method	EEG+fTCD	Left MI/baseline	<b>89.48%</b>	10	NA
Proposed method	EEG+fTCD	Right /left MI	<b>82.38%</b>	10	NA

\*NA: Not applicable

## 4.4 Conclusion

In this chapter, we propose a novel motor imagery hybrid BCI that uses EEG as the primary sensing modality that measures brain electrical activity and the fTCD as the secondary sensing modality that measures cerebral blood flow velocity. To test the feasibility of binary BCIs, 3 binary selection problems were studied including right arm MI versus baseline, left arm MI versus baseline, and right arm MI versus left arm MI. It was shown that right/left arm MI versus baseline achieved higher accuracies compared to right arm MI versus left arm MI. Specifically, right arm MI versus baseline obtained 88.33% average accuracy and left arm MI versus baseline achieved 89.48% average accuracy while right arm MI vs left arm MI got average accuracy of 82.38%. However, right arm MI versus left arm MI obtained the highest bit rate of 10.57 bits/min compared to 4.17 bits/min, and 5.45 bits/min obtained by right arm MI versus baseline and left arm MI versus baseline. Based on these results, we believe that the proposed hybrid BCI is a promising tool for developing real-time BCI applications.

## 5.0 Towards Optimal Visual Presentation Design for Hybrid EEG-fTCD Brain-Computer Interfaces <sup>3</sup>

In the previous chapter, we have studied the feasibility of a motor imagery (MI) hybrid system that combines both EEG and fTCD as measurement modalities [98] using the visual presentation shown in Fig. 15 (a). A horizontal arrow pointing to the right represents right arm motor imagery while another horizontal arrow pointing to the left represents left arm motor imagery. In addition, a fixation cross was used to represent the baseline. During each trial, a vertical arrow points randomly to one of the 3 tasks that the user has to perform for duration of 10 s. It was found that, since both cognitive tasks are imagery tasks, there are slight differences between the recorded fTCD signals in response to right and left motor imagery tasks which indeed negatively affected the overall performance accuracy of the hybrid system [98].

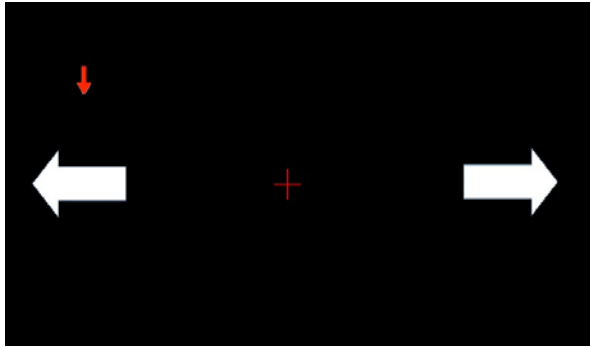
In this chapter, we introduce a visual presentation for the EEG-fTCD hybrid system in order to achieve higher overall performance accuracy compared to the hybrid system that employs MI presentation. To develop the system described in this chapter, instead of using 2 imagery tasks (right and left MI) to induce responses simultaneously in EEG and fTCD, we use two different but complementary paradigms. Specifically, we design mental rotation (imagery) and word generation (analytical) tasks through visual instructions since, it was proved that word generation (WG) induces higher blood flow velocity in left middle cerebral arteries (MCAs) while the mental rotation (MR) induces bilateral activation enabling different responses fTCD [46]. However, such

---

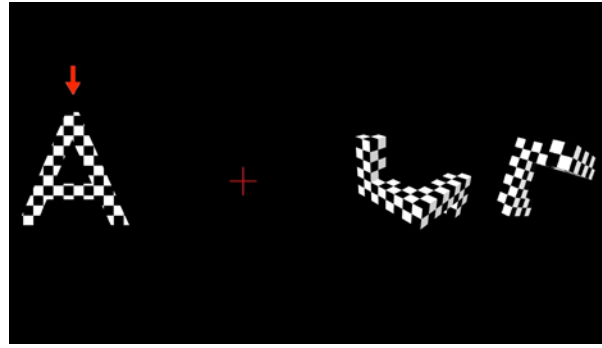
<sup>3</sup> Based on Aya Khalaf, Ervin Sejdic, Murat Akcakaya, “Towards Optimal Visual Presentation Design for Hybrid EEG-fTCD Brain Computer Interfaces,” *Journal of Neural Engineering*, vol. 15, no. 5, 2018. © [2018] IOP Publishing.

tasks cannot be distinguished using the EEG. Therefore, they cannot be directly employed in a hybrid EEG-fTCD system design. To build an efficient hybrid BCI in which cognitive tasks can be differentiated using both brain activity sensing modalities, we propose to combine the WG and MR tasks with an SSVEP paradigm such that WG and MR tasks will include a flickering checkerboard texture as shown in Fig. 15 (b) [129]. Consequently, this approach enables EEG to differentiate between MR and WG tasks because each task is designed to elicit a different SSVEP response. On the other hand, as also described above, our design enables fTCD to distinguish the differences between MR and WG tasks due to differences in cerebral blood flow velocity in different parts of the brain. The SSVEP paradigm is used in the proposed system with the expectation to achieve higher accuracies compared to the one that used MI visual presentation. This is because the SSVEP-BCIs are known to give higher performance measures compared to motor imagery BCIs [51]. Moreover, in terms of fTCD, it is expected that analytical versus imagery tasks will be differentiated with higher accuracy compared to imagery versus imagery tasks.

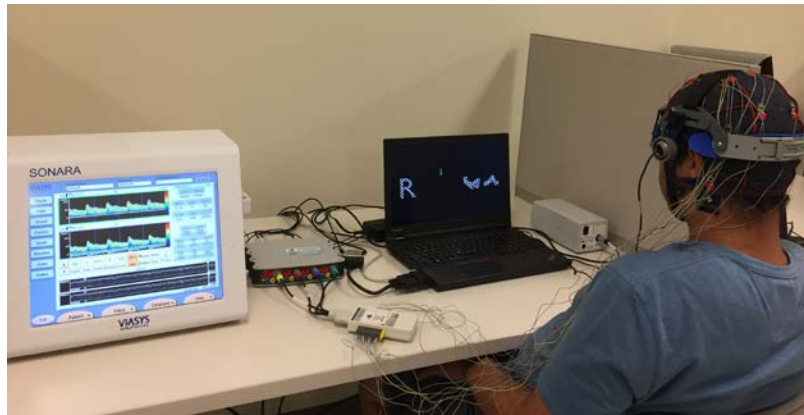
To investigate the feasibility of a 2-class hybrid BCI, 3 binary selection problems are formulated using the recordings corresponding to the flickering MR and WG task icons as well as the baseline. Specifically, a problem is formulated to distinguish flickering MR tasks against WG tasks while the other two problems aim at differentiating each cognitive task against the baseline. For the 3 selection problems, features derived from the power spectrum for both EEG and fTCD signals are calculated and mutual information and SVM are used for feature selection and classification respectively.



a)



b)



c)

**Figure 15 Stimulus presentation for our motor imagery EEG-fTCD BCI (a) and the proposed flickering MR/WG hybrid BCI (b) as well as the hybrid system setup captured during one of the data collection sessions (c).**

## **5.1 Materials and Methods**

### **5.1.1 Simultaneous Data Acquisition**

Sixteen electrodes were used to collect the EEG data. For the sake of fair comparison with the motor imagery EEG-fTCD hybrid BCI we designed in chapter 4.0 [98], in this chapter, the electrode locations are the same locations used for the MI hybrid system. The electrodes were positioned over frontal, central, and parietal lobes at positions Fp1, Fp2, F3, F4, Fz, Fc1, Fc2, Cz, P1, P2, C1, C2, Cp3, Cp4, P5, and P6 according to the 10-10 system. Although SSVEPs give the strongest response over occipital area, we anticipated getting responses similar to those obtained from the occipital area using the electrodes mentioned above. Especially, we have electrodes on locations P5, and P6 which are close to the occipital area given that EEG is known to have low spatial resolution. Fig. 15 (c) shows the hybrid system setup during one of the data collection sessions. EEG and fTCD data were collected using the same equipment mentioned in chapter 4.0. Please see section 4.1.1 in chapter 4.0 for detailed description of simultaneous data acquisition.

### **5.1.2 Visual Presentation Design**

The presented tasks have to be differentiated by both EEG and fTCD modalities in order to obtain a successful hybrid BCI system. Since fTCD is known to be successful in distinguishing analytical and imagination tasks due to differences in blood perfusion in both sides of the brain, word generation (WG) and mental rotation (MR) cognitive tasks were used for designing the hybrid system visual presentation. As these tasks are not expected to show differences in terms of EEG, they have to be modified such that the introduced modification induces the minimum

possible cognitive load since the participant will be already mentally busy with performing WG and MR tasks. Therefore, the icons/visual stimuli that instruct the users to perform WG and MR tasks were textured with a flickering checkerboard pattern as seen in Fig. 15 (b) to induce SSVEPs in EEG. For SSVEPs to be elicited, the flickering frequency of the stimuli has to be in the range from 7 to 60 Hz [130]. In addition, it was found that flickering frequencies higher than 20 Hz elicit SSVEPs with low amplitudes [130]. Based on this information, WG and MR stimuli flickered with frequencies of 7 and 17 Hz. In addition, the system included a third class which is a fixation cross that represents the baseline. For flickering WG, a randomly chosen letter flickers on the screen in order to instruct the user to silently generate words starting with that letter. The flickering MR task is represented on the screen by a pair of flickering 3D similar shapes rotated with different angles and the user is asked to mentally rotate the shapes to decide if they are identical or mirrored. These shapes were inspired from a database of 3D shapes constructed from cubes [107]. The tasks were designed using Blender computer graphics software. During each trial, a vertical arrow points randomly to one of the 3 tasks for duration of 10 s and the user has to focus on performing the mental task specified by that arrow. A total of 150 trials are presented per session.

In summary, using the proposed presentation scheme, flickering checkerboard-textured tasks will induce SSVEPs in the EEG corresponding to the flickering frequency of each task leading to different EEG responses while word generation and mental rotation will induce different cerebral blood flow in the two hemispheres of the brain, therefore, they will generate distinct fTCD responses. The baseline EEG and fTCD will be recorded when the participants are performing no mental activity (while looking at the red cross located at the center of the screen).

### **5.1.3 Participants**

All research procedures were approved by the local institutional review board (IRB) at the University of Pittsburgh under the University of Pittsburgh IRB number of PRO16080475. Eleven healthy participants (3 females, and 8 males) provided informed consent and participated in this study with ages ranging from 25 to 32 years. None of the participants had a history of migraines, concussions, strokes, heart murmurs, or other brain related injuries. Each participant attended one session that lasted for 25 minutes. The participants were seated in a comfortable chair approximately 100 cm away from the laptop screen on which the visual presentation was shown. Before starting the session, the visual presentation to be shown on the screen was described to the participants and they were instructed to keep focusing on the task indicated by the vertical arrow as long as the arrow did not change its position. Since the fTCD device displays how the fTCD signals change over time, the device was placed outside the participant's field of view so that the participant does not get distracted by the device display.

### **5.1.4 Feature Extraction and Fusion**

To ensure fair comparison between the performance measures due to the presentation paradigm suggested here and the one suggested in the previous chapter, we applied the same feature extraction techniques mentioned in the previous chapter. The process of feature extraction, averaging and concatenation is shown in Fig. 16. Please see section 4.1.4 in chapter 4 for detailed description of feature extraction and fusion.

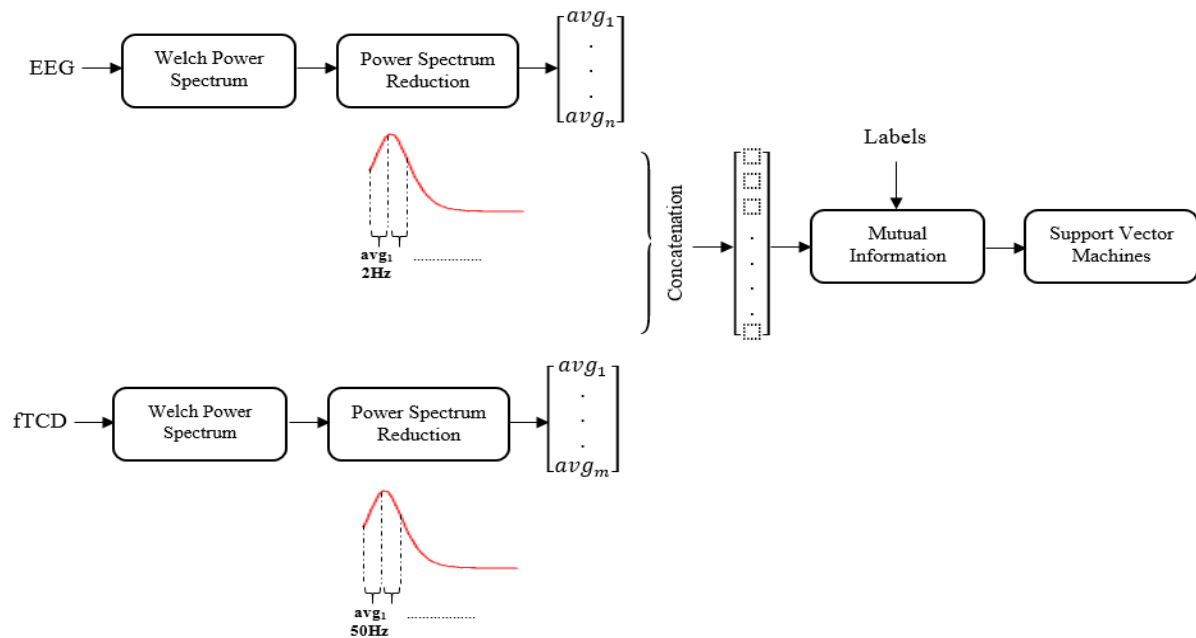


Figure 16 Diagram showing feature extraction, selection, and classification stages applied on EEG and fTCD signals.

### 5.1.5 Feature Selection

Mutual information was used to select the significant features out of concatenated EEG-fTCD feature vector that contains 420 features. Please see section 4.1.5 in chapter 4 for detailed description of using mutual information for feature selection.

### 5.1.6 Classification

Three binary selection problems were formulated and classified using linear SVM. They include MR versus baseline, WG versus baseline, and MR versus WG. For each participant, a subject-specific classifier was trained and tested using leave-one-out cross validation. Performance

measures including accuracy, sensitivity, specificity, and information transfer rate (ITR) given by (1) were computed to evaluate the hybrid system.

The objective behind calculating sensitivity and specificity is to test if the classifier recognizes both classes with similar accuracies or it is biased towards one of the classes. Specifically, sensitivity is the accuracy of detecting MR/WG stimulus while specificity reflects the accuracy of detecting the baseline.

### **5.1.7 Evaluation of the Effectiveness of the Hybrid System**

Wilcoxon signed rank test was used to assess the significance of the EEG-fTCD combination by statistically comparing the resultant performance measures with those obtained using EEG data only. Specifically, EEG-fTCD accuracy vector containing accuracies for the 11 participants as well as the corresponding EEG only accuracy vector for the same 11 participants represented the 2 populations to be test using Wilcoxon signed rank test.

### **5.1.8 Incremental Analysis**

An incremental window of 1 s initial width was used to calculate performance measures for each participant. The window width was increased by 1 s increment up to 10 s which is the trial length and the performance measures were evaluated at each increment. The objective behind using incremental window is to check if we can possibly decrease the trial length in future versions of this system. For each participant, the performance measures were computed versus time using 12 different CDF thresholds corresponding to probabilities ranging from 0.5 to 0.95 with 0.05 step as well as 0.98 and 0.99. Therefore, for every person, we obtained 12 different profiles for the

performance measures across time. Two groups of average performance measures over all participants were obtained by using subject-independent and subject-specific CDF thresholds.

To get the average performance measures using subject-independent threshold, for each participant, the maximum accuracy at each CDF threshold and the corresponding sensitivity, and specificity were obtained. Therefore, each participant has 12 sets of performance measures corresponding to the 12 CDF thresholds. For each CDF threshold, the average performance measures over all the 11 participants were obtained. The threshold at which the maximum average accuracy over all participant was achieved was selected as the general CDF threshold to be used with all participants. Considering subject-specific CDF thresholds, for each participant, all the accuracies at all CDF thresholds were considered and the maximum accuracy and the corresponding performance measures as well as the corresponding CDF threshold were used to represent that participant. Average of the maximum accuracy and the corresponding sensitivity, and specificity across all participants were obtained.

## **5.2 Results**

Tables 12-14 show the performance measures for MR versus baseline, WG versus baseline, and MR versus WG using subject-independent and subject-specific thresholds. Each of these tables shows the maximum accuracy obtained using EEG-fTCD combination for each participant. The time corresponding to the maximum possible EEG-fTCD accuracy that can be obtained by each participant was also reported. Accuracy was also calculated using EEG only and fTCD only at times yielding EEG-fTCD maximum accuracy to show the significance of the hybrid system.

Sensitivities and specificities corresponding to the accuracies reported in Tables 12-14 were represented using error bars in Fig. 17 and Fig. 18. Transmission rates were calculated for EEG, fTCD, and their combination using the accuracies and times listed in Tables 12-14. Fig. 19, 20, and 21 show these transmission rates obtained for each individual using subject-independent and subject-specific thresholds. Fig. 22 shows the comparison between the average bit rates for EEG-fTCD combination obtained using subject-independent and subject-specific thresholds. To show the significance of the EEG-fTCD combination compared to EEG only, a statistical significance test was performed using the EEG-fTCD and EEG accuracy vectors and the p-values for each binary selection problem were calculated and shown in Table 15. In Fig. 23, the distribution of the fTCD significant features obtained using subject-specific thresholds was shown. Finally, comparisons with hybrid BCIs from literature were performed and listed in Table 16.

### **5.2.1 MR/WG versus Baseline**

By analyzing MR versus baseline problem using subject-independent threshold, EEG-fTCD combination achieved 86.65% average accuracy in 7.82 *s* compared to 83.24% achieved using EEG only as seen in Table 12. Higher accuracies were obtained using EEG-fTCD combination with subject-specific thresholds (89.11% average accuracy) in approximately 7.73 *s*. The combination outperformed EEG only by an average accuracy difference of 4.06%. Since accuracy as a performance measure is not sufficient to decide if the classification model is biased towards one of the classes, both sensitivity and specificity were calculated. As seen in Fig.17 (a) and Fig. 18 (a), considering the error bars representing variability in sensitivities and specificities obtained using both threshold types, it can be noticed that the classification model is balanced since the average sensitivities and specificities show very similar values. Moreover, the variability

in sensitivities and specificities obtained using the hybrid system is lower compared to those obtained using EEG only.

**Table 12 Maximum accuracy (Acc) and the corresponding and time for each subject using hybrid system, EEG only, and fTCD only. These measures were obtained for MR vs baseline problem using subject-independent and subject-specific thresholds.**

Sub_ID	Subject-Independent Threshold				Subject-Specific Threshold			
	Time (s)	Acc_Hybrid	Acc_EEG	Acc_fTCD	Time (s)	Acc_Hybrid	Acc_EEG	Acc_fTCD
1	10	82.29%	82.29%	48.96%	6	89.58%	91.67%	50.00%
2	10	<b>86.46%</b>	84.38%	57.29%	8	<b>89.58%</b>	84.38%	57.29%
3	7	91.67%	91.67%	55.21%	10	<b>93.75%</b>	90.63%	56.25%
4	7	<b>79.17%</b>	69.79%	53.13%	9	<b>84.38%</b>	83.33%	52.08%
5	8	<b>85.42%</b>	82.29%	42.71%	9	<b>88.54%</b>	82.29%	46.88%
6	9	91.67%	91.67%	63.54%	9	<b>94.79%</b>	90.63%	60.42%
7	5	92.71%	92.71%	57.29%	4	<b>94.79%</b>	93.75%	39.58%
8	7	<b>89.58%</b>	86.46%	47.92%	7	<b>89.58%</b>	88.54%	47.92%
9	9	85.42%	87.50%	47.92%	9	<b>86.46%</b>	83.33%	50.00%
10	8	<b>80.21%</b>	58.33%	67.71%	8	<b>80.21%</b>	58.33%	67.71%
11	6	88.54%	88.54%	38.54%	6	88.54%	88.54%	38.54%
Mean	<b>7.82</b>	<b>86.65%</b>	83.24%	52.75%	<b>7.73</b>	<b>89.11%</b>	85.04%	51.52%

**Table 13 Maximum accuracy (Acc) and the corresponding and time for each subject using hybrid system, EEG only, and fTCD only. These measures were obtained for WG vs baseline problem using subject-independent and subject-specific thresholds.**

Sub_ID	Subject-Independent Threshold				Subject-Specific Threshold			
	Time (s)	Acc_Hybrid	Acc_EEG	Acc_fTCD	Time (s)	Acc_Hybrid	Acc_EEG	Acc_fTCD
1	8	87.63%	88.66%	43.30%	5	<b>89.69%</b>	82.47%	55.67%
2	4	59.79%	62.89%	44.33%	4	<b>67.01%</b>	63.92%	43.30%
3	8	<b>80.41%</b>	73.20%	53.61%	8	<b>80.41%</b>	73.20%	53.61%
4	3	<b>76.29%</b>	68.04%	42.27%	3	<b>76.29%</b>	68.04%	42.27%
5	10	<b>82.47%</b>	72.16%	59.79%	10	<b>86.60%</b>	68.04%	57.73%
6	7	<b>88.66%</b>	84.54%	68.04%	7	<b>89.69%</b>	84.54%	53.61%
7	4	<b>94.85%</b>	93.81%	47.42%	4	<b>95.88%</b>	94.85%	55.67%
8	5	<b>64.95%</b>	57.73%	58.76%	5	<b>68.04%</b>	63.92%	50.00%
9	4	78.35%	78.35%	54.64%	4	78.35%	78.35%	54.64%
10	7	<b>73.20%</b>	69.07%	54.64%	3	<b>75.26%</b>	68.04%	62.89%
11	4	68.04%	78.35%	41.24%	9	<b>82.47%</b>	80.41%	52.58%
Mean	<b>5.82</b>	<b>77.69%</b>	75.16%	51.64%	<b>5.64</b>	<b>80.88%</b>	75.07%	52.91%

The EEG-fTCD combination scored higher accuracies than EEG only for 5 out of 11 participants using subject-independent threshold and for 9 out of 11 participants using subject-specific thresholds. Performance measures obtained using fTCD only were nonsignificant. However, fTCD boosted the overall performance when it was combined with the EEG. As seen in Table 15, in case of subject-specific thresholds, the combination was proved to be significant compared to EEG only with a p-value of 0.0156 while it was shown to be nonsignificant when using subject-independent threshold. In terms of transmission rates, as shown in Fig. 19, for most of the participants, the combination achieved higher bit rates compared to EEG only especially

using subject-specific thresholds. On average, as seen in Fig. 22, average bit rate of 3.66 bits/min was achieved using subject-independent threshold while subject-specific thresholds obtained 4.39 bits/min.

**Table 14 Maximum accuracy (Acc) and the corresponding and time for each subject using hybrid system, EEG only, and fTCD only. These measures were obtained for MR vs WG problem using subject-independent and subject-specific thresholds.**

Sub_ID	Subject-Independent Threshold			Subject-Specific Threshold				
	Time (s)	Acc_Hybrid	Acc_EEG	Acc_fTCD	Time (s)	Acc_Hybrid	Acc_EEG	Acc_fTCD
1	7	<b>98.10%</b>	96.19%	49.52%	7	<b>99.05%</b>	95.24%	51.43%
2	5	<b>82.86%</b>	75.24%	52.38%	10	<b>85.71%</b>	82.86%	52.38%
3	6	<b>92.38%</b>	86.67%	53.33%	9	<b>97.14%</b>	96.19%	73.33%
4	3	<b>87.62%</b>	77.14%	49.52%	9	<b>89.52%</b>	84.76%	54.29%
5	9	80.00%	80.00%	64.76%	8	86.67%	89.52%	63.81%
6	8	88.57%	88.57%	64.76%	8	<b>93.33%</b>	90.48%	68.57%
7	5	<b>94.29%</b>	93.33%	58.10%	9	<b>96.19%</b>	94.29%	57.14%
8	7	<b>92.38%</b>	88.57%	45.71%	7	<b>93.33%</b>	88.57%	43.81%
9	4	87.62%	87.62%	43.81%	4	<b>88.57%</b>	87.62%	47.62%
10	8	<b>89.52%</b>	86.67%	63.81%	8	91.43%	91.43%	60.95%
11	8	<b>94.29%</b>	89.52%	54.29%	7	<b>95.24%</b>	91.43%	52.38%
Mean	<b>6.36</b>	<b>89.78%</b>	86.32%	54.55%	<b>7.82</b>	<b>92.38%</b>	90.22%	56.88%

**Table 15 P-values representing significance of the EEG-ftCD system for the binary problems using subject-independent and subject-specific CDF thresholds.**

Threshold	MR vs Baseline	WG vs Baseline	MR vs WG
Subject-independent	0.0938	0.1900	0.0078
Subject-specific	0.0156	0.0020	0.0195

Considering WG versus baseline problem, as seen in Table 13, average accuracy of 77.69% was obtained in 5.82 s using subject-independent threshold while EEG only obtained 75.16% with an average accuracy difference of 2.53%. In contrast, higher average accuracy difference of 5.81% between the EEG-ftCD combination and EEG only was achieved using subject-specific thresholds as shown in Table 13. Specifically, the combination achieved 80.88% average accuracy in 5.64 s while EEG only obtained 75.07%. As seen in Fig. 17 (b) and Fig. 18 (b), error bars show that both classes (WG and baseline) can be recognized almost with the same percentage.

The EEG-ftCD combination scored higher accuracies for 7 out of 11 participants using subject-independent threshold and for 10 out of 11 participants using subject-specific thresholds. The hybrid system was shown to provide a significant accuracy improvement using subject-specific thresholds compared to EEG only with a p-value of 0.012 as shown in Table 15 while that improvement was not significant in case of subject-independent threshold. The combination achieved higher bit rates than EEG only for most of the participants as seen in Fig. 20. Considering the average bit rates shown in Fig. 22, subject-specific thresholds achieved higher bit rate (3.92 bits/min) compared to subject-independent threshold (3.12 bits/min).

## 5.2.2 MR versus WG

Unexpectedly, MR versus WG obtained higher performance measures compared to MR/WG versus baseline. Specifically, as shown in Table 14, in 6.36 *s*, we obtained 89.78% average accuracy with an average accuracy difference of 3.46% compared to EEG only which obtained 86.32%. Higher performance measures were obtained using subject-specific thresholds as seen in Table 14 as EEG-ftCD combination obtained 92.38% average accuracy in 7.82 *s* while EEG only got 90.22%. Similar to MR/WG versus baseline problems, average sensitivity and specificity have similar values reflecting the ability of the classification model to identify both classes almost equally as seen in Fig. 17 (c) and Fig. 18 (c). Moreover, Fig. 17 and Fig. 18 show that WG versus MR has the lowest variance in sensitivity and specificity compared to the other problems.

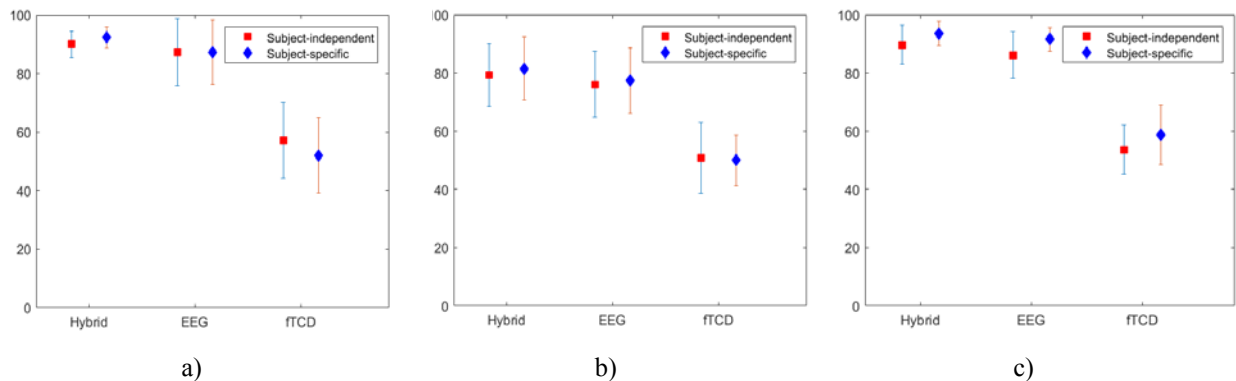


**Figure 17 Sensitivities (mean and standard deviation) calculated using both EEG and ftCD, EEG only, and ftCD only for flickering MR vs baseline problem (a), flickering WG vs baseline problem (b), and flickering MR vs flickering WG (c).**

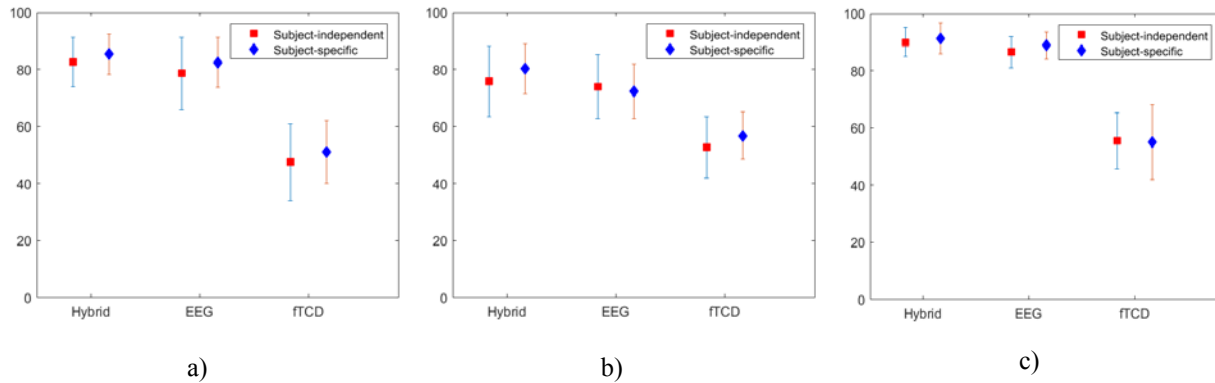


**Figure 18 Specificities (mean and standard deviation) calculated using both EEG and fTCD, EEG only, and fTCD only for flickering MR vs baseline problem (a), flickering WG vs baseline problem (b), and flickering MR vs flickering WG (c).**

The hybrid combination achieved higher accuracies for 8 out of 11 participants using subject-independent threshold and for 9 out of 11 participants using subject-specific thresholds. As seen in Table 15, the hybrid combination was shown to be significant with p-value of 0.0078 and 0.0195 for subject-specific and subject-independent thresholds respectively. Bit rates obtained using the EEG-fTCD combination were higher for most of the participants compared to those obtained using EEG as shown in Fig. 21. Average bit rates of 5.60 bits/min and 5.07 bits/min were obtained using subject-independent and subject-specific thresholds respectively as shown in Fig. 22.

Through investigation of the common EEG and fTCD significant features across all participants for the classification problem that yielded the highest accuracy (WG versus MR), as expected, the top common EEG power spectrum features were found approximately around the 1<sup>st</sup>, 2<sup>nd</sup>, and 3<sup>rd</sup> harmonics of 7 Hz and around 1<sup>st</sup> and 2<sup>nd</sup> harmonics of 17 Hz. Considering the fTCD features, the most common selected significant power spectrum features were found at frequency bands of 0-50, 1200-1250, and 1350-1400 for the left fTCD channel and at frequency

bands of 0-100, 300-350, and 1950-2000 Hz for the right ftCD channel as seen in Fig. 23. We observed also that there is no specific feature that is common across all the participants, which indicates that the selected features are participant specific.

In this chapter, we initially focused on the feasibility analysis of the EEG-ftCD hybrid system to understand the most efficient visual presentation in terms of accuracy and bit rate compared to the study we did before [28]. However, since the online performance is of great interests to the BCI community, we included an online analysis for the system performance. In particular, each participant attended one session (a total of 150 trials). The first 100 trials were used for training of the system and calculating the optimal CDF subject-specific threshold while the last 50 trials were used for testing the online performance. Accuracy of 90.91% was obtained for MR versus WG compared to 92.38% obtained using offline analysis. In addition, 85.63% was achieved for MR versus baseline compared to 89.11% achieved offline. Finally, WG versus baseline yielded accuracy of 79.77% while the offline analysis obtained 80.88% accuracy.

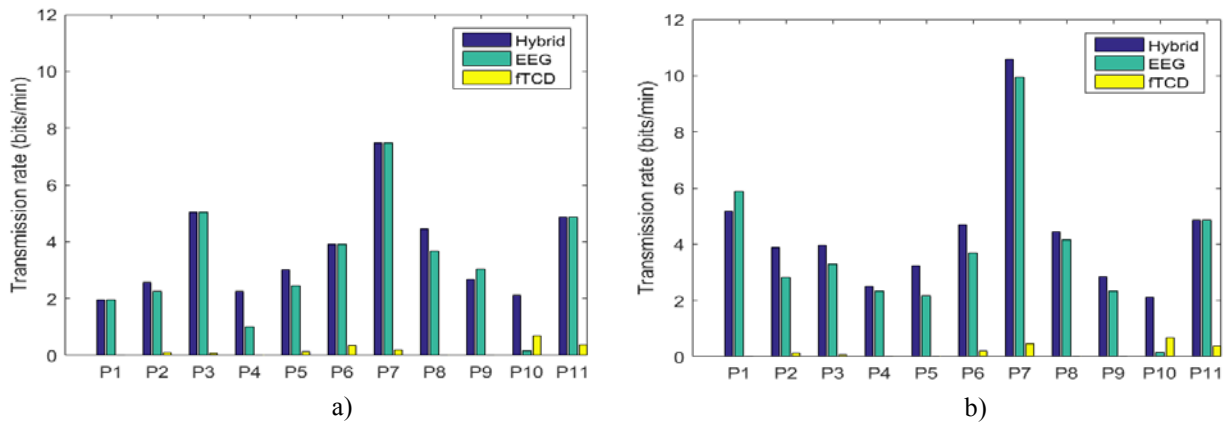


**Figure 19** Transmission rates for each participant (p) calculated using both EEG and ftCD, EEG only, and ftCD only for for flickering MR vs baseline problem with subject-independent threshold (a) and subject-specific thresholds (b).

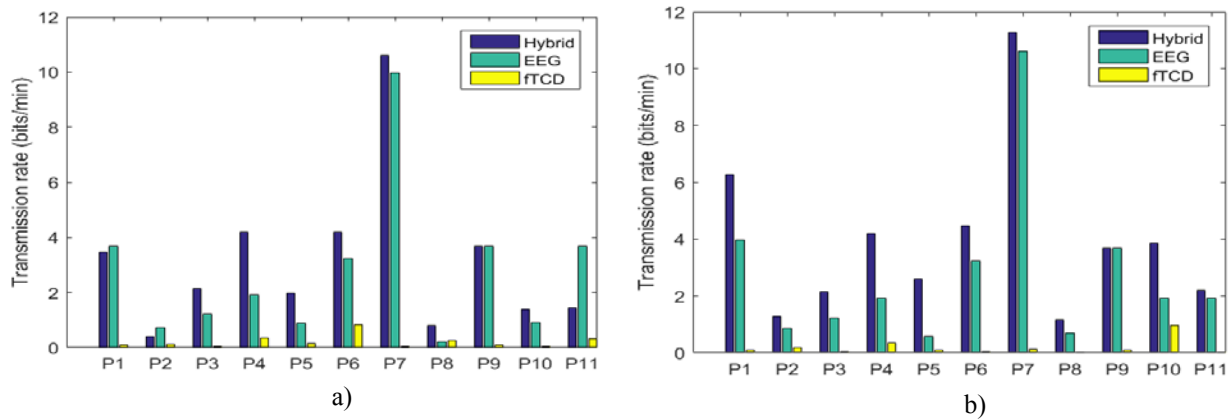


**Figure 20** Transmission rates for each participant (p) calculated using both EEG and fTCD, EEG only, and fTCD only for flickering WG vs baseline problem with subject-independent threshold (a) and subject-specific thresholds (b).

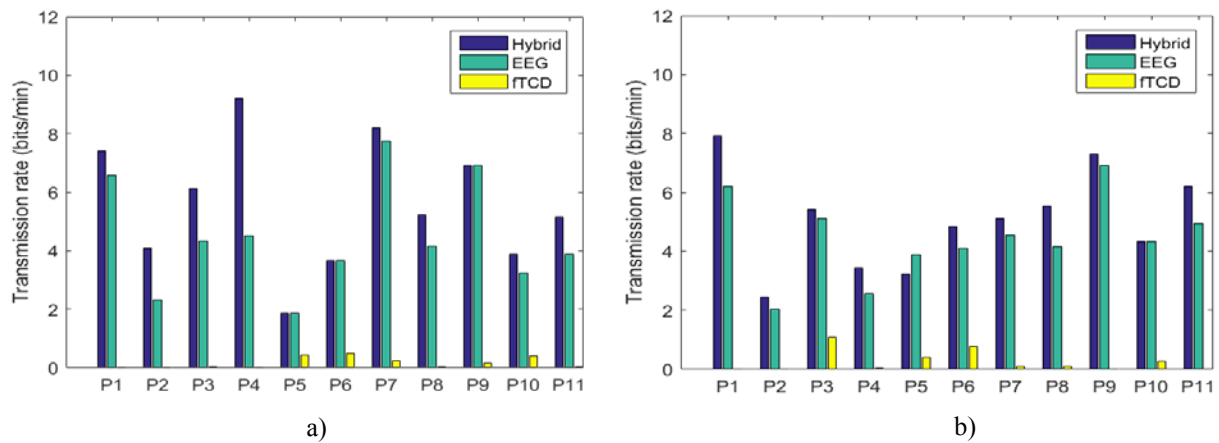


**Figure 21** Transmission rates for each participant (p) calculated using both EEG and fTCD, EEG only, and fTCD only for flickering MR vs flickering WG problem with subject-independent threshold (a) and subject-specific thresholds (b).

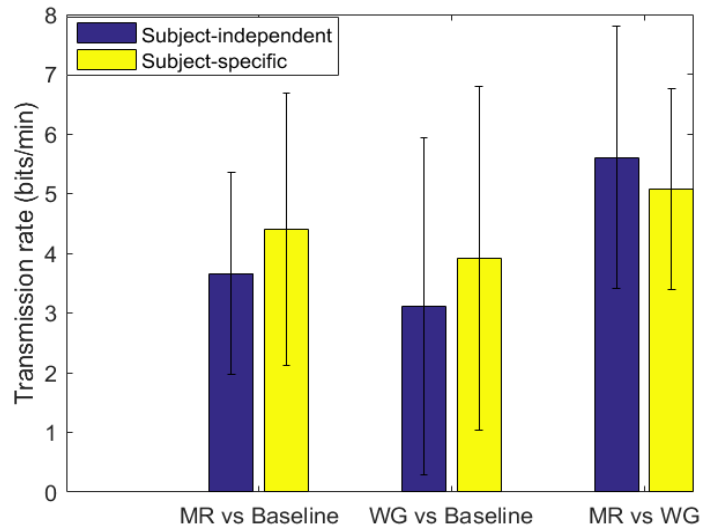


**Figure 22** Average transmission rates calculated using EEG-ftCD combination for the 3 binary problems with subject-independent and subject-specific thresholds.

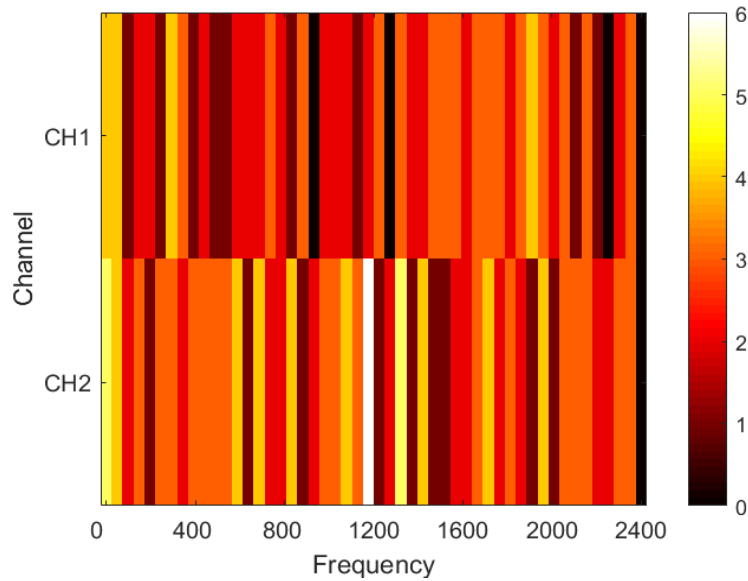


**Figure 23** 2D histogram of the ftCD significant features appearing at right ftCD channel (CH1) and left ftCD channel (CH2) among the 11 individuals participated in the study.

### 5.3 Discussion

In general, subject-specific thresholds achieved higher accuracies compared to subject-independent thresholds for the 3 binary selection problems. For MR/WG versus baseline, the average accuracy difference between the hybrid combination and EEG was higher for subject-specific thresholds (4.06% / 5.81%) compared to the difference achieved by subject-independent threshold (3.46% / 2.53%). In contrast, EEG-ftCD combination achieved higher average accuracy difference using subject-independent threshold compared to subject-specific thresholds for MR versus WG binary selection problem. Specifically, subject-independent threshold obtained 3.46% average accuracy difference compared to subject-specific thresholds which obtained 2.16% average difference. The combination was proved to be significant compared to EEG only for MR/WG versus baseline using only subject-specific thresholds while it was found to be significant using both subject-independent and subject-specific thresholds for MR versus WG. Therefore, it is possible to use subject-independent threshold for MR versus WG. One advantage of employing such threshold is that no parameter selection (CDF threshold) needs to be performed for each participant separately. In contrast, for MR/WG versus baseline, the CDF threshold parameter has to be optimized for each participant.

Compared to a previous ftCD study [49] in which we obtained approximately 80% average accuracy, in this study, we obtained lower ftCD accuracies for several reasons. Here, for each participant, we find the maximum accuracy for the hybrid system. Such accuracy is more controlled by the EEG which is the primary input modality, thus, the corresponding ftCD accuracy is not necessarily the maximum ftCD accuracy. In addition, in this study, the tasks were flickering to elicit SSVEPs. Such flickering reduced the concentration of each subject on the mental task to be performed. In addition, in the previous study, a baseline period of 15 min was included before

stating the tasks to stabilize the cerebral blood flow. In addition, a 45-s resting period was included between consecutive tasks. Here, no baseline/ resting periods were inserted before/after each task to stabilize the cerebral blood flow. In fact, the baseline was shown at random times since the objective behind having the baseline was not to stabilize the blood flow after each task, but it was considered as a separate task that resembles the case when the BCI user does not intend to issue a specific command. Moreover, the baseline is planned to be used in the future to normalize data across participants so that data from all participants can be used in one machine learning problem.

In Table 16, we compared the proposed hybrid BCI with the state of the art EEG-fNIRS hybrid BCIs [127], [83], [79], [64] [59], [60], [78], [80] as well as the motor imagery based EEG-ftCD hybrid system we introduced before [98]. Accuracies of the 3 binary selection problems were listed in Table 16. Comparisons were performed in terms of trial length and accuracy. Compared to the motor imagery EEG-ftCD hybrid system we developed [98] in the previous chapter, an average accuracy increase of 10% was achieved as seen in Table 16. However, the proposed system is slower since it requires an average time of 6.36 *s* to achieve 92.38 % accuracy while the MI one requires only 3.5 *s* on average to reach 82.38% accuracy. In line with the differences in speed, the flickering MR/WG presentation achieved maximum bit rate of 5.6 bits/min while the MI visual presentation obtained 10.57 bits/min. On the other hand, right/left arm MI versus baseline achieved higher accuracies compared to right arm versus left arm MI. In contrast, it was found that MR/WG versus baseline problems achieved lower accuracies compared to MR versus WG problem. Since the location of the baseline cross is very close to the flickering MR and WG tasks as seen in Fig. 15 (b), flickering affected the subject attention even during focusing at the baseline cross and caused reduction in accuracy for MR/WG versus baseline problems.

**Table 16 Comparison between the proposed hybrid system and the state of the art hybrid BCIs.**

Method	BCI Type	Accuracy	Trial length (s)	
			Task	Baseline/rest
[127] Fazli et al., 2012	EEG+fNIRS	83.20%	15	6/0
[83] Blokland et al., 2014	EEG+fNIRS	79.00%	15	0/30±3
[79] Khan et al., 2014	EEG+fNIRS	83.60%	10	0/5
[64] Putze et al., 2014	EEG+fNIRS	94.70%	12.5±2.5	0/20 ±5
[59] Yin et al., 2015	EEG+fNIRS	89.00%	10	0/21±1
[60] Koo et al. 2015	fTCD+NIRS	88.00%	15	0/60
[78] Buccino et al., 2016	EEG+fNIRS	72.20%	6	6/0
[78] Buccino et al., 2016	EEG+fNIRS	94.20%	6	6/0
[80] Shin et al., 2017	EEG+fNIRS	88.20%	10	0/16±1
[98] Khalaf et al.,2019 (right/baseline)	EEG+fTCD	88.33%	10	NA
[98] Khalaf et al.,2019 left/baseline)	EEG+fTCD	89.48%	10	NA
[98] Khalaf et al.,2019 (right/left)	EEG+fTCD	82.38%	10	NA
Proposed method (MR/baseline)	EEG+fTCD	89.11%	10	NA
Proposed method (WG/baseline)	EEG+fTCD	80.88%	10	NA
Proposed method (MR/WG)	EEG+fTCD	92.38%	10	NA

\*NA: Not applicable

Compared to the other BCIs listed in Table 16, in terms of trial length, the proposed system has the shortest trial length of 10 s. In addition, the proposed system is faster since it requires no baseline/rest period before/after each task. In terms of accuracy, the proposed hybrid BCI outperforms most of the methods in comparison. However, the systems introduced by Putze et al. [64] and Buccino et al. [78] achieved higher accuracy compared to ours as they obtained 94.70% and 94.20% average accuracy respectively. Yet, these system are slower than our system since the one introduced by Putze et al. [64] requires at least 12.5 s as a task period and 20 s as a resting

period while the one presented by Buccino et al. [78] requires a baseline period of 6 s before starting each task.

The proposed BCI can be used to improve the quality of life for disabled individuals by increasing the contact with the society though using the BCI for communication with the external environment. Also, the level of independency for such individuals can be increased when using such BCI to control assistive devices such as prosthetic limbs and wheel chairs [118]. Moreover, the BCI can be used for environmental control purposes. Specifically, individuals using the BCI in homes can control lights, temperature, TVs, etc. [119]. In addition, the BCI can be used as a neurorehabilitation tool that helps individuals with disabilities to restore lost neuromuscular functions [121].

Compared to the existing work on hybrid BCI that combines EEG with other modalities, we have made important progress towards making such systems real-world-worthy in terms of speed and accuracy, see Table 16 for comparison with other hybrid systems. However, the system still has limitations such that the temporal resolution of fTCD is lower than EEG resulting in longer trial lengths and decreasing the speed of the system. We will focus on this limitation in our future work. For example, such mismatch between the temporal resolution of these modalities can be minimized by introducing advanced analysis techniques for fTCD data to improve the obtained accuracy within the minimum possible task period. In particular, Wavelet analysis can be employed for fTCD analysis since it was used in a recent study [49] to prove that fTCD is a viable candidate for real-time BCIs and it achieved accuracies of approximately 80% and 60% for binary and 3-class BCIs within 3 and 5 s respectively. On the other hand, based on the feedback from the BCI users, a bigger screen will be used to run the experiment to reduce the flickering

effect on the subject's attention while focusing on the baseline cross. Moreover, the 25-min session will be divided into 2 sessions to reduce the user fatigue due to the flickering.

## **5.4 Conclusion**

We propose a novel hybrid BCI that uses EEG to measure brain electrical activity and fTCD to measure cerebral blood velocity. Flickering MR and flickering WG tasks as well as a baseline cross were used in designing the visual presentation. Three binary selection problems were formulated including MR versus baseline, WG versus baseline, MR versus WG. Each problem was analyzed using subject-independent and subject-specific thresholds. It was found that subject-specific thresholds achieve higher performance measures for MR versus baseline, WG versus baseline and WG versus MR problems as it obtained average accuracy of 89.11%, 80.88%, and 92.38% respectively compared to 86.65%, 77.69%, and 89.78% achieved by subject-independent threshold. Bit rates of 4.39, 3.92, 5.60 bits/min were obtained for MR versus baseline, WG versus baseline, MR versus WG respectively. Such promising results show that the proposed hybrid BCI is a feasible candidate for real-time BCI applications.

## 6.0 Common Spatial Pattern and Wavelet Decomposition for Motor Imagery EEG- fTCD Brain-Computer Interface <sup>4</sup>

In this chapter, we extend our previous work, detailed in chapter 4.0, on MI multimodal hybrid BCI that utilizes EEG and fTCD modalities. In particular, we extend our feature extraction approach by considering features computed based on multiscale analysis and common spatial pattern (CSP) instead of using power spectrum based features we employed previously [98] in chapter 4.0. It was shown that multiscale analysis captures the changes in fTCD in a timely fashion making it a modality suitable for real-time BCIs [49]. Moreover, CSP is commonly used for EEG-based MI BCIs due to its computational simplicity and ability to find the spatial patterns characteristic to different motor imagery tasks [131]. Using the classical feature extraction approaches described above, we mainly contribute to multi-modal fusion of EEG and fTCD features. In particular, we propose a probabilistic fusion of EEG and fTCD evidences instead of simple concatenation of EEG and fTCD feature vectors. Through such a probabilistic fusion, the contributions of each modality towards the correct decision can be optimized. More specifically, EEG data was analyzed using common spatial pattern while fTCD data was analyzed using wavelet decomposition. Significant fTCD features were selected using Wilcoxon test. To fuse EEG and fTCD features of each trial, we developed a Bayesian framework and combined EEG and fTCD evidences under 3 different assumptions. Intent inference was made based on maximum

---

<sup>4</sup> Based on Aya Khalaf, Ervin Sejdic, Murat Akcakaya, “Common Spatial Pattern and Wavelet Decomposition for Motor Imagery EEG-fTCD Brain-Computer Interface,” *Journal of Neuroscience Methods*, vol. 320, pp. 98-106, 2019 © [2019] Elsevier.

likelihood estimation. The proposed analysis technique was used to evaluate 3 binary selection problems including right MI vs baseline, left MI versus baseline, and right MI versus left MI.

## **6.1 Materials and Methods**

This section includes detailed explanation of preprocessing, feature extraction and selection methods as well as feature fusion and classification.

### **6.1.1 Preprocessing**

EEG data was filtered using g. USBamp, a bio-signal amplifier, with 8th order bandpass filter of corner frequencies 2 and 62 Hz as well as 4th order notch filter with corner frequencies 58 and 62 Hz. Since fTCD data are sampled at 44.1 kHz while the fTCD signals are approximately bandlimited to 4.4 kHz, the data were downsampled by a factor of 5 after a low-pass filter with 4.4 kHz corner frequency was applied to avoid aliasing.

### **6.1.2 Common Spatial Pattern (CSP)**

In this study, common spatial pattern (CSP) was used to extract features from EEG data. CSP is one of the most efficient feature extraction techniques for MI-based EEG BCIs since characteristic EEG spatial patterns obtained using CSP make MI different tasks significantly differentiable [132]. Basic CSP algorithm is used to analyze multi-channel data based on observations from two classes. In particular, it designs a linear transform that maps the

observations from two classes to a new space where they are more discriminative in terms of variance [133]. More specifically, the aim of CSP is to learn the optimal spatial filters which maximize the variance of one class while minimizing the variance of the other class simultaneously [82]. Finding such spatial filters can be performed through solving the following optimization problem:

$$\begin{aligned} \max_w \quad & \text{tr } W^T \Sigma_c W \\ \text{s. t.} \quad & W^T (\Sigma_{(+)} + \Sigma_{(-)}) W = 1 \end{aligned} \quad (4)$$

where  $\Sigma_c$  is the average trial covariance matrix for class  $c \in \{+, -\}$  and  $w^T \Sigma_c w$  is the variance in direction  $w$ .

Assume each trial is represented by matrix  $R^{N \times T}$  where  $N$  is the number of EEG channels and  $T$  is the number of samples. Sample covariance matrix for each trial  $m$  is estimated as follows:

$$S_m = \frac{RR^T}{\text{tr}(RR^T)} \quad (5)$$

The average trial covariance matrix can be calculated as follows:

$$\Sigma_c = \frac{1}{M} \sum_{m=1}^M S_m \quad (6)$$

where  $M$  is the number of trials belonging to class  $c$ . The optimization problem in (4) can be solved by simultaneous diagonalization of the covariance matrices  $\Sigma_c$ . This can be written as follows:

$$\begin{aligned} W^T \Sigma_{(+)} W &= \Lambda_{(+)} \\ W^T \Sigma_{(-)} W &= \Lambda_{(-)} \\ \text{s. t.} \quad \Lambda_{(+)} + \Lambda_{(-)} &= I \end{aligned} \quad (7)$$

where  $\Lambda_c$  is a diagonal matrix with the eigenvalues  $\lambda_j^c$ ,  $j = 1, 2, \dots, N$  on diagonal. Solving (7) is equivalent to solving the generalized eigenvalue problem given by:

$$\Sigma_{(+)} w_j = \lambda \Sigma_{(-)} w_j \quad (8)$$

where  $w_j$  is the  $j^{th}$  generalized eigenvector and  $\lambda = \frac{\lambda_j^{(+)}}{\lambda_j^{(-)}}$ . (7) is satisfied for transformation matrix

$W = [w_1, w_2, \dots, w_N]$  and  $\lambda_j^c$  given by:

$$\lambda_j^c = w_j^T \Sigma_c w_j \quad (9)$$

where  $\lambda_j^c$  are the diagonal elements of  $\Lambda_c$ . Given that  $\Lambda_{(+)} + \Lambda_{(-)} = I$ , consequently, it can be concluded that  $\lambda_j^{(+)} + \lambda_j^{(-)} = 1$ .

For instance, when value of  $\lambda_j^{(+)}$  is large, it reflects higher variance in the positive class when filtering it using the spatial filter  $w_j$ . In the meantime, a high value of  $\lambda_j^{(+)}$  yields low value of  $\lambda_j^{(-)}$ . Therefore, the same spatial filter  $w_j$  will result in low variance when used for filtering the negative class. For classification purposes, eigenvectors from both ends of matrix  $W$  are considered to maximize the differentiation between the 2 classes. In previous studies [134]–[136], it was found that 3 eigenvectors from both ends of  $W$  are sufficient to perform the classification task. However, since such choice of the number of eigenvectors used for EEG spatial filtering can vary depending on many parameters such as the number and the location of the electrodes used in each study, in this chapter, we solved the 3 binary classification problems at all possible numbers of eigenvectors. In particular, we spatially filtered EEG data using 1, 2, 3, ..., and 8 eigenvectors from both ends of  $W$ . To extract EEG features, we calculated the log variance of each spatially filtered signal.

### 6.1.3 Wavelet Decomposition

fTCD data were analyzed using 5-level wavelet decomposition that utilized Daubachies 4 mother wavelet. Such analysis was performed since it was used before with fTCD data and it yielded the most efficient fTCD-based BCI in literature [137] as explained in chapter 3.0. To reduce the dimensionality of the fTCD feature vector, 4 features were computed for each wavelet band instead of using all wavelet coefficients as features. The 4 features included mean, variance, skewness, and kurtosis. Feature vector corresponding to each trial included 24 features for each channel and 48 features in total.

### 6.1.4 Feature Reduction and Classification

The Wilcoxon signed rank test [113] was used to select the significant features from fTCD feature vectors. p-values of 0.001, 0.005, 0.01, and 0.05 were used. As for EEG, the feature vector of each trial contained  $2f$  features obtained by projecting the trial data using  $f = 1, 2, 3, \dots$ , and 8 eigenvectors from both ends of  $W$ . To assess the performance of single-modal BCIs (EEG only and fTCD only BCIs), selected features from each modality were classified solely using the SVM classifier. In particular, the performance of fTCD only system was evaluated at p-values of 0.001, 0.005, 0.01, and 0.05. Also, the performance of EEG only system was evaluated using  $2f$  (2, 4, 6,  $\dots$ , and 16) CSP features. The best set of performance measures for each modality were reported in the results section below.

To evaluate the performance of the hybrid system, the EEG feature vector of each trial containing  $f$  features was projected into one scalar SVM score (EEG evidence). Moreover, the selected features from the fTCD feature vector were also projected into one scalar SVM score

(fTCD evidence). In particular, the EEG and fTCD feature vectors corresponding to training trials were used to learn 2 SVM classifiers separately. The 2 classifiers were used to obtain 2 SVM scalar scores representing projected EEG and fTCD feature vectors of each trial under test. EEG and fTCD SVM scores were evaluated at p-values of 0.001, 0.005, 0.01, and 0.05 and  $2f$  (2, 4, 6, ..., and 16) CSP features. The best set of performance measures were reported in the results section.

### 6.1.5 Bayesian Fusion and Decision Making

We designed a Bayesian framework to fuse EEG and fTCD evidences (SVM scores described in Section 6.1.4) under 3 different assumptions including joint EEG-fTCD distributions (A1), independent EEG and fTCD distributions (A2) as well as weighted independent EEG and fTCD distributions (A3). For each binary selection problem, EEG and fTCD evidences corresponding to trials of that problem were partitioned randomly into training and testing sets using 10-fold cross validation scheme. Assume  $N$  is the number of trials presented to a certain BCI user. Given a set of EEG and fTCD evidences  $Y = \{y_1, \dots, y_N\}$  where  $y_n = \{e_n, f_n\}$ ,  $e_n$  and  $f_n$  are EEG and fTCD evidences respectively. As shown in Fig. 24, for a test trial  $k$ , inference of the unknown user intent  $x_k$  will be achieved through state estimation using the EEG and fTCD evidences jointly. Here, since we solve the binary classification problem through state estimation, we assume that  $x_k$  takes only two distinct values for each binary classification problem. Fig. 24 (b) assumes independence between the EEG and fTCD evidences conditioned on the unknown state  $x_k$  while Fig. 24 (a) does not make this assumption. Inference of the user intent without restricting EEG and fTCD evidences to any assumption can be found through solving the following optimization problem.

$$\widehat{x}_k = \arg \max_{x_k} p(x_k | Y = y_k) \quad (10)$$

In (10),  $p(x_k | Y)$  is the posterior distribution of the state  $x_k$  conditioned on the observations  $Y$ . From Bayes rule and noting that the conditional distribution of  $Y$ ,  $P(Y)$  does not depend on the state variable  $x_k$ , (10) is equivalent to:

$$\widehat{x}_k = \arg \max_{x_k} p(Y = y_k | x_k) p(x_k) \quad (11)$$

where  $p(Y | x_k)$  is the state conditional distribution of the evidences  $Y$  and  $p(x_k)$  is the prior distribution defined over the values of state. Since the number of trials belonging to each class is randomized in our study, we assume that  $p(x_k)$  is uniformly distributed. Accordingly, we rewrite (11) as:

$$\widehat{x}_k = \arg \max_{x_k} p(Y = y_k | x_k) \quad (12)$$

The distribution  $p(Y | x_k)$  is computed from the training data. In particular,  $p(Y | x_k = c_1)$  and  $p(Y | x_k = c_2)$  are state conditional distributions of the evidences  $Y$  belonging to class  $c_1$  ( $x_k = c_1$ ) and class  $c_2$  ( $x_k = c_2$ ) respectively. The conditional distribution representing each class were estimated using kernel density estimation with a Gaussian kernel. Silverman's rule of thumb [138] was used to calculate the kernel bandwidth. User intent at trial  $k$  is inferred by solving eqn. (12) at the evidences  $Y = y_k$ . In this study, the distribution  $p(Y | x_k)$  was evaluated under 3 different assumptions.

#### 6.1.5.1 Assumption 1: Joint Distribution

Since the  $k^{\text{th}}$  evidences are  $y_k = \{e_k, f_k\}$ , (11) can be written as:

$$\widehat{x}_k = \arg \max_{x_k} p(e = e_k, f = f_k | x_k) \quad (13)$$

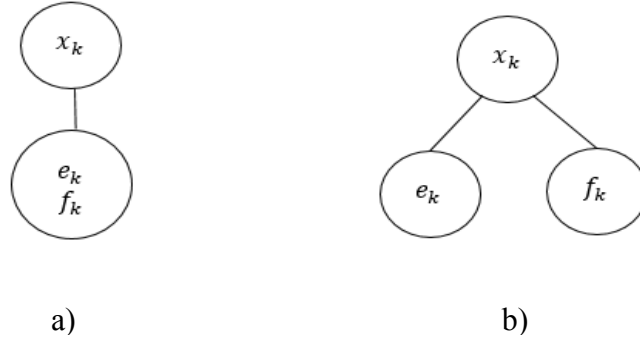


**Figure 24 Probabilistic graphical model illustrating the state and measurement relationships assuming EEG and fTCD evidences are jointly distributed (a) and independent (b).**

where  $p(e, f|x_k)$  is the state conditional joint distribution of  $e$  and  $f$ . This is represented graphically in Fig. 24 (a). To compute  $p(e, f|x_k)$  for  $N-10$  training trials, the joint distribution of the EEG and fTCD scores was assumed to follow a multivariate Gaussian distribution. Kernel density estimation with a Gaussian kernel was employed to compute the distributions  $p(e, f|x_k), k = 1, 2$ . For evidences under test  $y_k = \{e_k, f_k\}$ ,  $e_k$  and  $f_k$  are plugged in (13) and the user intent  $x_k$  that yields the maximum likelihood is selected.

### 6.1.5.2 Assumption 2: Independent Distributions

In order to compute  $p(Y|x_k)$ , we will assume that conditioned on the latent state, the EEG and fTCD evidences are independent from each other as seen in Fig. 24 (b), then accordingly also considering the uniform prior over the states, we rewrite (13) as:

$$\widehat{x}_k = \arg \max_{x_k} p(e = e_k|x_k)p(f = f_k|x_k) \quad (14)$$

where  $p(e|x_k)$  and  $p(f|x_k)$  are the distributions of EEG and fTCD evidences conditioned on the state  $x_k$  respectively.

SVM EEG and fTCD scores of the N-10 training trials are used separately to compute 2 distributions  $[p(e|x_k)$  and  $p(f|x_k)]$  using kernel density estimation with Gaussian kernel. For evidences under test  $y_k = \{e_k, f_k\}$ ,  $e_k$  and  $f_k$  are plugged in (14) and the user intent  $x_k$  that yields the maximum likelihood is selected.

### 6.1.5.3 Assumption 3: Weighted Independent Distributions

Since the contribution of EEG and fTCD evidences towards making a correct decision might be unequal, we suggest weighting the distributions  $p(e|x_k)$  and  $p(f|x_k)$ , and thus rewriting (13) as:

$$\widehat{x}_k = \arg \max_{x_k} p(e = e_k | x_k)^\alpha p(f = f_k | x_k)^{1-\alpha} \quad (15)$$

where  $\alpha$  and  $1 - \alpha$  represent the optimum contribution of the EEG and fTCD modalities, respectively.  $\alpha$  ranges from 0 to 1.  $p(e|x_k)$  and  $p(f|x_k)$  were computed as mentioned in section 6.1.5.2. To simplify (15), natural logarithm was employed. In particular, since natural logarithm is a monotonically increasing function, maximization of the right-hand side of (15) is equivalent to maximization of the natural logarithm of this right-hand side. Therefore, (15) is equivalent to the convex combination of the log likelihoods given by (16).

$$\widehat{x}_k = \arg \max_{x_k} [\alpha \ln p(e = e_k | x_k) + (1 - \alpha) \ln p(f = f_k | x_k)] \quad (16)$$

The training of our hybrid system requires the identification of the optimum task period for each individual. For assumption A3, unlike A1 and A2, we performed 2D optimization since we seek optimizing both the task period and the  $\alpha$  value. Such optimization is achieved through grid search over a task period ranging from 1 to 10 seconds with a step of 1 second and over  $\alpha$  values ranging from 0 to 1 with a step of 0.01.

### 6.1.6 EEG-fTCD Analysis Across Time

To evaluate the performance of the hybrid system compared to the single-modal systems (EEG only and fTCD only systems), accuracy and information transfer rate (ITR) were calculated across 10-s periods (trial length) for the 3 systems.

Both EEG and fTCD data were analyzed across time at time points 1, 2, ..., 10 s. An incremental window with initial length of 1 second and increments of 1 second was used to analyze EEG data while a moving window of 1 second length was used to analyze fTCD data. The moving window was chosen for fTCD analysis based on an fTCD-based BCI study in which performance of both incremental and moving windows was compared (see chapter 3.0) [49]. In particular, CSP EEG features and fTCD features at each time window were computed and the performance measures of EEG only and fTCD only systems were calculated at each time point. To compute the performance measures of the hybrid system, EEG and fTCD evidences were combined using the Bayesian framework described in section 6.1.5 for joint user intent inference. In particular, at each time point (1, 2, ..., 10 s), for every trial, EEG and fTCD evidences corresponding to the EEG and fTCD feature vectors at that time point were calculated. Then, these evidences were combined under the 3 different assumptions described in section 6.1.5 and the corresponding performance measures were calculated.

## 6.2 Results

To assess the significance of combining EEG and fTCD for hybrid BCI design, for each participant, maximum possible accuracies obtained using EEG only and fTCD only were

compared with maximum accuracy achieved using the hybrid system under the 3 different assumptions (A1, A2, and A3). These accuracies are reported for each individual separately in Tables 17, 18, and 19 for right MI vs baseline, left MI versus baseline, and right MI vs left MI problems respectively. Moreover, to evaluate the balance of the prediction model, error bars of sensitivities and specificities corresponding to the accuracies reported in Tables 17, 18, and 19 were plotted in Fig. 25. In addition, to statistically evaluate the significance of the hybrid combination compared to EEG only, p-values, reported in Table 20 representing the statistical difference between the accuracy vector of A1, A2, and A3 and accuracy vector of EEG only were calculated using the Wilcoxon signed rank test. However, statistical comparison in terms of maximum accuracy only is not sufficient to judge the effectiveness of the BCI since accuracy does not reflect the speed of the BCI in contrast to ITR which is a measure that combines both speed and accuracy. Therefore, we compared the hybrid system under A1, A2, and A3 with EEG only and fTCD only in terms of ITRs that are computed at 1 second trial length. We chose 1 second as the trial length because such a selection will enable us to use this system in online applications. Moreover, average ITRs of A1, A2, A3, EEG only, and fTCD only were plotted across the 10-s trial length and presented in Fig. 26.

For right MI versus baseline, Table 17 shows that EEG only achieved average accuracy of 90.52% and fTCD only achieved average accuracy of 64.48% while the hybrid system obtained 91.35%, 92.29%, and 93.85% under A1, A2, and A3 assumptions respectively. Statistical comparisons showed that accuracy vectors of A2 and A3 are significant compared to accuracy vector obtained using EEG only with p-values of 0.002 and 0.0009 while in terms of ITRs, A2 and A3 were found to be significant with p-values 0.0098 and 0.001. For both accuracy and ITR, A1 was found to be insignificant as seen in Tables 20 and 21. As for left MI versus baseline, A1, A2,

**Table 17 Maximum accuracy achieved for each subject using hybrid combinations (A1, A2, A3), EEG only, and fTCD only for right MI vs baseline problem.**

Sub_ID	EEG	fTCD	A1	A2	A3
1	92.71%	64.58%	93.75%	93.75%	94.79%
2	90.63%	60.42%	89.58%	90.63%	92.71%
3	81.25%	63.54%	82.29%	82.29%	84.38%
4	87.50%	68.75%	89.58%	93.75%	95.83%
5	96.88%	61.46%	95.83%	97.92%	97.92%
6	86.46%	68.75%	88.54%	89.58%	92.71%
7	93.75%	59.38%	94.79%	94.79%	96.88%
8	95.83%	60.42%	95.83%	96.88%	96.88%
9	87.50%	65.63%	89.58%	89.58%	91.67%
10	92.71%	71.88%	93.75%	93.75%	94.79%
<b>Mean</b>	90.52%	64.48%	91.35%	92.29%	93.85%

**Table 18 Maximum accuracy achieved for each subject using hybrid combinations (A1, A2, A3), EEG only, and fTCD only for left MI vs baseline problem.**

Sub_ID	EEG	fTCD	A1	A2	A3
1	92.78%	58.76%	92.78%	91.75%	93.81%
2	93.81%	68.04%	92.78%	92.78%	93.81%
3	91.75%	62.89%	92.78%	94.85%	96.91%
4	87.63%	59.79%	86.60%	83.51%	89.69%
5	92.78%	61.86%	91.75%	89.69%	92.78%
6	87.63%	62.89%	83.51%	93.81%	94.85%
7	93.81%	54.64%	93.81%	94.85%	94.85%
8	95.88%	59.79%	89.69%	90.72%	90.72%
9	91.75%	61.86%	91.75%	93.81%	94.85%
10	93.81%	61.86%	91.75%	93.81%	94.85%
<b>Mean</b>	92.16%	61.24%	90.72%	91.96%	93.71%

and A3 obtained average accuracies of 90.72%, 91.96%, and 93.71% respectively while EEG only and fTCD only obtained 92.16% and 61.24% respectively. A1, A2, and A3 were statically compared with accuracy vector due to EEG only. As seen in Table 20, in terms of accuracy, A3 was shown to be statistical ly insignificant compared to EEG only with a p-value of 0.0625 while A1 and A2 were insignificant compared to EEG only with p-values greater than 0.5. In contrast, in terms of ITR, A3 was found to be significant compared to EEG only with a p-value of 0.001 as shown in Table 21. fTCD average sensitivities and specificities of right MI versus baseline and left MI versus baseline problems were found to be imbalanced as shown in Fig. 25 (a) and Fig. 25 (b).

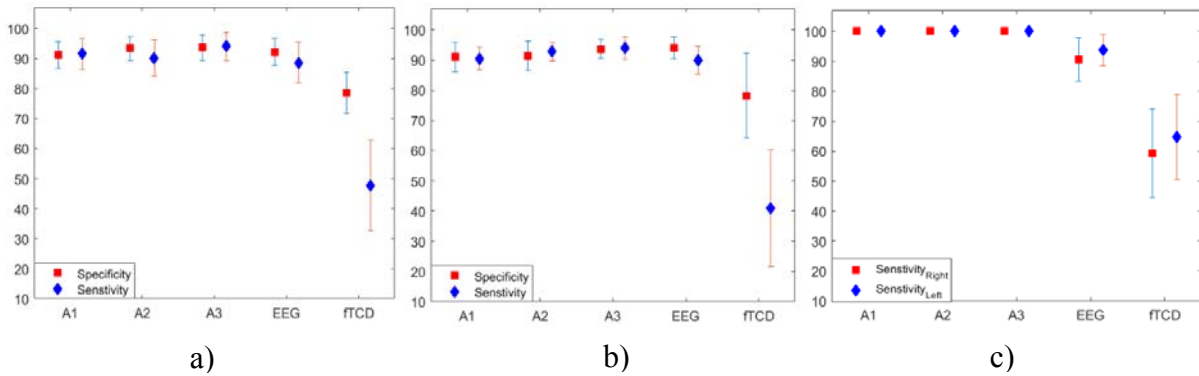


**Figure 25 Sensitivities and specificities (mean and standard deviation) calculated using A1, A2, A3, EEG only, and fTCD only for right MI vs baseline problem (a), left MI vs baseline problem (b), and right MI vs left MI (c).**

**Table 19 Maximum accuracy achieved for each subject using hybrid combinations (A1, A2, A3), EEG only, and fTCD only for right MI vs left MI problem.**

Sub_ID	EEG	fTCD	A1	A2	A3
1	93.33%	63.81%	100.00%	100.00%	100.00%
2	88.57%	58.10%	100.00%	100.00%	100.00%
3	92.38%	70.48%	100.00%	100.00%	100.00%
4	91.43%	62.86%	100.00%	100.00%	100.00%
5	93.33%	59.05%	100.00%	100.00%	100.00%
6	90.48%	61.90%	100.00%	100.00%	100.00%
7	96.19%	60.95%	100.00%	100.00%	100.00%
8	100.00%	62.86%	100.00%	100.00%	100.00%
9	95.24%	57.14%	100.00%	100.00%	100.00%
10	80.95%	62.86%	100.00%	100.00%	100.00%
Mean	92.19%	62.00%	100.00%	100.00%	100.00%

**Table 20 P-values showing accuracy significance of A1, A2, and A3 compared to EEG only for the 3 binary problems.**

Comparison	Right MI vs Baseline	Left MI vs Baseline	Right MI vs Left MI
A1/EEG	0.1055	0.9922	0.0020
A2/EEG	0.0020	0.5332	0.0020
A3/EEG	0.0009	0.0625	0.0020

**Table 21 P-values showing ITR significance of A1, A2, and A3 compared to EEG only for the 3 binary problems.**

Comparison	Right MI vs Baseline	Left MI vs Baseline	Right MI vs Left MI
A1/EEG	0.0938	0.2461	0.0059
A2/EEG	0.0098	0.1250	0.0029
A3/EEG	0.0010	0.0010	0.0010

As seen in Table 19, the 3 hybrid combinations (A1, A2, and A3) achieved 100% accuracy for right MI versus left MI problem compared to 92.19% and 62.00% obtained using EEG only and fTCD only respectively. In line with these results, p-values of Tables 20 and 21 showed that A1, A2, and A3 are statistically significant compared to EEG only in terms of both accuracy and ITR. Moreover, balanced sensitivities and specificities were achieved using the hybrid system under the 3 assumptions A1, A2, and A3 as well as EEG only and fTCD only as shown in Fig. 25 (c).

The results above show that, on average, the accuracy differences between the hybrid system and EEG only are relatively low, however, in terms of ITRs, as seen in Fig. 26, average ITRs of A1, A2, and A3 are clearly higher than those achieved using EEG only and fTCD only for the 3 binary selection problems although, according to Table 21, A3 is the only assumption that shows statistical significance for the 3 selection problems when compared to EEG only. In particular, for right MI versus left MI, A1, A2, and A3 achieved maximum ITRs of 39.09, 39.46, and 40.83 bits/min respectively compared to 12.08 and 12.11 bits/min achieved by EEG only and fTCD only. As for right MI versus baseline, A1, A2, A3, EEG only, and fTCD only achieved maximum ITRs of 22.71, 19.89, 22.27, 12.08, and 12.11 bits/min respectively. Finally, left MI versus baseline problem yielded maximum ITRs of 10.68 and 17.43 bits/min using EEG only and fTCD only while A1, A2, and A3 obtained 23.87, 24.29, and 26.55 bits/min. In summary, A3 is

the only fusion assumption that provided significantly higher performance compared to EEG only system for all the binary selection problems.

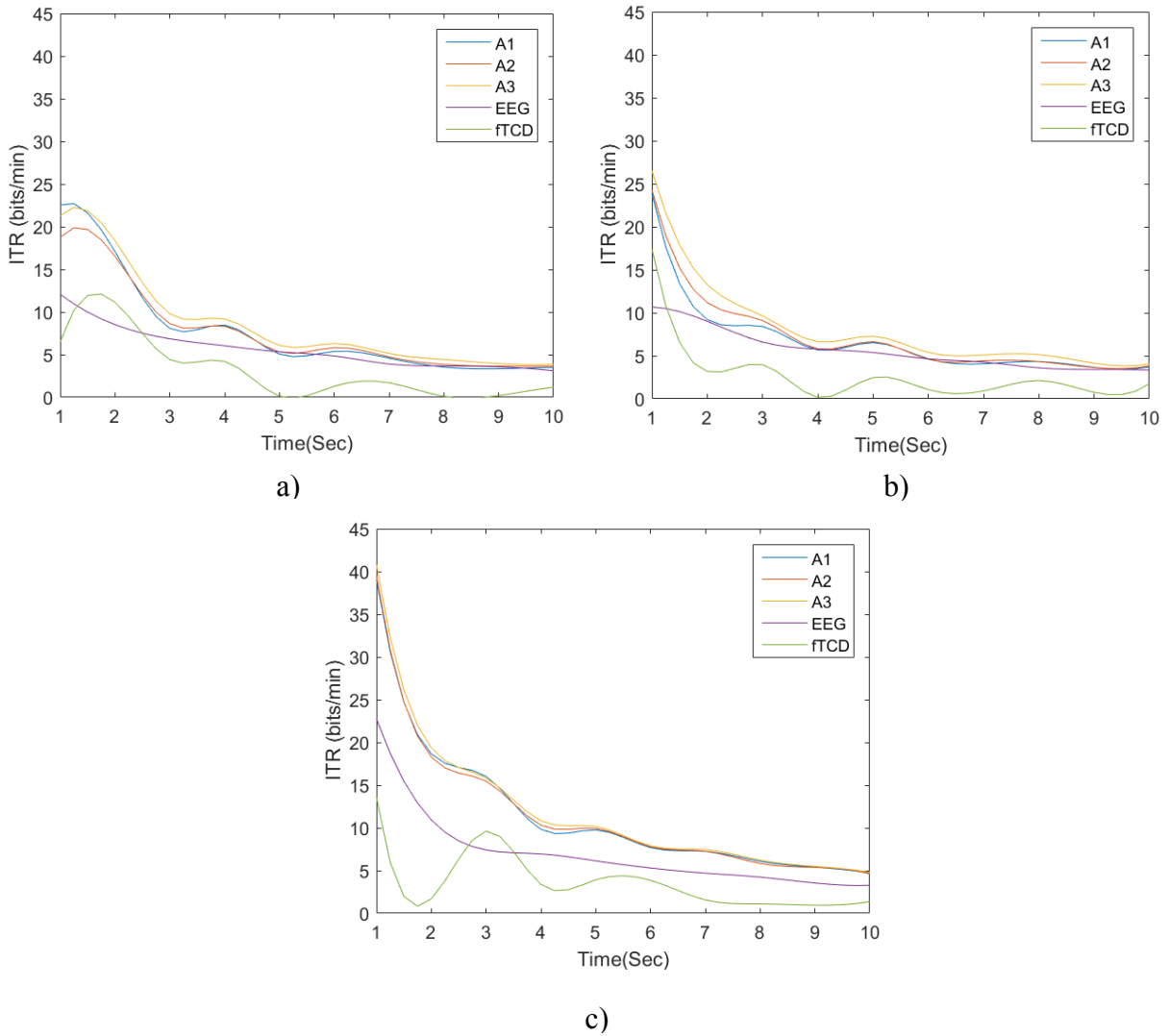


**Figure 26 Average ITRs calculated using EEG only, fTCD only, and the 3 hybrid combinations (A1, A2, and A3) for right MI vs baseline problem (a), left MI vs baseline problem (b), and right MI vs left MI problem (c).**

### 6.3 Discussion

In general, it can be noted that the proposed analysis approach including feature extraction and probabilistic fusion stages did not significantly boost the performance of the hybrid system compared to EEG only in terms of accuracy. However, the proposed analysis resulted in average ITR that is 5 times the average ITR obtained previously for right/left MI versus baseline [98]. Moreover, the average ITR of the right MI versus left MI problem is 4 times the ITR achieved before for the same problem [98].

Considering the performance of the hybrid system for the 3 binary selection problems, it was found that right MI versus left MI problem obtained significantly higher average accuracy and average ITR compared to left/right MI versus baseline problems under assumptions A1, A2, and A3. Specifically, 100% accuracy was obtained under the 3 different assumptions compared to 93.85% and 93.71% achieved by right MI versus baseline and left MI versus baseline respectively while average ITRs of 40.83, 19.89, and 26.55 bits/min were obtained for right MI versus left MI, right MI versus baseline, and left MI versus baseline respectively. Such results indicate that the information provided by the EEG and fTCD modalities during task versus task problem are well suited to complement each other.

In terms of both accuracy and ITR, as seen in Tables 17-21, the hybrid system under assumptions A2 and A3 outperformed EEG only for right MI versus baseline and right MI versus left MI problems. For left MI versus baseline problem, although the hybrid system under A1, A2, and A3 did not provide significant improvement compared to EEG only in terms of accuracy, the hybrid system under A3 provided a significant improvement in terms of ITRs as shown in Table 21. Considering the 3 binary selection problems, it can be concluded that A3 provides significantly higher accuracies and/or ITRs compared to EEG only as seen in Tables 17-19, Fig. 26, and

confirmed by the statistical comparisons shown in Tables 20 and 21. Therefore, we believe that the system can perform efficiently under the weighted independence assumption (A3).

Although the accuracy due to EEG only for left MI versus baseline problem was higher than the EEG accuracy of right MI versus baseline problem, assumptions A2 and A3 failed to significantly improve the accuracy of the hybrid system compared to EEG only for left MI versus baseline while the same assumptions succeeded to significantly improve the hybrid performance for right MI versus baseline compared to EEG only. Therefore, we claim that such failure occurred because fTCD could not boost the performance of the system due to limitations related to the features extracted from fTCD data and how well these features are able to highlight the differences between left MI and baseline. To prove such a claim, at different decomposition levels, we investigated wavelet coefficients from which the fTCD statistical features were derived. As seen in Fig. 27, for each fTCD channel, the difference between the right MI coefficients and the baseline coefficients (Fig. 27 (a) and Fig. 27 (c)) is higher than the difference between the left MI coefficients and the baseline coefficients (Fig. 27 (b) and Fig. 27 (d)). Moreover, the differences between the wavelet coefficients due to MI tasks and the baseline seem to be localized rather than global while the statistical features we extract in this chapter are calculated for all coefficients within each wavelet band. For instance, out of around 2700 approximation coefficients, only 500 coefficients highlight the differences between left MI and baseline coefficients as shown in Fig. 27 (b) while many more coefficients highlight the differences between right MI and baseline as seen in Fig. 27 (a). Considering level 4 detail coefficients, for left MI versus baseline, the differences between the coefficients were more noticeable for the last 3000 coefficients out of 11000 in total for both channels while for right MI versus baseline, the differences were obvious

over all the coefficients representing channel 2 and over the last 3000 coefficients representing channel 1.

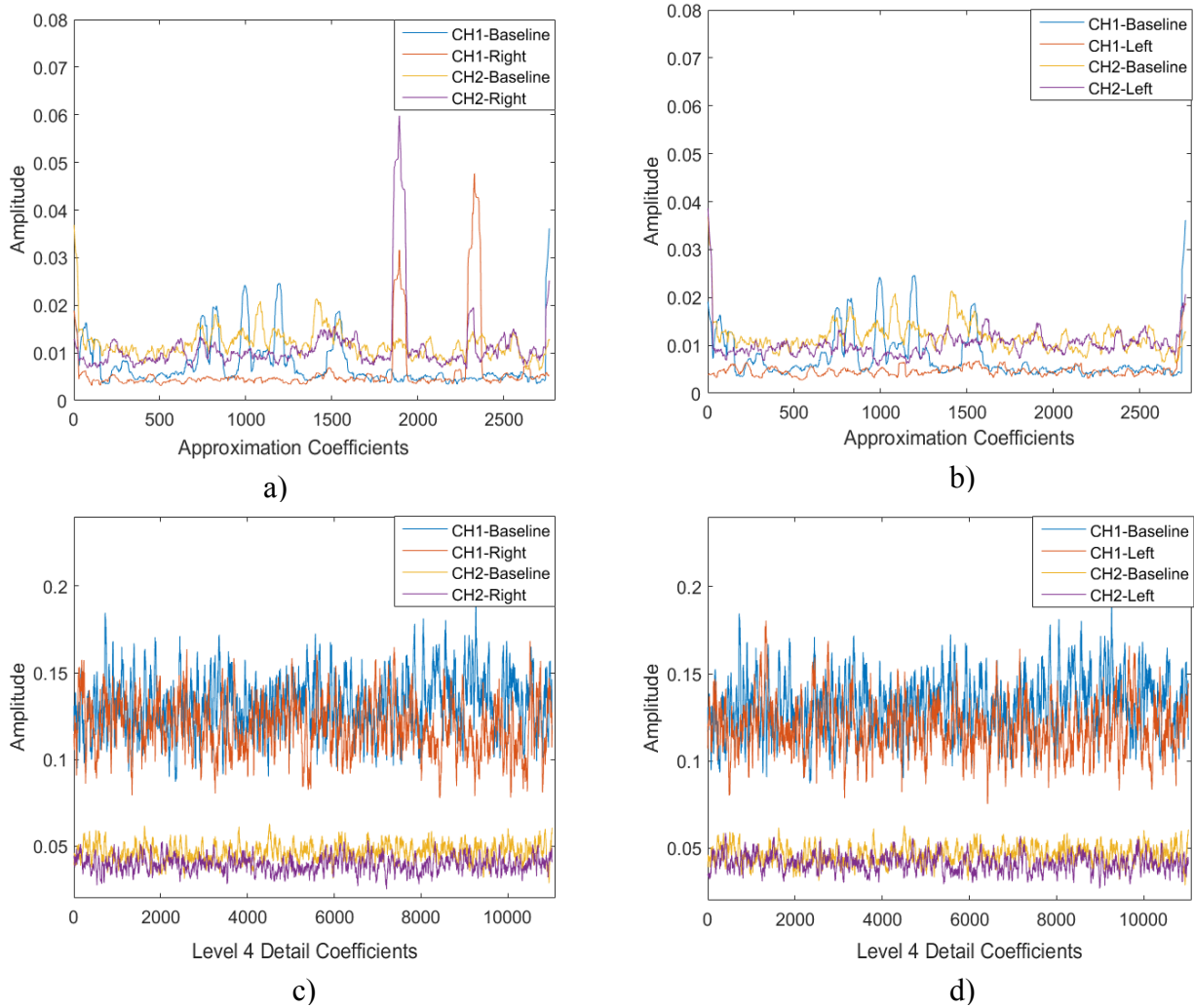


**Figure 27** For each task, wavelet coefficients of each wavelet band were averaged across trials corresponding to that task. The figure shows average approximation and level 4 detail wavelet coefficients for right MI vs baseline problem (a, c) and left MI vs baseline problem (b, d). It can be noted that, for each fTCD channel, the difference between right MI coefficients and baseline coefficients (Fig.4. a and Fig.4. c) is higher than the difference between left MI coefficients and baseline coefficients (Fig.4. b and Fig.4. d).

In general, since the difference between the right MI and baseline coefficients is more obvious than the difference between the left MI and baseline coefficients, the global features were able to better highlight the differences between right MI and baseline and, therefore, improve the hybrid performance compared to EEG only for right MI versus baseline. Considering Fig. 27 (a) and Fig. 27 (b), for both channels, it can be noted that the difference between the right MI and left MI coefficients is more noticeable than the right MI-baseline difference and left MI-baseline difference. Such observation explains the reason why fTCD provided more significant information for right MI versus left MI problem.

In this chapter, extraction of fTCD global statistical features was performed with the aim of reducing the computational complexity of the system through extracting few numbers of features rather than utilizing the wavelet coefficients themselves as features which will result in a very high-dimensional feature vector. To address local changes in the wavelet coefficients, as one of our future directions, we will calculate localized statistical features for each wavelet band though dividing each band into segments with equal length where the segment length can be determined based on the calibration sessions of each participant.

In our preliminary study (chapter 4.0) in which we introduced MI hybrid EEG-fTCD BCI, average accuracies of 88.33%, 89.48%, and 82.38% and average ITRs of 4.17, 5.45, and 10.57 bits/min were achieved for right MI versus baseline, left MI versus baseline, and right MI versus left MI respectively [98]. In the current study, we succeeded to significantly improve both accuracy and ITR of the proposed MI-based hybrid system. In particular, the current analysis yielded 93.85%, 93.71%, and 100% average accuracy and 19.89, 26.55, and 40.83 bits/min average ITRs for right MI versus baseline, left MI versus baseline, and right MI versus left MI respectively.

Moreover, to evaluate the performance of the 2 visual presentations we designed for the hybrid EEG-ftCD system, we compared the current performance measures obtained using MI visual presentation with the preliminary performance measures we obtained in chapter 5.0 using MR/WG visual presentation [97]. As seen in Table 22, MI visual presentation using the current analysis approach outperformed MR/WG visual presentation in terms of accuracy. In terms of ITR, average ITRs obtained using MR/WG visual presentation were 4.39, 3.92, and 5.60 bits/min for MR versus baseline, WG versus baseline, and WG versus MR classification respectively [97]. Such ITRs are significantly lower than the ITRs we obtained in the current study using MI visual presentation especially for task versus baseline problems.

Since the hybrid EEG-ftCD system is suggested as a faster alternative for EEG-fNIRS BCIs, we compared our results with the binary EEG-fNIRS BCIs in literature in terms of accuracy and trial length. As seen in Table 22, the MI EEG-ftCD system with the proposed analysis approach outperforms all the studies in comparison in terms of accuracy for the task versus task problem. For task versus baseline problems, the achieved accuracies are comparable to those obtained in studies [79], [64], [78]. However, unlike the hybrid BCIs in comparison, the proposed system does not require baseline/rest periods before/after each task yielding a total trial length that is shorter than trial length of all studies in comparison. Therefore, inference of the user intent can be achieved faster using the proposed hybrid system with the current analysis approach.

**Table 22 Comparison between the proposed hybrid system and the state-of-the-art hybrid BCIs.**

Method	Activity	Modalities	Accuracy	Trial length (s)	
				Task	Baseline/rest
[127] Fazli et al., 2012	Motor Imagery	EEG+fNIRS	83.20%	5	6/0
[127] Fazli et al., 2012	Motor Execution	EEG+fNIRS	93.20%	5	6/0
[83] Blokland et al., 2014	Motor Imagery	EEG+fNIRS	79.00%	15	0/30±3
[83] Blokland et al., 2014	Motor Execution	EEG+fNIRS	87.00%	15	0/30±3
[79] Khan et al., 2014	Mental Arithmetic	EEG+fNIRS	83.60%	10	0/5
[79] Khan et al., 2014	Motor Execution	EEG+fNIRS	94.70%	10	0/5
[64] Putze et al., 2014	Visual/auditory stimuli	EEG+fNIRS	94.70%	12.5±2.5	0/20 ±5
[59] Yin et al., 2015	Motor Imagery	EEG+fNIRS	89.00%	10	0/21±1
[60] Koo et al. 2015	Motor Imagery	fTCD+NIRS	88.00%	15	0/60
[78] Buccino et al., 2016	Motor Execution	EEG+fNIRS	72.20%	6	6/0
[78] Buccino et al., 2016	Motor Execution	EEG+fNIRS	94.20%	6	6/0
[80] Shin et al., 2017	Mental Arithmetic	EEG+fNIRS	88.20%	10	0/16±1
[97] Khalaf et al.,2019 (MR/baseline)	SSVEP+ MR/WG	EEG+fTCD	89.11%	10	NA
[97] Khalaf et al.,2019 (WG/baseline)	SSVEP+ MR/WG	EEG+fTCD	80.88%	10	NA
[97] Khalaf et al.,2019 (MR/WG)	SSVEP+ MR/WG	EEG+fTCD	92.38%	10	NA
[98] Khalaf et al.,2019 (right/baseline)	Motor Imagery	EEG+fTCD	88.33%	10	NA
[98] Khalaf et al.,2019 (left/baseline)	Motor Imagery	EEG+fTCD	89.48%	10	NA
[98] Khalaf et al.,2019 (right/left)	Motor Imagery	EEG+fTCD	82.38%	10	NA
Proposed method (right/baseline)	Motor Imagery	EEG+fTCD	<b>93.85%</b>	10	NA
Proposed method (left/baseline)	Motor Imagery	EEG+fTCD	<b>93.71%</b>	10	NA
Proposed method (right/left)	Motor Imagery	EEG+fTCD	<b>100.00%</b>	10	NA

\*NA: Not applicable

## 6.4 Conclusion

In this chapter, through fTCD multiscale analysis and CSP-based EEG analysis, we improved the performance of our novel MI hybrid system in which EEG and fTCD data are acquired simultaneously during visual presentation of MI tasks to the BCI users. Moreover, we proposed a probabilistic fusion approach of EEG and fTCD evidences instead of concatenating EEG and fTCD feature vectors of each trial. The proposed approach fuses EEG and fTCD evidences under 3 different assumptions. To evaluate the performance of the hybrid system compared to single-modal EEG and fTCD systems, we formulated 3 binary selection problems including right MI versus baseline, left MI versus baseline, and right MI versus left MI. It was found the hybrid system achieves the highest performance under assumption (A3) that assumes that EEG and fTCD are independent, but they do not have equal contribution towards making a correct decision. In particular, the hybrid system achieved average accuracies of 93.85%, 93.71%, and 100% and ITRs of 19.89, 26.55, and 40.83 bits/min for right MI versus baseline, left MI versus baseline, and right MI versus left MI respectively while the same problems yielded 90.52%, 92.16%, and 92.19% average accuracy and ITRs of 12.08, 10.68, and 22.76 bits/min respectively using EEG only. Compared to both hybrid EEG-fNIRS and EEG-fTCD BCIs in literature, the system with the current analysis approach outperformed all the studies in comparison.

## 7.0 EEG-ftCD Hybrid Brain-Computer Interface Using Template Matching and Wavelet Decomposition <sup>5</sup>

In this chapter, we aim at improving accuracies and ITRs of the system employing flickering MR/WG visual presentation. To achieve such aim, we extend our feature extraction approach by considering features derived from multiscale analysis and template matching instead of employing features derived from EEG and ftCD power spectrums as performed in chapter 5.0 [97]. In particular, considering ftCD data, it was shown before that the task performed by the BCI user can be identified with sufficient accuracy within 3-5 seconds of the task onset through analyzing the corresponding ftCD data using 5-level wavelet decomposition which makes ftCD a modality suitable for real-time BCI design [49]. Therefore, in this chapter, we employ 5-level wavelet decomposition to extract features from ftCD data. As for EEG analysis, one of the most successful target detection algorithms designed to detect SSVEPs is canonical correlation analysis (CCA) [139] [140] in which artificial sinusoidal signals are used as reference signals to identify the stimulus of interest. To enhance target identification accuracy, CCA is extended such that templates generated from the EEG data are used instead of artificial sinusoidal signals [141]. However, extended CCA method is computationally expensive since the spatial filters used to project trial data are constructed for each single trial [142]. In this chapter, we use a simple template matching algorithm in which templates generated from EEG training data are used as reference signals instead of using artificial reference signals as performed in CCA. Moreover, our

---

<sup>5</sup> Based on Aya Khalaf, Ervin Sejdic, Murat Akcakaya, “EEG-ftCD Hybrid brain-computer interface using template matching and wavelet decomposition,” *Journal of Neural Engineering*, vol. 16, no. 3, 2019 © [2019] IOP Publishing.

algorithm, unlike extended CCA, is computationally inexpensive since it requires only calculation of cross correlation between EEG segments of each trial and the corresponding EEG templates. These cross-correlations are used to generate EEG features. To select EEG and fTCD significant features, the Wilcoxon signed-rank test is employed. In this work, using the classical features described above, we mainly contribute to multi-modal fusion of EEG and fTCD features. In particular, instead of simple concatenation of EEG and fTCD feature vectors before classification as performed in our previous work [97], we propose a probabilistic fusion approach of EEG and fTCD evidences. Through such a probabilistic fusion, the contributions of each modality towards making a correct decision can be optimized. To perform such a probabilistic fusion, two SVM classifiers are used to project selected EEG and fTCD features of each trial separately into 2 scalar SVM scores. These scores (evidences) are fused under 3 different assumptions through the Bayesian framework we developed. To assess the performance of the hybrid system, 3 binary selection problems are evaluated including MR versus baseline, WG versus baseline, and WG versus MR.

## **7.1 Materials and Methods**

This section includes a detailed description of preprocessing, feature extraction, and feature selection methods as well as feature fusion and decision-making algorithms.

### **7.1.1 Preprocessing**

EEG data were bandpass-filtered using the g. USBamp bio-signal amplifier with corner frequencies 2 and 62 Hz. EEG data were also filtered using 4th order notch filters with corner frequencies 58 and 62 Hz. Since fTCD data are sampled at 44.1 kHz while the fTCD signals are approximately bandlimited to 4.4 kHz, the data were downsampled by a factor of 5 after a low-pass filter with 4.4 kHz corner frequency was applied to avoid aliasing.

### **7.1.2 Feature Extraction**

During each data collection session, 150 trials were presented to the BCI user. To extract features of each trial, both EEG and fTCD data corresponding to each 10-s trial were segmented. The data of each trial consisted of 16 EEG segments collected from the 16 EEG electrodes as well as 2 fTCD segments collected from the 2 fTCD transducers.

Cross correlation coefficients generated using template matching represented EEG features while fTCD features were statistical features derived from the Wavelet decomposition of fTCD data corresponding to each trial. Features of all EEG/fTCD segments were concatenated to form EEG/fTCD feature vectors.

#### **7.1.2.1 Template Matching**

One of the most popular techniques to identify stimulus of interest in SSVEP-based BCI systems is canonical correlation analysis (CCA). In CCA, artificial sinusoidal signals with frequencies of the same value as the flickering frequencies of the stimuli presented to the users are used as reference signals to recognize the frequency of the stimulus under test [139] [140].

However, using such artificial reference signals does not yield the best performance accuracy since these signals lack the features of real EEG signals. Therefore, CCA is extended such that templates generated from the EEG data are used instead of artificial sinusoidal signals [141]. However, such extension is computationally expensive since the spatial filters used to project EEG trial data are constructed for each single trial [142]. In this chapter, we used a simple template matching algorithm to identify the stimulus of interest and instead of using artificial reference signals as performed in CCA, templates generated from EEG training data were used as reference signals. Moreover, compared to extended CCA, our template matching algorithm is computationally inexpensive since it requires only calculation of cross correlations between EEG segments of each trial and the EEG templates while extended CCA requires, for each trial, optimizing the spatial filters used to project EEG data. In particular, for each class, average of EEG data of the training trials was calculated where each EEG electrode was represented by one template and thus 16 templates per class were generated. Assume each trial is represented by a matrix  $D$  where  $D$  is an  $N \times S$  matrix,  $N$  is the number of EEG channels and  $S$  is the number of samples. The template of channel  $n$  belonging to class  $C$  ( $T^{C_n}$ ) can be obtained as follows:

$$T^{C_n} = \frac{1}{L_c} \sum_{l=1}^{L_c} D_l(n, :) \quad (17)$$

where  $D_l(n, :)$  represents the  $n^{th}$  channel of the  $l^{th}$  trial matrix  $D$ ,  $L_c$  is the number of training trials belonging to class  $c$ , and  $n = 1, 2, \dots, N$ .

To identify the class of a test trial  $D$ , cross correlations were calculated between the  $N$  templates of each class ( $T^{C_n}$ ) and the corresponding  $N$  EEG segments ( $D(n, :)$ ) of the test trial as given below.

$$\hat{R}_{T^{c_n}D(n,:)}(\mathbf{m}) = \begin{cases} \sum_{s=0}^{S-m-1} T^{c_n}(s+m) D^*(n,s) & m \geq 0 \\ \widehat{R}_{D(n,:)T^{c_n}}^*(-m) & m < 0 \end{cases} \quad (18)$$

where  $m = 1, 2, \dots, 2S - 1$ . For each channel  $n$ , maximum cross correlation value between the test segment  $D(n, :)$  and the corresponding template  $T^{c_n}$  was selected as the feature representing that channel. Therefore, total of  $N$  features represented the cross correlations between the test trial  $D$  and the templates belonging to class  $C$ . These  $N$  features were normalized by their maximum value. Since we have 2 classes in each selection problem, and hence 2 sets of templates, we computed  $2N$  features representing each trial.

### 7.1.2.2 Wavelet Decomposition

Instead of extracting features derived from the fTCD power spectrum as performed in chapter 5.0 [97], we employed multi-scale analysis since the most efficient fTCD-based BCI in literature in terms of both accuracy and ITR employed 5-level wavelet decomposition for extracting features from fTCD data corresponding to MR and WG mental tasks [49]. Please see section 6.1.3 in chapter 6.0 for detailed description of this analysis.

### 7.1.3 Feature Selection and Reduction

For both EEG and fTCD feature vectors, significant features were selected using the Wilcoxon signed-rank test [113] at p-value of 0.05. However, for MR/WG versus baseline problems, the Wilcoxon test with 0.05 significance level failed sometimes during some cross-validation folds to find significant features that distinguish WG/MR task against baseline.

Therefore, a p-value of 0.1 was also used for task versus baseline problems and 2 sets of performance measures corresponding to p-values of 0.05 and 0.1 were generated. The best set of performance measures was reported in the results section below. To evaluate the performance of single modality BCIs (EEG only and fTCD only BCIs), selected features from each modality were classified solely using the SVM classifier [114] and performance measures corresponding to each modality were generated.

EEG and fTCD feature vectors were combined to assess the performance of the hybrid system. Instead of concatenating the 2 feature vectors corresponding to each trial, SVM was used to reduce each feature vector of each trial into a 1-D SVM score. In particular, 2 SVM classifiers were trained separately using selected EEG and fTCD feature vectors of the training trials. For each trial under test, the selected features from the 32-D EEG and 48-D fTCD feature vectors of that trial were reduced into 2 scalar SVM scores corresponding to EEG and fTCD evidences of that trial.

#### **7.1.4 Feature Fusion and Decision Making**

Please see section 6.1.4 in chapter 6.0 for a detailed description of feature fusion and decision making processes.

#### **7.1.5 Temporal Analysis**

With the aim of finding the optimal task period, both EEG and fTCD data were analyzed and performance measures were evaluated across time. Calculated performance measures included accuracy and information transfer rate (ITR) [143].

Both EEG and fTCD data were analyzed across time at time points 1, 2, ..., 10 s. For EEG data, an incremental window of 1 second initial length and increment size of 1 second was used to analyze the data across time while a moving window of 1 second length with no overlap was used to analyze fTCD data. The choice of the moving window for fTCD analysis was based on a study we carried out before to enhance the performance of an fTCD-based BCI that employs MR and WG tasks [49]. In particular, when computing the performance measures using EEG only, EEG template matching features of the EEG 1 second window are calculated, and performance measures are computed. Afterwards, the window size is increased by 1 second, EEG template matching features are calculated, and performance measures are reevaluated. The same process is performed until the window length is equal to task period (10 seconds). Similar to EEG only system, performance measures due to fTCD only are evaluated using a moving window of 1-s width instead of an incremental window.

To evaluate the performance of the hybrid combination, we developed a Bayesian framework that combines the evidences from fTCD and EEG modalities for joint user intent inference. At each time point (1, 2, ..., 10 s), 1-D EEG and fTCD evidences corresponding to the EEG and fTCD feature vectors at that time point are generated. EEG and fTCD evidences corresponding to each time window are combined under 3 different assumptions including joint EEG-fTCD distributions, independent EEG and fTCD distributions as well as weighted independent EEG and fTCD distributions as described in section 6.1.4 and the corresponding performance measures are calculated.

## 7.2 Results

To evaluate the effectiveness of the hybrid system, the maximum possible accuracy that can be obtained using EEG only and fTCD only was compared with the maximum accuracy achieved by the hybrid system under the 3 different assumptions (*A1*, *A2*, and *A3*) explained in section 6.1.4. These accuracies are reported in Tables 23, 24, and 25 for MR vs baseline, WG versus baseline, and WG vs MR problems respectively. In addition, error bars of sensitivities and specificities corresponding to the accuracies listed in Tables 23, 24, and 25 were plotted in Fig. 28. Moreover, ITRs of *A1*, *A2*, *A3*, EEG only, and fTCD only were compared in Fig. 29. P-values showing the statistical significance of *A1*, *A2*, and *A3* compared to EEG only and fTCD only across subjects were calculated using Wilcoxon signed rank test and reported in Table 26.

As seen in Table 23, for the MR versus baseline problem, *A1*, *A2*, and *A3* achieved significantly higher average accuracies compared to EEG only and fTCD only. In particular, 79.45%, 83.24%, and 86.27% average accuracies were achieved by *A1*, *A2*, and *A3* while EEG only and fTCD only obtained average accuracies of 75.28% and 68.66% respectively. As shown in Fig. 28, error bars of the corresponding sensitivities and specificities show that *A2* and *A3* have the highest average values and lowest standard deviation across participants especially compared to EEG only. Although *A1*, *A2*, and *A3* outperformed EEG only and fTCD only in terms of average accuracy, *A1* outperformed EEG for only 8 out of 11 participants while *A2* and *A3* outperformed EEG for 9 and 10 out of 11 participants respectively. Moreover, both *A2* and *A3* scored higher accuracies than fTCD only for all the participants while *A1* outperformed fTCD only for 10 out of 11 participants. In line with these observations, the p-values of Table 26 showed that *A1* is not statistically significant compared to EEG only. Meanwhile, both *A2* and *A3* are statistically

significant compared to EEG only. Compared to fTCD only, A1, A2, and A3 are statistically significant. In terms of ITRs, as seen in Fig. 29 (a), A3 outperformed A1, A2, EEG, and fTCD for most of the participants. On average, as shown in Fig. 29 (d), A3 achieved 8.95 bits/min while A1, A2, EEG, and fTCD yielded 7.55, 5.14, 3.49, and 2.46 bits/min respectively.

Tables 24 shows a comparison of the performance measures obtained for the WG versus baseline problem. A1, A2, and A3 obtained 78.26%, 82.85%, 85.29% average accuracy compared to 68.04%, and 67.67% obtained by EEG only and fTCD only. As shown in Fig 28 (b), the corresponding sensitivities and specificities have very similar values especially those of A1 and A2, therefore, the proposed classification model is balanced. In addition, A2 and A3 obtained higher accuracies than EEG only and fTCD only for all 11 participants. However, A1 achieved higher accuracies than EEG only and fTCD only for 9 and 10 participants respectively. These results are supported by the p-values of WG versus baseline problem listed in Table 26. Fig. 29 (b) shows that A1, A2, and A3 yielded higher ITRs for most of the participants compared to EEG only and fTCD. Unexpectedly, A2 obtained higher average ITR than A3 as shown in Fig. 29 (d). In particular, A2 obtained 8.89 bits/min while A3 obtained 8.34 bits/min. Meanwhile, A1, EEG only, and fTCD only got ITRs of 5.11, 1.98, and 1.37 bits/min respectively.

MR versus WG problem yielded the highest performance measures compared to MR/WG versus baseline problems as seen in Table 25. More specifically, A1, A2, and A3 obtained average accuracies of 97.84%, 97.40%, and 98.18% compared to 79.65% obtained by EEG only and 66.93% by fTCD only. Moreover, A1, A2, and A3 showed very low variance in sensitivities of MR and WG tasks across participants compared to EEG only and fTCD only as shown in Fig. 28 (c). Supported by the p-values in Table 26, for all participants, A1, A2, and A3 yielded higher accuracies than EEG only and fTCD only. In addition, A1, A2, and A3 achieved higher ITRs than

EEG only and fTCD only for all participants as seen in Fig. 29 (c). In terms of average ITRs, as shown in Fig. 29 (d), EEG only obtained 3.62 bits/min while fTCD only obtained 2.84 bits/min. However, when combined together, A1, A2, and A3 yielded average ITRs of 20.99, 19.63, and 21.29 respectively.

**Table 23 Maximum accuracy achieved for each subject using hybrid combinations (A1, A2, A3), EEG only, and fTCD only for MR vs baseline problem.**

Sub_ID	EEG	fTCD	A1	A2	A3
1	68.75%	70.83%	80.21%	86.46%	91.67%
2	83.33%	60.42%	86.46%	89.58%	92.71%
3	78.13%	76.04%	83.33%	84.38%	87.50%
4	75.00%	65.63%	71.88%	76.04%	82.29%
5	73.96%	78.13%	75.00%	79.17%	81.25%
6	72.92%	64.58%	79.17%	80.21%	82.29%
7	78.13%	65.63%	82.29%	84.38%	85.42%
8	75.00%	65.63%	84.38%	89.58%	91.67%
9	58.33%	73.96%	84.38%	89.58%	91.67%
10	83.33%	68.75%	71.88%	76.04%	78.13%
11	81.25%	65.63%	75.00%	80.21%	84.38%
<b>Mean</b>	<b>75.28%</b>	<b>68.66%</b>	<b>79.45%</b>	<b>83.24%</b>	<b>86.27%</b>

**Table 24 Maximum accuracy achieved for each subject using hybrid combinations (A1, A2, A3), EEG only, and fTCD only for WG vs baseline problem.**

Sub_ID	EEG	fTCD	<i>A1</i>	<i>A2</i>	<i>A3</i>
1	79.38%	63.92%	81.44%	86.60%	88.66%
2	58.76%	62.89%	85.57%	90.72%	93.81%
3	75.26%	71.13%	85.57%	81.44%	84.54%
4	61.86%	61.86%	72.16%	78.35%	81.44%
5	70.10%	72.16%	70.10%	77.32%	79.38%
6	72.16%	74.23%	78.35%	78.35%	79.38%
7	63.92%	68.04%	78.35%	85.57%	88.66%
8	46.39%	72.16%	75.26%	81.44%	83.51%
9	72.16%	61.86%	82.47%	88.66%	91.75%
10	75.26%	64.95%	79.38%	85.57%	87.63%
11	73.20%	71.13%	72.16%	77.32%	79.38%
<b>Mean</b>	<b>68.04%</b>	<b>67.67%</b>	<b>78.26%</b>	<b>82.85%</b>	<b>85.29%</b>

**Table 25 Maximum accuracy achieved for each subject using hybrid combinations (A1, A2, A3), EEG only, and fTCD only for MR vs WG problem.**

Sub_ID	EEG	fTCD	A1	A2	A3
1	93.33%	62.86%	99.05%	99.05%	99.05%
2	81.90%	65.71%	100.0%	100.0%	100.0%
3	87.62%	68.57%	100.0%	100.0%	100.0%
4	75.24%	62.86%	100.0%	100.0%	100.0%
5	78.10%	64.76%	100.0%	96.19%	96.19%
6	72.38%	72.38%	99.05%	99.05%	99.05%
7	80.00%	70.48%	96.19%	95.24%	98.10%
8	72.38%	66.67%	83.81%	85.71%	88.57%
9	64.76%	69.52%	100.0%	100.0%	100.0%
10	90.48%	70.48%	100.0%	100.0%	100.0%
11	80.00%	61.90%	98.10%	96.19%	99.05%
<b>Mean</b>	<b>79.65%</b>	<b>66.93%</b>	<b>97.84%</b>	<b>97.40%</b>	<b>98.18%</b>

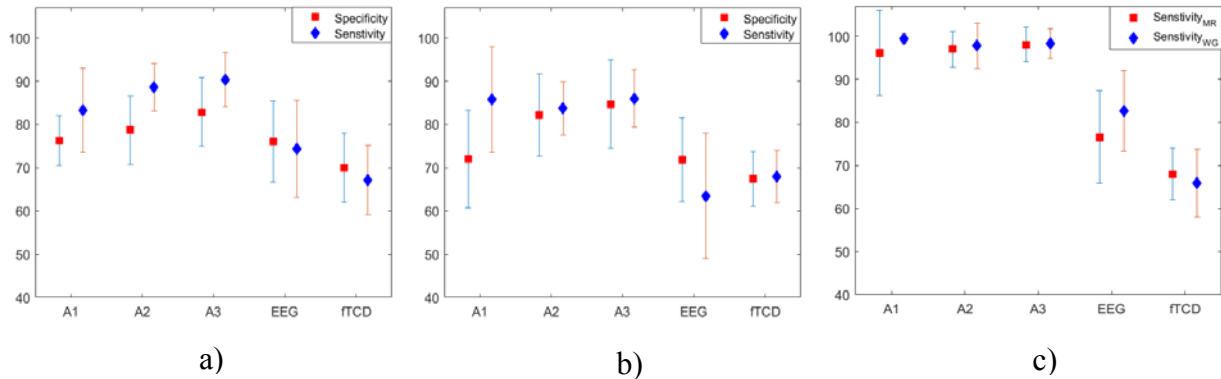


**Figure 28 Sensitivities and specificities (mean and standard deviation) calculated using A1, A2, A3, EEG only, and fTCD only for flickering MR vs baseline problem (a), flickering WG vs baseline problem (b), and flickering MR vs flickering WG (c).**

**Table 26 P-values showing \significance of A1, A2, and A3 compared to EEG only and fTCD only for the 3 binary problems.**

Comparison	MR vs Baseline	WG vs Baseline	MR vs WG
A1/EEG	0.1816	0.0039	0.0009
A1/fTCD	0.0029	0.0029	0.0009
A2/EEG	0.0293	0.0009	0.0009
A2/fTCD	0.0009	0.0009	0.0009
A3/EEG	0.0029	0.0009	0.0009
A3/fTCD	0.0009	0.0009	0.0009

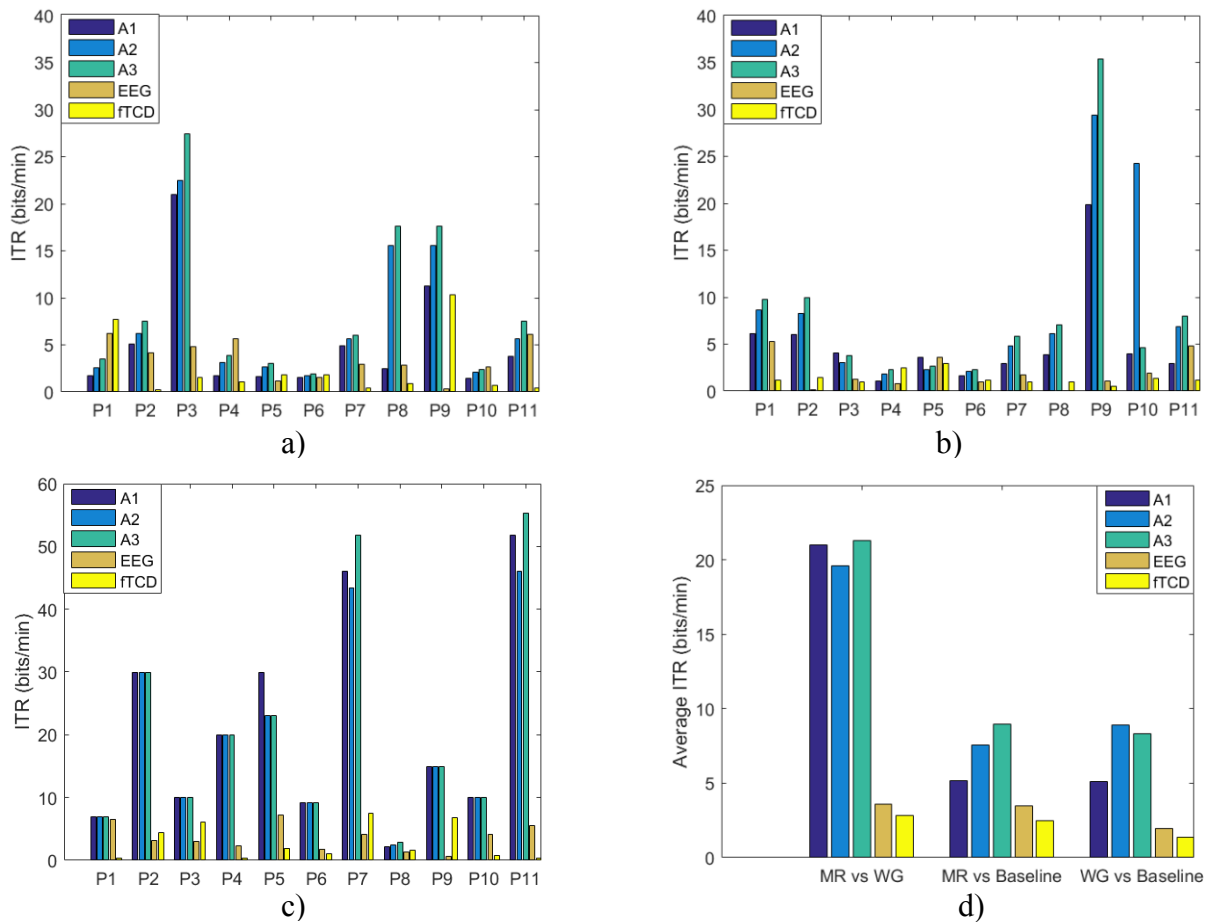


**Figure 29 Information transfer rates (ITRs) for each participant (P) calculated using EEG only, fTCD only, and the 3 hybrid combinations (A1, A2, and A3) for MR vs baseline problem (a), WG vs baseline problem (b), and MR vs WG problem (c). Average ITRs for the 3 classifications problems.**

### 7.3 Discussion

Based on the accuracies shown in Tables 23, 24, and 25 as well as the average ITRs shown in Fig. 29 (d), it can be noticed that the EEG and fTCD independence hypothesis (*A2*) yielded more efficient performance compared to the general hypothesis where EEG and fTCD are assumed to be jointly distributed (*A1*). Moreover, although weighted independence hypothesis (*A3*) offers higher accuracies compared to those obtained under *A2*, the increase in accuracy is not that significant considering the increase in computational complexity due to the  $\alpha$  parameter optimization required when combining EEG and fTCD evidences under *A3*. Moreover, despite the differences in accuracies, the ITRs due to *A2* and *A3* are very close in value to each other. Therefore, we believe that the system can perform efficiently under the independence assumption (*A2*).

It was shown that the MR versus WG problem obtained significantly higher average accuracy and average ITR compared to MR/WG versus baseline problems. Specifically, accuracies of 86.27%, 85.29%, and 98.11% were obtained by MR versus baseline, WG versus baseline, and MR versus WG respectively while the same binary problems yielded average ITRs of 8.95, 8.34, and 21.29 bits/min respectively. One limitation of this study is that the BCI user gets distracted while focusing on the fixation cross during the baseline trials since such user experiences flickering effect coming from both visual icons representing MR and WG tasks during those baseline trials. However, the user is less distracted by this flickering effect while performing MR and WG tasks since they are separated by a larger distance on the screen as shown in Fig. 15. Such flickering effect is the reason behind the significant difference in both accuracy and ITR obtained for MR

versus WG problem compared to accuracy and ITR achieved for MR/WG versus baseline problems. To reduce the distraction encountered by the user during baseline trials, a screen with larger dimensions can be used instead of the current 15.6" laptop screen. Another solution is to reduce the size of the visual icons representing the MR and WG tasks. Another limitation of the current study is the long data collection sessions (25 min) which leads to user fatigue and eye strain due to long exposure to flickering objects. Therefore, in the future version of this system, each session will be divided into 2 separate sessions.

From fTCD literature, it was found that the imagination nature of MR task induces bilateral activation in both brain hemispheres while the analytical nature of WG task induces higher activation in left middle cerebral arteries (MCAs) enabling different responses fTCD [46]. To confirm such observation, we plotted the envelope of fTCD signals measured using left and right channels while performing MR and WG tasks separately. As shown in Fig. 30 (a), the fTCD signal collected from the left channel (records from left MCAs) during WG task has a higher amplitude than the fTCD signal collected from the right channel as well as both fTCD signals corresponding to MR task. Moreover, as seen in Fig. 30 (b), the amplitude of the difference between right and left channels during the WG task is higher than the amplitude of the difference during the MR task. To a large extent, such findings are in line with the observations reported in the literature about cerebral activation due to MR and WG tasks.

Note that to induce changes in EEG to infer user intent, we use checkerboard patterns with different frequencies to represent MR and WG tasks as seen in Fig. 15. In Fig. 30 (c) and Fig. 30 (d), power spectrum of EEG due to MR (flickering frequency= 7 Hz) and WG (flickering frequency= 17Hz) tasks are presented. In both subfigures, a peak around 2 Hz can be noticed. However, this peak is due to the bandpass filter used to preprocess the EEG data (described in

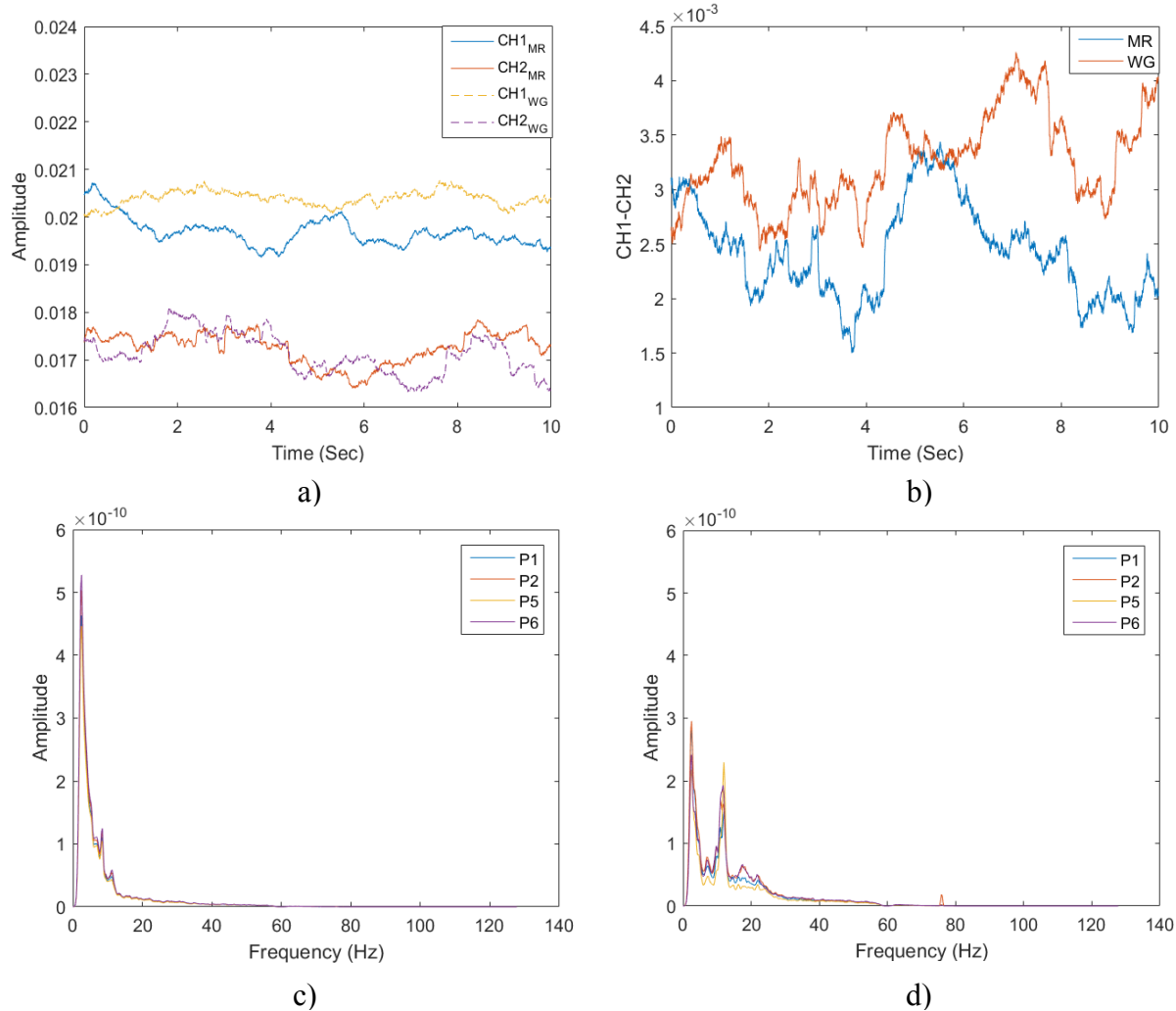


**Figure 30 (a) Right ftCD channel (channel 1) and left ftCD channel (channel 2) normalized envelope signals during MR and WG tasks, (b) Difference between right ftCD channel (channel 1) and left ftCD channel (channel 2) envelope signals shown in (a) for MR and WG tasks, (c) power spectrum of EEG signals collected from electrodes P1, P2, P5, and P6 during MR task (flickering frequency= 7 Hz) (d) power spectrum of EEG signals collected from electrodes P1, P2, P5, and P6 during WG task (flickering frequency= 17 Hz).**

section 7.1.1) not due to the flickering frequencies of MR and WG tasks. As for the other peaks in the power spectra, considering the fact that although the BCI user gets distracted while observing a specific task since such user experiences flickering effect coming from both tasks, it is expected

that, even though the BCI user might be focusing on a single task, the effects of both flickering frequencies can be observed from the power spectrum of the corresponding EEG data. For instance, in Fig. 30 (c), the power spectrum of the EEG response due to the MR task (flickering frequency= 7 Hz) shows peaks at approximately 7 Hz which is the MR flickering frequency as well as 9 Hz which is around the first subharmonic frequency of the WG task. Such results are in line with the literature since it was found that the subharmonic responses can be observed for flickering frequencies in the range of 17–22 Hz especially over the parietal lobe [144] from which the EEG data used to obtain the power spectra in Fig. 30 are recorded. Moreover, based on the power spectrum due to the WG task (flickering frequency= 17 Hz) shown in Fig. 30 (d), it can be noted that there is a peak at  $\approx 17$  Hz which is the flickering frequency of the WG task as well as a peak at  $\approx 9$  Hz which is approximately the first subharmonic of the 17 Hz. Moreover, a small peak at 7 Hz was noticed which is most likely due to the flickering effect of the MR task on the BCI user while performing the WG task.

Compared to the preliminary results we obtained before using the flickering MR/WG visual presentation, in this chapter, we improved the ITRs for the 3 binary problems at least 2 times compared to the ITRs we obtained previously. In particular, previously we obtained 4.39, 3.92, and 5.60 bits/min average ITRs for MR versus baseline, WG versus baseline, and MR versus WG respectively while in this work, ITRs of 8.95, 8.34, and 21.29 bits/min were obtained for the same binary problems respectively. In terms of accuracy, as shown in Table 27, the analysis we performed in the previous study yielded 89.11%, 80.88%, and 92.38% average accuracy for MR versus baseline, WG versus baseline, and MR versus WG respectively compared to 86.27%, 85.29%, and 98.11% obtained with the current analysis. It can be noted that the MR versus baseline problem achieved lower accuracy with the current analysis. However, it obtained twice

the ITR obtained in the previous study where the ITR is known to be a measure that combines both accuracy and speed of the BCI system. Moreover, as shown in Table 27, the flickering MR/WG visual presentation with the current analysis outperforms the motor imagery hybrid EEG- fTCD BCI we designed before.

In terms of accuracy, as seen in Table 27, the flickering MR/WG visual presentation with the current analysis outperforms the state of the art hybrid EEG-fNIRS BCIs [78], [60], [127], [83], [79], [98], [97], [64], [59], [80] especially the MR versus WG binary selection problem. In terms of trial length, the proposed system has the shortest trial length of 10 s compared to the other systems in literature. Moreover, the proposed system does not require baseline or rest period before or after performing each task. Instead, the baseline cross in this study is selected randomly without any specified order during the visual presentation since it is considered as one of the tasks that reflects the case when no action is required to be performed. Even though the systems introduced in [78], [79], [64] achieved accuracies comparable to ours, such systems are slower than the proposed system. In particular, the system introduced by Putze et al. [64] requires a task period of 12.5 s and a rest period of 20 s while the system introduced by Khan et al. [79] needs a 5 s rest period and a 10 s task period. Moreover, baseline and task periods of 6 s are required for the system proposed by Buccino et al. [78]. In addition, 2 of these 3 studies exploited motor execution to design their BCIs [78], [79] while the proposed system is intended to be used in the future by individuals with disabilities, therefore, it does not require any movement to execute any BCI command.

**Table 27 Comparison between the proposed hybrid system and the state-of-the-art hybrid BCIs.**

Method	Activity	Modalities	Accuracy	Trial length (s)	
				Task	Baseline/re st
[127] Fazli et al., 2012	Motor Imagery	EEG+fNIRS	83.20%	15	6/0
[127] Fazli et al., 2012	Motor Execution	EEG+fNIRS	93.20%	15	6/0
[83] Blokland et al., 2014	Motor Imagery	EEG+fNIRS	79.00%	15	0/30±3
[83] Blokland et al., 2014	Motor Execution	EEG+fNIRS	87.00%	15	0/30±3
[79] Khan et al., 2014	Mental Arithmetic	EEG+fNIRS	83.60%	10	0/5
[79] Khan et al., 2014	Motor Execution	EEG+fNIRS	94.70%	10	0/5
[64] Putze et al., 2014	Visual/auditory stimuli	EEG+fNIRS	94.70%	12.5±2.5	0/20 ±5
[59] Yin et al., 2015	Motor Imagery	EEG+fNIRS	89.00%	10	0/21±1
[60] Koo et al. 2015	Motor Imagery	fTCD+NIRS	88.00%	15	0/60
[78] Buccino et al., 2016	Motor Execution	EEG+fNIRS	72.20%	6	6/0
[78] Buccino et al., 2016	Motor Execution	EEG+fNIRS	94.20%	6	6/0
[80] Shin et al., 2017	Mental Arithmetic	EEG+fNIRS	88.20%	10	0/16±1
[97] Khalaf et al.,2019 (right/baseline)	Motor Imagery	EEG+fTCD	88.33%	10	NA
[97] Khalaf et al.,2019 (left/baseline)	Motor Imagery	EEG+fTCD	89.48%	10	NA
[97] Khalaf et al.,2019 (right/left)	Motor Imagery	EEG+fTCD	82.38%	10	NA
[98] Khalaf et al.,2018 (MR/baseline)	SSVEP+ MR/WG	EEG+fTCD	89.11%	10	NA
[98] Khalaf et al.,2018 (WG/baseline)	SSVEP+ MR/WG	EEG+fTCD	80.88%	10	NA
[98] Khalaf et al.,2018 (MR/WG)	SSVEP+ MR/WG	EEG+fTCD	92.38%	10	NA
Proposed method (MR/baseline)	SSVEP+ MR/WG	EEG+fTCD	<b>86.27%</b>	10	NA
Proposed method (WG/baseline)	SSVEP+ MR/WG	EEG+fTCD	<b>85.29%</b>	10	NA
Proposed method (MR/WG)	SSVEP+ MR/WG	EEG+fTCD	<b>98.11%</b>	10	NA

\*NA: Not applicable

## 7.4 Conclusion

In this chapter, to improve the performance measures of the hybrid EEG-fTCD BCI we designed before, we employed template matching and wavelet decomposition for EEG and fTCD analysis, respectively. Moreover, we proposed a probabilistic fusion approach of EEG and fTCD evidences. Through such an approach, the contributions of each modality towards making a correct decision can be optimized. In this hybrid BCI, EEG and fTCD data are recorded simultaneously while a visual presentation showing flickering MR and WG tasks is presented to the BCI user. To assess the hybrid system performance, 3 classification problems were solved including MR versus baseline, WG versus baseline, and MR versus WG. Average accuracies of 86.27%, 85.29%, and 98.11 were obtained for MR versus baseline, WG versus baseline, and MR versus WG respectively while the same problems achieved average ITRs of 8.95, 8.34, and 21.29 bits/min respectively. These performance measures outperform the preliminary results we obtained before using flickering MR/WG visual presentation. Moreover, the system with the current analysis outperforms the hybrid EEG-fNIRS BCIs in literature in terms of accuracy and trial length. Such results show that the proposed hybrid BCI with the current analysis techniques is a promising step towards making such hybrid systems efficient to be used in real-life BCI applications.

## 8.0 3-Class EEG-fTCD Brain-Computer Interfaces

In this chapter, we aim at extending our feature extraction approaches explained in chapters 6.0 and 7.0 to solve the 3-class problems of both the MI and flickering MR/WG paradigms. In particular, for the MI paradigm, we analyzed the 3-class fTCD data using wavelet decomposition and extended the basic binary CSP algorithm to multi-class CSP to extract features from 3-class EEG data. As for the flickering MR/WG paradigm, we modified our template matching algorithm to analyze the 3-class EEG data while features were extracted from fTCD data using wavelet decomposition.

### 8.1 Materials and Methods

In this section, we explain extending our feature extraction, selection, and fusion approaches to solve 3-class problems of both the MI and flickering MR/WG paradigms.

#### 8.1.1 EEG Feature Extraction

##### 8.1.1.1 MI Paradigm

Given that CSP is a binary feature extraction technique while the classification problem to be solved is a 3-class problem, in this chapter, we extended basic CSP algorithm to multi-class CSP using one versus one approach [114] which decomposes a  $k$ -class problem into  $k \frac{k-1}{2}$  binary problems that include all possible pairs of the  $k$  classes. Therefore, the 3-class problem was

decomposed into 3 binary problems. In particular, the training trials of the 3 classes were arranged into 3 different groups such that each group contained the training trials corresponding to each pair of classes. CSP was applied to the training trials of each group separately and the corresponding eigenvectors were computed. During testing a trial  $x$ , the EEG data of that trial were projected on the set of eigenvectors of each group separately. In particular, for each group, we spatially filtered EEG data of trial  $x$  using  $f = 1, 2, 3, \dots, \text{ and } 8$  eigenvectors from both ends of  $W$  matrix as explained in chapter 6.0. To extract EEG features, we calculated the log variance of each spatially filtered signal yielding  $2f$  ( $2, 4, 6, \dots, \text{ and } 16$ ) CSP features. The overall feature vector was formed by concatenating the features due to the 3 groups of eigenvectors. Therefore, the overall feature vector contained  $6f$  CSP features.

### **8.1.1.2 Flickering MR/WG Paradigm**

Here, we extended our EEG template matching technique explained in chapter 7.0 to solve the 3-class problem of the flickering MR/WG paradigm. In particular, for each class, since each trial is represented by 16 EEG segments collected from 16 EEG channels, we extracted 16 templates corresponding to the 16 EEG channels by averaging EEG training trials over each channel. To extract EEG features of certain trial, cross correlations between the 16 templates of each class and the corresponding 16 EEG segments of that trial were calculated. At each channel, the maximum cross correlation value between the EEG segment of that channel and the corresponding template was selected as the feature representing that channel. Therefore, a total of 16 features represented the correlations between the 16 EEG segments of each test trial and the templates belonging to each class. These 16 features were normalized by their maximum value. Since we have 3 classes in each selection problem; and hence, 3 sets of templates, we computed  $3 \times 16$  features for each trial.

### 8.1.2 fTCD Feature Extraction

Wavelet analysis was employed to analyze fTCD data collected using both MI and flickering MR/WG paradigms. In particular, 5-level wavelet decomposition was applied to the 2 fTCD data segments corresponding to each trial (one segment per fTCD channel) as explained in chapters 6.0 and 7.0. Four statistical features including mean, variance, skewness, and kurtosis were calculated for each of the 6 wavelet bands obtained from the decomposition leading to computation of 24 features per segment and 48 features per trial.

### 8.1.3 Feature Selection and Reduction

Given that the Wilcoxon rank-sum test is a binary feature selection technique while the classification problem to be solved is a 3-class problem, we employed a one versus one approach [114] which decomposes a  $k$ -class problem into  $k \frac{k-1}{2}$  binary problems that include all possible pairs of the  $k$  classes. In particular, each 3-class classification problem was decomposed into 3 binary problems. For each binary problem, the significant features were evaluated separately using the Wilcoxon rank-sum test. The set of selected features for each binary problem was used as an input to one SVM classifier. Each 3-class problem was solved at p-values of 0.001, 0.005, 0.01, and 0.05. As explained in chapters 6.0 and 7.0, the Wilcoxon rank-sum test was used to select significant features of fTCD data as well as EEG data of flickering MR/WG paradigm.

SVM was used to reduce EEG and fTCD feature vectors of each trial separately into scalar SVM scores. As mentioned above, each of the 3-class problems was decomposed into 3 binary problems. Each binary problem has its own significant features and its own SVM classifier where each classifier is trained using data from different pair of classes. During testing a trial belonging

to class  $k$  ( $k = 1, 2, 3$ ) the selected EEG/fTCD feature vector of that trial is used as input to the 3 binary classifiers. Therefore, for each trial under test, the selected features from the EEG and fTCD feature vectors of that trial are reduced into 3 scalar EEG SVM scores and 3 scalar fTCD SVM scores, respectively corresponding to EEG and fTCD evidences of that trial.

#### 8.1.4 Feature Fusion and Decision Making

The probabilistic fusion approach introduced in chapter 6.0 was extended to solve the 3-class problem of the MI and flickering MR/WG paradigms. Inference of the user intent without restricting EEG and fTCD evidences to any assumption can be found through solving the following optimization problem.

$$\widehat{x}_k = \arg \max_{x_k} p(x_k|Y = y_k) \quad (10)$$

In (10),  $p(x_k|Y)$  is the posterior distribution of the state  $x_k$  conditioned on the observations  $Y$  where  $x_k = 1, 2, \text{ or } 3$ . To reduce computational complexity, we solved (10) only under the independence assumption (A2). Therefore, as explained in chapter 6.0, (10) can be written as:

$$\widehat{x}_k = \arg \max_{x_k} p(e = e_k|x_k)p(f = f_k|x_k) \quad (14)$$

where  $p(e|x_k)$  and  $p(f|x_k)$  are the distributions of EEG and fTCD evidences conditioned on the state  $x_k$  respectively.

SVM EEG and fTCD scores of training trials are used separately to compute two 3-dimensional distributions [ $p(e|x_k)$  and  $p(f|x_k)$ ] that are assumed to be multivariate Gaussian distributions. To estimate these distributions, EEG and fTCD evidences of the training trials were fitted to a 3-dimensional Gaussian mixture model [145]. For evidences under test  $y_k = \{e_k, f_k\}$ ,  $e_k$  and  $f_k$  are plugged in (14) and the user intent  $x_k$  that yields the maximum likelihood is selected.

## 8.2 Results

As shown in Table 28, for the MI paradigm, EEG-fTCD combination under the independence assumption (A2) obtained higher accuracies compared to accuracies obtained using EEG only and fTCD only. In particular, 96.58%, 85.50%, and 43.89% average accuracies were achieved using EEG-fTCD, EEG only, and fTCD only. On the other hand, EEG-fTCD, under A2, obtained average accuracy of 90.60% using the flickering MR/WG paradigm while EEG only and fTCD only yielded 57.54% and 44.66% average accuracies as seen in Table 29.

To assess if the classification model is balanced, for both paradigms, we calculated the accuracy of identifying each task (task sensitivity) as well as the accuracy of identifying the baseline (specificity). As seen in Fig. 31 (a) and Fig. 31 (b), considering the error bars representing variability in sensitivities and specificities across participants, it can be concluded that the EEG-fTCD classification models of the MI and MR/WG paradigms are balanced since the average sensitivities and specificities show very similar values. Moreover, for the MI paradigm, the variability in sensitivities and specificities obtained using the hybrid system is much lower compared to those obtained using fTCD only, while for the MR/WG paradigm the variability in sensitivities and specificities obtained using the hybrid system is much lower than those obtained using EEG only and fTCD only.

**Table 28 Maximum accuracy achieved for each subject using A3, EEG only, and fTCD only for the MI paradigm.**

Sub_ID	EEG	fTCD	A2
1	92.62%	44.33%	96.64%
2	81.88%	46.31%	100.00%
3	83.22%	50.34%	98.66%
4	79.87%	44.97%	93.29%
5	88.59%	41.61%	99.33%
6	83.22%	43.62%	91.95%
7	90.60%	42.28%	90.60%
8	93.29%	44.30%	98.66%
9	84.56%	37.58%	99.33%
10	77.18%	43.62%	97.32%
<b>Mean</b>	<b>85.50%</b>	<b>43.89%</b>	<b>96.58%</b>

**Table 29 Maximum accuracy achieved for each subject using A2, EEG only, and fTCD only for the flickering MR/WG paradigm.**

Sub_ID	EEG	fTCD	A2
1	65.10%	38.26%	94.63%
2	57.72%	48.32%	96.64%
3	63.76%	42.95%	96.64%
4	57.72%	43.62%	97.32%
5	61.07%	45.64%	95.30%
6	57.05%	47.65%	86.58%
7	51.01%	50.34%	85.23%
8	49.66%	40.94%	70.47%
9	47.65%	48.99%	85.23%
10	63.09%	39.60%	97.99%
11	59.06%	44.97%	90.60%
<b>Mean</b>	<b>57.54%</b>	<b>44.66%</b>	<b>90.60%</b>

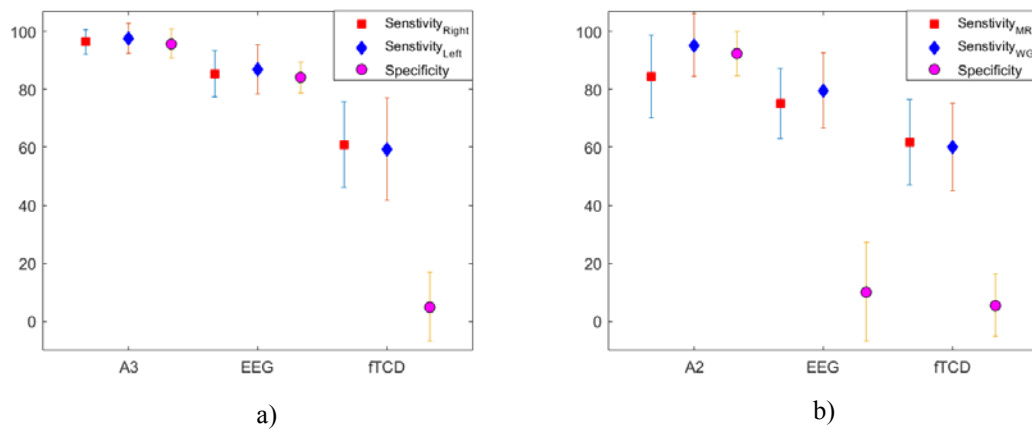


**Figure 31 Sensitivities and specificities (mean and standard deviation) calculated using EEG-ftCD, EEG only, and fTCD only for the MI paradigm (a), and the flickering MR/WG paradigm (b).**

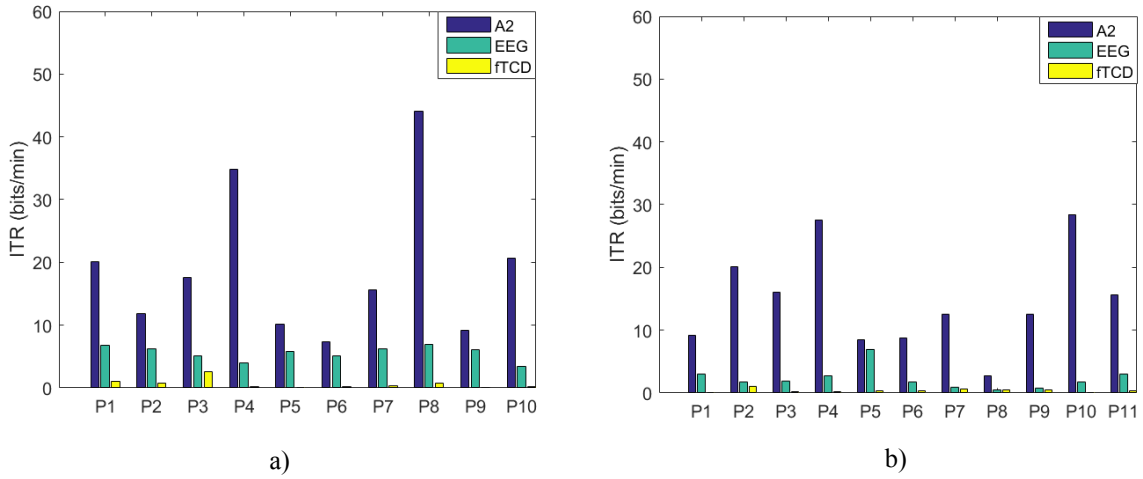


**Figure 32 Information transfer rates (ITRs) for each participant (P) calculated using EEG only, fTCD only, and the EEG-fTCD combination for the MI paradigm (a), and the flickering MR/WG paradigm (b).**

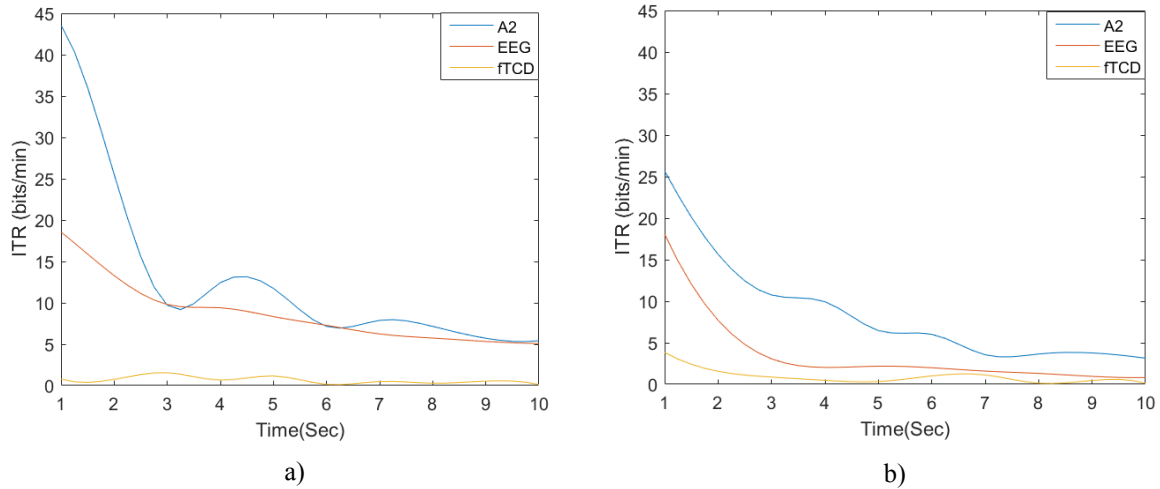


**Figure 33 Average ITRs calculated using EEG only, fTCD only, and the hybrid combination for the MI paradigm (a), and the flickering MR/WG paradigm (b).**

In terms of ITRs, for each participant, we calculated ITRs corresponding to the maximum accuracies obtained using EEG-fTCD, EEG only, and fTCD only. As shown in Fig. 32, ITRs due to the hybrid combination are significantly higher than those obtained using EEG only and fTCD

only. In particular, for the MI paradigm, EEG- fTCD obtained average ITR of 19.16 bits/min while EEG only and fTCD only obtained 5.57 and 0.66 bits/min, respectively while for the flickering MR/WG paradigm, average ITRs of 14.73, 2.27, and 0.40 were achieved using EEG- fTCD, EEG only, and fTCD only.

Alternatively, for both paradigms, the average ITRs were computed and plotted across the 10 second trial length and presented in Fig. 33. It can be noted that at 1 second trial length, EEG- fTCD yielded 43.59 and 25.70 bits/min for the MI and MR/WG paradigms, respectively while EEG only obtained 18.56 and 18.09, respectively. Using fTCD only, average ITRs of 0.78 and 3.84 bits/min were obtained for the MI and MR/WG paradigms, respectively.

### **8.3 Discussion**

As shown in Tables 28 and 29, the accuracies of the 3-class problems obtained using the hybrid combination are significantly higher than those obtained using EEG only and fTCD only for both the MI and flickering MR/WG paradigms. In particular, for the MI paradigm, EEG-fTCD obtained an average accuracy of 96.58% which is 10% higher than the accuracy obtained using EEG only (the primary modality in the EEG-fTCD multimodal BCI). As for the MR/WG paradigm, the combination achieved 90.60% average accuracy which is 33% higher than that obtained using EEG only.

In line with these results, for both paradigms, ITRs of EEG-fTCD combination significantly outperformed ITRs obtained using EEG only and fTCD only as shown in Fig. 33 especially at 1-second trial length. More specifically, for the MI paradigm, EEG-fTCD achieved approximately an average ITR that is 2.5 times the average ITR obtained using EEG only while

for the MR/WG paradigm, the average ITR achieved using EEG-ftCD combination is 1.5 times the average ITR of EEG only.

In terms of both accuracy and ITR, it can be noted that the MI paradigm achieved higher performance compared to the flickering MR/WG system. In particular, the combination achieved 96.58% average accuracy using the MI paradigm and 90.60% average accuracy using the MR/WG paradigm. Moreover, at 1-second trial length, ITRs of 43.59 and 25.70 bits/min were achieved using the MI and MR/WG paradigms, respectively. Such findings in addition to the performance measures obtained in chapters 6.0 and 7.0 suggest that the MI paradigm is a more promising candidate for real-time BCI applications.

#### **8.4 Conclusion**

In this chapter, we extended our feature extraction approaches that we proposed in chapters 6.0 and 7.0 to solve the 3-class problem of both the MI and flickering MR/WG paradigms. In particular, we solved 2 classification problems including right MI versus left MI versus baseline and MR versus WG versus baseline. Experimental results showed that the hybrid combination significantly outperformed EEG only and ftCD only for both paradigms. Moreover, it was found that the hybrid combination of MI paradigm is more efficient than the hybrid combination of the flickering MR/WG paradigm in terms of both accuracy and ITR. In particular, an average accuracy of 96.58% and an average ITR of 43.59 bits/min were achieved using MI paradigm compared to 90.60% average accuracy and 25.70 bits/min average ITR obtained using flickering MR/WG paradigm. Consequently, it can be concluded that the hybrid system utilizing MI paradigm is a more viable candidate for real-time BCI applications.

## **9.0 A Probabilistic Transfer Learning Approach for Calibration Time Reduction in Hybrid EEG-ftCD Brain-Computer Interfaces**

### **9.1 Introduction**

Generally, before being used by each individual, a BCI requires calibration to ensure that it can identify user intent with sufficient accuracy in a reasonable amount of time. Moreover, since the BCI performance is directly proportional to the amount of available training data, each BCI user has to attend a certain number of calibration sessions which may be burdensome for individuals with limited speech and physical abilities.

One potential solution for such a problem is combining data from different BCI users to calibrate the system for a certain user. However, the statistical distribution of the data varies across subjects and even across sessions within the same subject [146]. This limits the transferability of training data across sessions and subjects. The concept of transfer learning focuses on developing algorithms that can improve learning capacity so that the prediction model either learns faster or better on a given data set through exposure to other datasets [147]. Recently, two categories of transfer learning methods have been studied including domain adaptation and rule adaptation methods [146]. Rule adaptation methods require learning a decision boundary for each subject separately. The decision boundary is considered as a random variable. The distribution of this random variable is found using the decision boundaries estimated based on datasets collected from previous subjects. However, for rule adaptation methods to be efficient, a high number of datasets is needed to estimate the distribution of the decision boundary.

In contrast, domain adaptation approaches have been extensively used for BCI applications. These approaches aim at finding a common structure in the data such that one decision boundary can be generalized across subjects. Finding a common structure can be performed either by finding a linear transformation where the data is invariant across all individuals [131] or by using similarity measures to find the top similar datasets to the dataset under test [148].

In this chapter, we propose a domain adaptation based transfer learning approach to reduce the calibration requirements of our multimodal EEG-fTCD BCI utilizing both the MI and flickering MR/WG paradigms through transferring BCI training experience across participants. To evaluate the performance of the proposed approach, we formulated 3 binary selection problems for each presentation paradigm including right arm MI versus baseline, left arm MI versus baseline, right versus left arm MI, MR versus baseline, WG versus baseline, and MR versus WG. As explained in chapters 5.0 and 6.0, common spatial pattern (CSP) and wavelet decomposition were used to extract features from EEG and fTCD data collected using the MI paradigm while template matching and wavelet decomposition were used to extract features from EEG and fTCD data of the flickering MR/WG paradigm.

To apply transfer learning, similarity between the EEG and fTCD data of the current BCI user and those of the previous users has to be measured. To achieve such aim, we reduced feature vectors of EEG and fTCD data of each trial into scalar SVM scores to learn EEG and fTCD class conditional distributions. Similarities across participants were identified based on these class conditional distributions. In particular, we computed Bhattacharyya distance between the class conditional distributions obtained using the training data of the current BCI user and class conditional distributions obtained using datasets collected from the previous BCI users. After

identifying the top similar datasets, we combined the training trials of the current user with trials of these top similar datasets to form a training set that can be used to calibrate the BCI system.

Using the new training set, we evaluated the performance of the system through assessing the test trials of the current BCI user. Depending on which presentation paradigm is presented to the user, we either followed the analysis approaches explained in chapter 5.0 or chapter 6.0. Based on the performance measures obtained in chapter 5.0 and 6.0, it can be noted that the best performance was achieved under assumption A3 for the MI paradigm; therefore, for MI, we utilized the assumption A3 in this chapter. On the other hand, for the flickering WG/MR paradigm, A2 and A3 both had high performance without any statistically significant differences. However, A3 is more computationally complex compared to A2; therefore, for the WG/MR paradigm, we performed probabilistic fusion under assumption A2.

## **9.2 Materials and Methods**

With the aim of decreasing calibration requirements and improving the performance of the hybrid system, we propose a transfer learning approach that identifies the top similar datasets collected from previous BCI users to a training dataset collected from a current BCI user and uses these datasets to augment the training data of the current BCI user. The proposed transfer learning approach is intended to be used for both the MI and flickering MR/WG paradigms. Therefore, the performance of the proposed approach was tested using the 6 binary selection problems of both paradigms.

### 9.2.1 Similarity Measure

To apply transfer learning to a certain binary selection problem, for each dataset from previous BCI users, EEG and fTCD feature vectors of trials corresponding to that problem were projected into scalar SVM scores. Therefore, each trial was represented by a scalar EEG SVM score and a scalar fTCD SVM score. Using KDE, 2 EEG class conditional distributions and 2 fTCD class conditional distributions were learnt from these scores. KDE was performed using gaussian kernel. EEG and fTCD class conditional distributions of the current BCI user were also estimated using his/her training trials.

To measure the similarity between the class conditional distributions of the current BCI user and those of the previous users, Bhattacharyya distance [149], given by (19), was used since it is a symmetric measure that can be applied to general distributions especially if these distributions are diverging from normal distributions and it provides bounds on Bayesian misclassification probability, which overall fits very well to our approach of making Bayesian decisions on binary classification problems using the estimated density functions.

$$d = -\ln \sum_{i=1}^N P_i Q_i \quad (19)$$

where  $P$  and  $Q$  are 2 probability distributions and  $N$  is the number of points composing each distribution.

Bhattacharyya distance between the EEG class conditional distribution of class  $i$  ( $i=1,2$ ) and the corresponding EEG class conditional distribution of the current BCI user were calculated. Bhattacharyya distance was also calculated between the fTCD class conditional distributions of each previous BCI user and the current BCI user. The sum of these 4 distances (2 EEG distances and 2 fTCD distances) represented the total distance between the current BCI user and a certain

previous BCI user. distances and 2 fTCD distances) represented the total distance between the current BCI user and a certain previous BCI user.

### **9.2.2 Proposed Transfer Learning Algorithm**

The proposed transfer learning approach is described in detail in Fig. 34 and Fig. 35. Given a group of previous BCI users where each user is represented by one dataset, the objective is to find the most similar datasets to the training dataset of the current BCI user and to combine the trials from these datasets with small number of training trials from the current user to train a classifier that can predict the labels of the test trials of that user with high accuracy. In particular, for each binary selection problem, the dataset of the current user was divided into training and testing sets. Initially, given that each binary selection problem is represented by 100 trials, we used the first 10 trials from the current BCI user for training the prediction model and the remaining 90 trials for testing. As seen in Fig. 34, features are extracted from training trials of the current user as well as the trials corresponding to the binary problem of interest from each of the previous BCI users. Extracted EEG and fTCD features vary depending on the paradigm used for data collection. In particular, CSP and wavelet decomposition were used to extract features from the MI paradigm while the flickering MR/WG paradigm employed template matching and wavelet decomposition for data analysis as explained in chapters 6.0 and 7.0. EEG and fTCD feature vectors of each trial were projected into 2 scalar SVM scores.

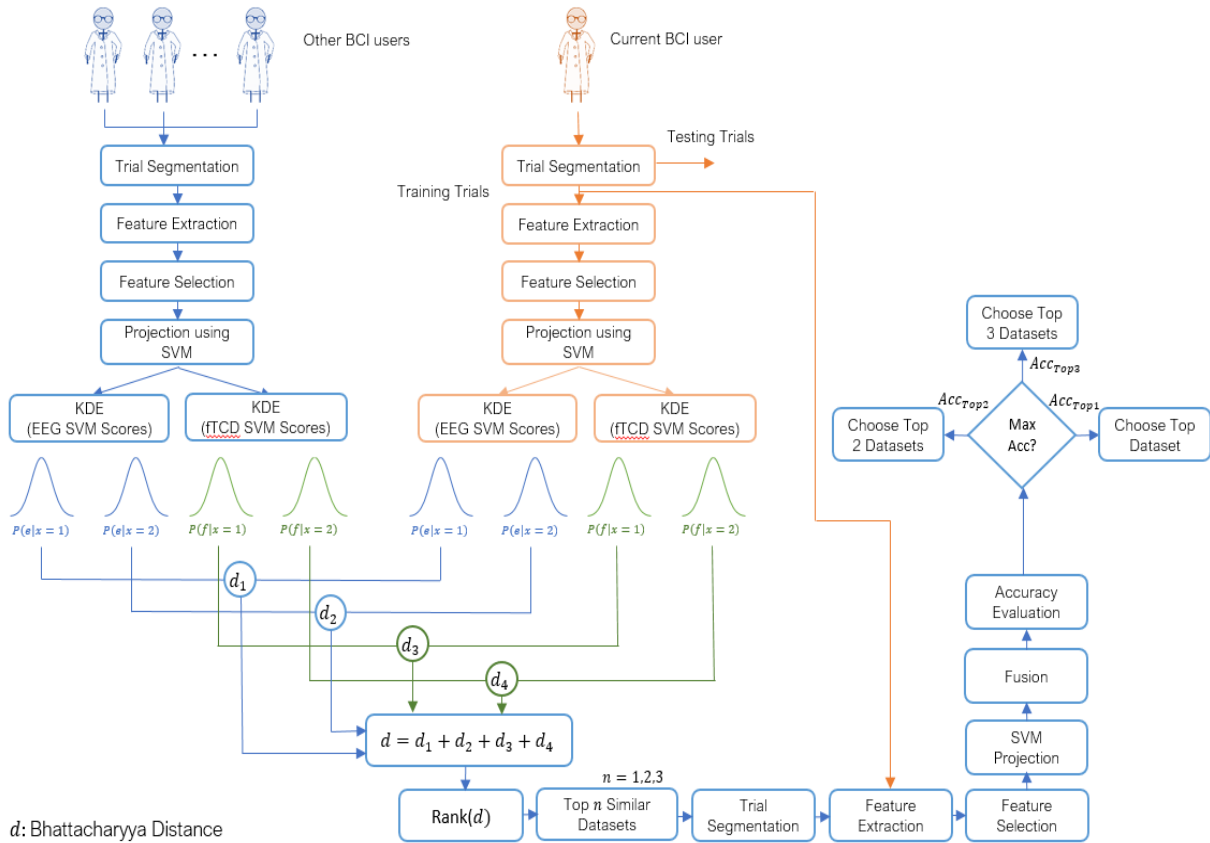


**Figure 34 Identifying the top similar datasets using the proposed transfer learning approach.**

For each class within the binary selection problem of interest, we learnt class conditional distributions of the EEG and fTCD scores obtained from SVM projection as seen in Fig. 34. The distance between class conditional distributions of the current BCI user and those of each of the previous BCI users was computed as explained in section 9.2.1. To identify the top similar datasets, these distances were sorted ascendingly. At this point, it was required to decide on how many similar datasets should be considered to train the classifier besides the training trials from the current BCI user. Here, we considered a maximum of 3 datasets to be combined with the training trials of the current BCI user. Through cross validation, the number of top similar datasets that maximize the performance accuracy when combined with the training trials of the current user was

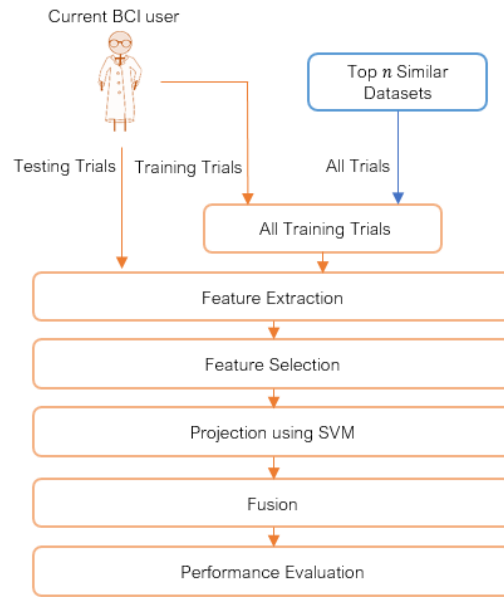


**Figure 35 Testing phase of the proposed transfer learning approach.**

chosen to be used later to predict test trials of the current BCI user as shown in Fig. 35. Here, for each participant, we used up to 3 datasets to be used for transfer learning. However, the maximum number of datasets could be increased or decreased depending on the needs of the designers. Moreover, the presented framework could be used to identify person-specific maximum number of datasets. For future versions of this algorithm, instead of using a maximum of 3 datasets to be combined with the training trials of the current BCI, such number can be optimized for each subject separately by means of model order selection techniques [150].

To study the impact of the training set size (from the current BCI user) on the performance of the proposed transfer learning approach, we applied the proposed approach on training sets of size ranging from 10 to 90 trials which corresponds to test sets of size ranging from 90 to 10 trials.

### 9.2.3 Performance Evaluation

For both the MI and flickering MR/WG paradigms, to assess the significance of the transfer learning (TL) compared to the no transfer learning case (NTL), for each participant, accuracy and ITR were calculated and compared at different number of training trials from the current BCI user. In particular, at every number of training trials, accuracy and ITR were calculated at time points 1, 2, ..., 10 s. For each number of training trials, maximum accuracy and ITR across the 10-s period (trial length) were reported for TL and NTL cases.

To compute the reduction in calibration requirements for each binary problem when using TL compared to the NTL case, at each training set size, we formed a vector containing performance accuracies obtained for all participant at that training set size. We statistically compared the accuracy vectors of TL at training set sizes of 10, 20, ..., 90 with accuracy vector obtained for the NTL case at maximum training set size (90 trials). Initially, at 10 training trials, we performed a one-sided Wilcoxon signed rank test between the accuracy vector of TL with 10 training trials and NTL accuracy vector at 90 training trials. Such statistical comparison is repeated with TL applied at bigger training set sizes until there is no statistically significant difference between the performance of TL and the performance of NTL at 90 trials. The number of trials N at which that statistical insignificance occurs is used in (20) to compute percentage of reduction.

$$\text{Reduction \%} = \frac{1}{P} \sum_{i=1}^P \frac{\text{Calibration Length}_{NTL}(i) - \text{Calibration Length}_{TL}(i)}{\text{Calibration Length}_{NTL}(i)} \times 100\% \quad (20)$$

Eq (20) is equivalent to:

$$\text{Reduction \%} = \frac{1}{P} \sum_{i=1}^P \frac{N \times \text{Trial Length}_N(i)|_{NTL} - m \times \text{Trial Length}_m(i)|_{TL}}{N \times \text{Trial Length}_N(i)|_{NTL}} \times 100\% \quad (21)$$

where  $N$  is the maximum number of training trials ( $N=90$ ) from the current BCI user and  $m$  is the minimum number of trials at which TL performance is at least equivalent to NTL performance where  $m$  ranges from 10 to 90 trials.

To guarantee that TL will improve or at least achieve the same average performance accuracy obtained for the NTL case, we checked if the TL average performance accuracy at  $m$  training trials was similar to or outperforms the average performance accuracy of the NTL case at 90 training trials. If this condition is not satisfied, we consider statistical comparisons at training set sizes  $> m$  until this condition is satisfied.

### 9.3 Results

For both the MI and flickering MR/WG paradigms, to evaluate the effectiveness of the proposed TL approach, for each binary selection problem, we reported the average accuracies and ITRs across participants obtained using different training set sizes. Moreover, we compare these accuracies/ITRs with those obtained without transfer learning. Fig. 36-41 reflect the impact of the amount of data available to train a prediction model on the accuracy/ITR that can be obtained with and without transfer learning. In particular, the x-axis shows the number of training trials, ranging from 10 to 90 trials, used to train a prediction model, while the y axis shows the average accuracy/ITR across participants corresponding to those training trials.

For both TL and NTL cases, at each training set size, a classifier is trained, and its performance is evaluated for each participant at trial lengths of 1, 2...10 seconds. The maximum accuracy/ITR at each training set size is reported regardless of the corresponding trial length. The average accuracy/ITR is computed across all participants at different training set sizes. Therefore,

in terms of calibration requirements, comparing the best possible performances obtained for TL and NTL cases is not entirely fair since these performances are not evaluated at the same calibration length. In particular, calibration length is not only a function of the number of training trials, but also is a function of trial length which varies depending on when maximum accuracy/ITR could be achieved. Therefore, as seen in Fig. 36-41, to ensure fair comparison, in addition to reporting the best possible TL and NTL performances, we evaluated the performance of NTL at the same trial lengths that yield the maximum possible TL performance. In addition, we evaluated the performance of TL and the same trial lengths that yield the maximum NTL performance.

### **9.3.1 MI Paradigm**

As seen in Fig. 36-38, the TL performance evaluated at the trial lengths that yield the maximum NTL performance is similar to the maximum NTL performance while the performance of NTL at the same trial lengths that yield the maximum possible TL performance is significantly worse than the maximum TL performance. Disregarding differences in trial length, average accuracies obtained using TL are significantly higher than those obtained without transfer learning (NTL) as shown in Fig. 36-38. Moreover, in terms of ITRs, it can be also noted that TL provides the highest ITRs compared to the NTL case.

In addition, we observed that, when TL is employed, using only 10 training trials, average accuracies of 80.58%, 75.29%, and 69.16% can be achieved for right MI versus baseline, left MI versus baseline, and right MI versus left MI, while for the NTL case, the average accuracies that can be obtained using 10 training trials are 56.63%, 58.14%, and 60.21%, respectively. In terms of ITRs, at 10 training trials, it can be noted that right MI versus baseline, left MI versus baseline,

and right MI versus left MI achieved average ITRs of 2.34, 2.13, and 2.98 bits/min, respectively compared to 1.51, 0.54, and 1.74 bits/min obtained for the NTL case.

Using 90% of the available data for training which corresponds to 90 training trials, TL achieved accuracies of 98.89%, 98.00%, and 94.67% and ITRs of 16.5, 20.51, and 11.3 bits/min for right MI versus baseline, left MI versus baseline, and right MI versus left MI, respectively compared to of accuracies of 80.00%, 78.33%, and 76.67% and ITRs of 7.83, 7.04, and 6.27 bits/min achieved without TL.

Using (21), we found that the calibration requirements for MI paradigm can be reduced by 80.00%, 60.43%, and 81.99% for right MI versus baseline, left MI versus baseline, and right MI versus left MI, respectively.

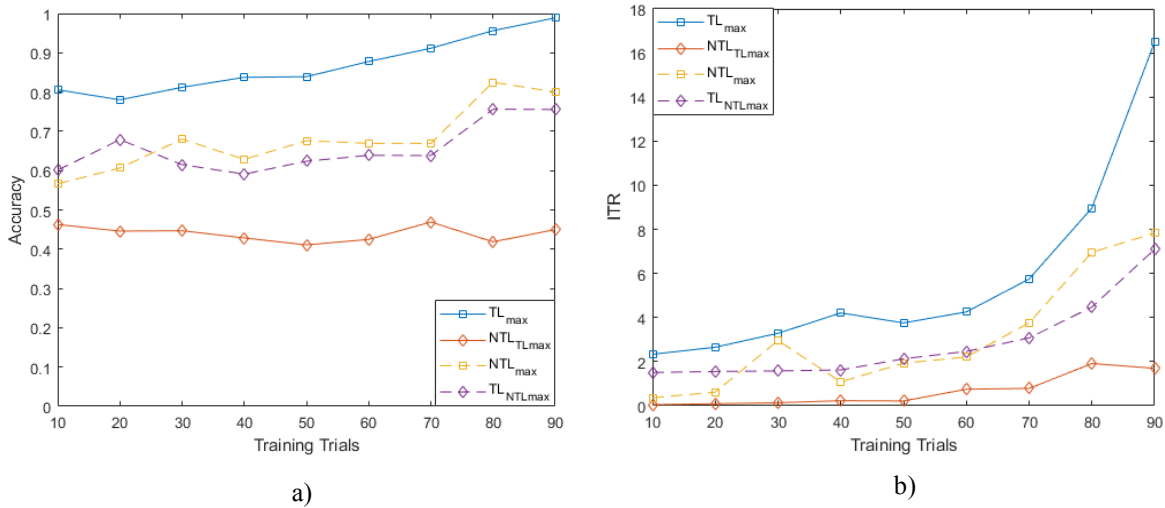
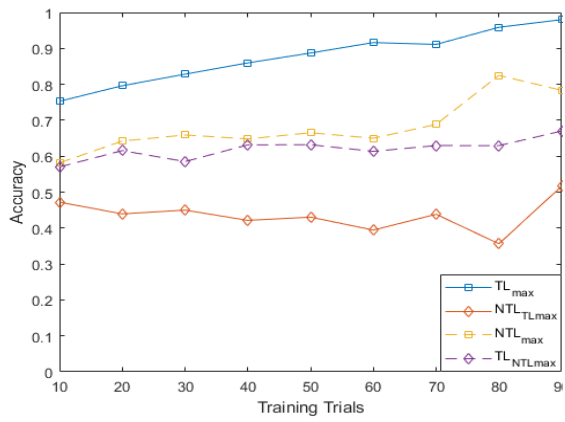
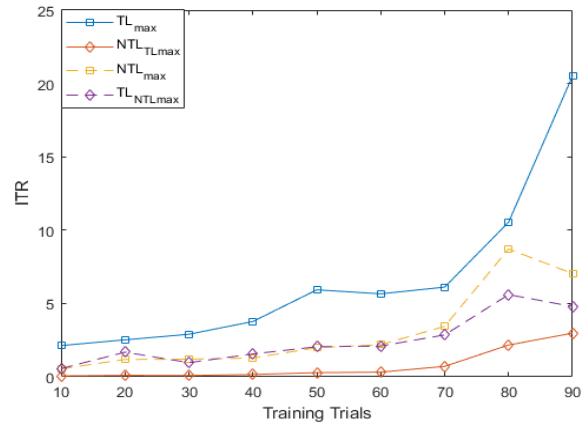


**Figure 36** Average accuracy (a) and average ITR (b) as a function of the number of training trials for right MI versus baseline problem.

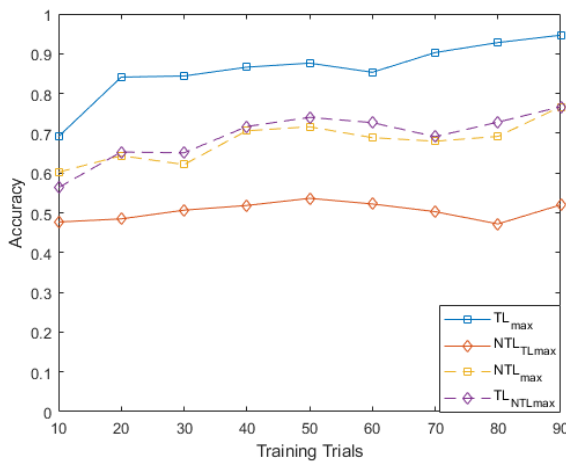


a)

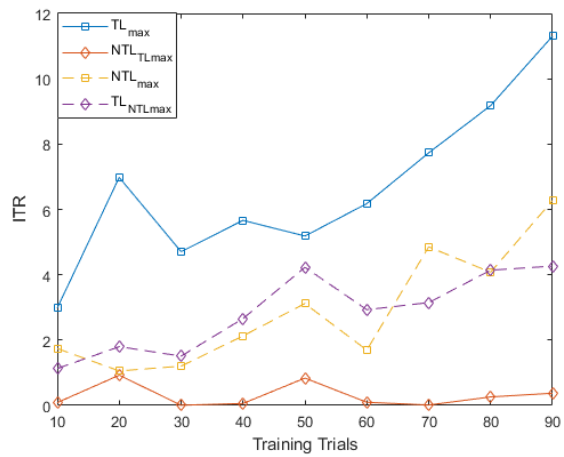


b)

**Figure 37 Average accuracy (a) and average ITR (b) as a function of the number of training trials for left MI versus baseline problem.**



a)



b)

**Figure 38 Average accuracy (a) and average ITR (b) as a function of the number of training trials for right MI versus left MI problem.**

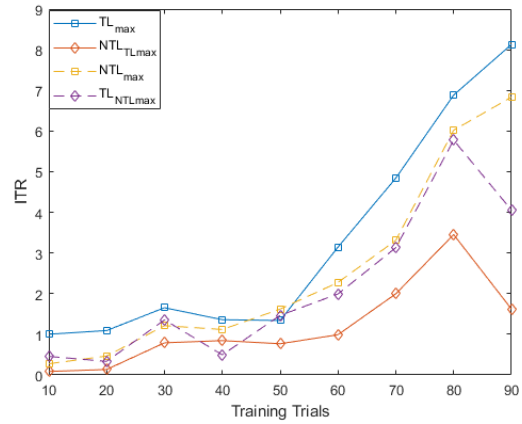
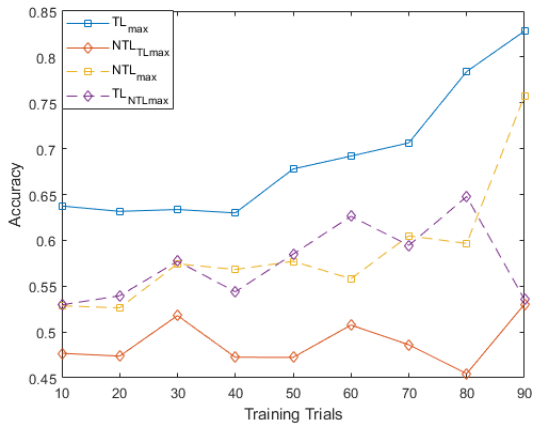
### 9.3.2 Flickering MR/WG paradigm

Fig. 39-41 show that the TL performance evaluated at the trial lengths yielding the maximum NTL performance is comparable to the maximum NTL performance while the performance of NTL at the same trial lengths yielding the maximum possible TL performance is significantly worse than the maximum TL performance. Disregarding trial length, for the 3 binary selection problems, average accuracy and ITR trends obtained using TL are significantly higher than those obtained without transfer learning (NTL) especially at smaller training set sizes as shown in Fig. 39-41. However, for the WG versus baseline problem, we observed that ITRs obtained using TL outperform those obtained without TL for training set sizes  $<50$  trials.

We observed also that when the training set size drops to 10 trials, transfer learning provides an improvement in the accuracy by approximately 11%, 5%, and 7% for MR versus baseline, WG versus baseline, and MR versus WG. In terms of ITRs, at 10 training trials, 1, 0.37, and 0.71 bits/min were obtained for MR versus baseline, WG versus baseline, and MR versus WG using TL, while without TL, 0.28, 0.29, and 0.17 bits/min were achieved for the same classification problems.

Using 90 training trials, TL achieved 82.83%, 79.09%, and 80.00% average accuracies and 8.13, 10.66, and 15.28 bits/min average ITRs MR for versus baseline, WG versus baseline, and MR versus WG, respectively, while NTL obtained 75.76%, 80.52%, and 69.97% average accuracies and 6.83, 11.13, 6.55 bits/min average ITRs for the same classification problems.

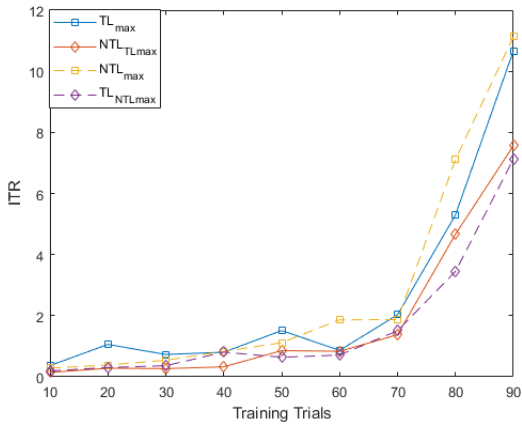
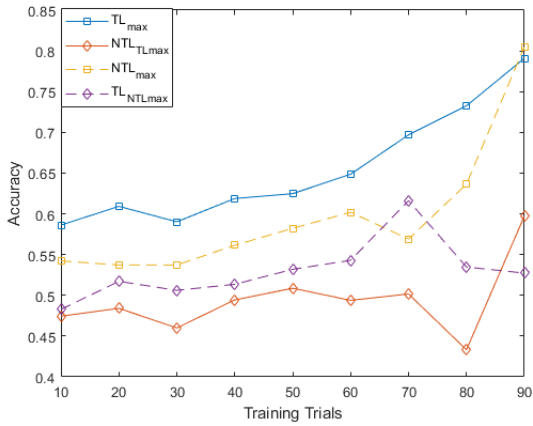
Using (21), we found that the calibration requirements for flickering MR/WG paradigm can be reduced by 17.31% and 12.96% for MR versus baseline and MR versus WG, respectively while for WG versus baseline, TL approach only boosted the performance accuracy without reducing the calibration requirement.



a)

b)

**Figure 39 Average accuracy (a) and average ITR (b) as a function of the number of training trials for MR versus baseline problem.**



a)

b)

**Figure 40 Average accuracy (a) and average ITR (b) as a function of the number of training trials for WG versus baseline problem.**

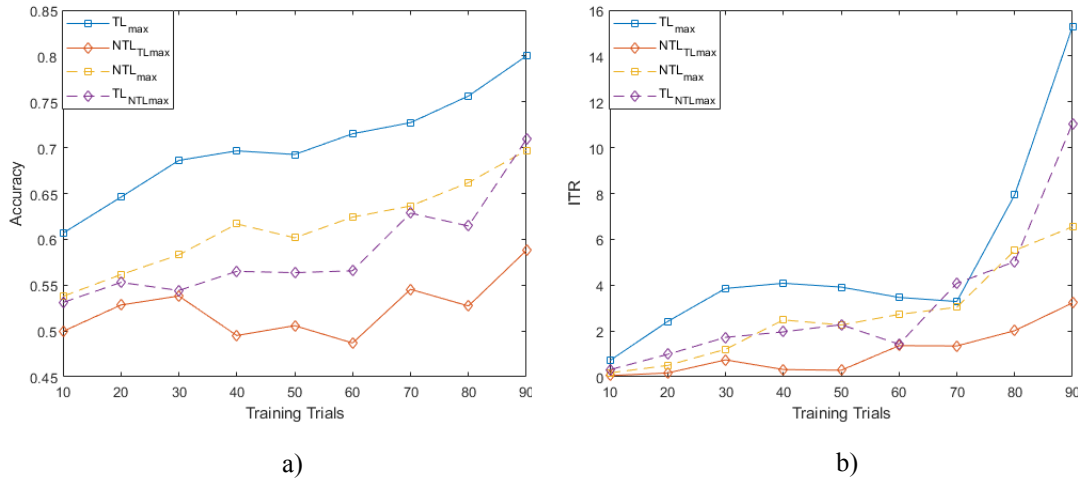


**Figure 41 Average accuracy (a) and average ITR (b) as a function of the number of training trials MR versus WG problem.**

## 9.4 Discussion

For the MI paradigm, it can be concluded that, using 10 training trials, TL can improve the average performance accuracy by 9-24% for the 3 binary selection problems compared to the NTL case, while using 100% of the available training data (90 trials), the performance of NTL case can be enhanced by 18-20% for the 3 classification problems. Moreover, ITRs obtained using TL at 10 training trials are 1.8-2.90 times the ITRs obtained without TL, while at 90 training trials, ITRs of TL case are 1.5-3.94 times the ITRs obtained without TL.

As for the MR/WG paradigm, at 10 training trials, improvements ranging from 5 to 11% in average accuracy as well as ITRs that are 1.28- 4.18 times ITRs of NTL case can be achieved for MR versus baseline and MR versus WG. At 90 training trials, performance can be enhanced

by 7-10% average accuracy with 1.19-2.33 times ITRs of NTL case. However, there is no improvement in performance for the WG versus baseline problem when using 100% of the available training data.

Comparing the average accuracies and ITRs obtained using both paradigms as well as their average accuracy and ITR improvements compared to the NTL case especially at 10 training trials, it can be concluded that the proposed transfer learning algorithm is more efficient when used with the MI paradigm. Therefore, TL can be used to reduce the calibration requirements of the system while maintaining sufficient performance that is comparable to NTL performance with a higher number of training trials. For instance, given only 10 training trials from the current BCI user who uses the MI paradigm, accuracies ranging from 70% to 80% can be achieved for the 3 classification problems when using the proposed transfer learning approach. This corresponds to a maximum of 100 seconds calibration length.

Considering the trade-off between the calibration length and the corresponding BCI performance, it is the BCI designer's decision to choose the optimal number of trials to be recorded from each BCI user to calibrate the system. Given that the proposed transfer learning approach has significantly reduced the calibration requirements of the MI-based hybrid BCI by at least 60.43%, we believe that our proposed approach gives more flexibility to the BCI designers to control and reduce the calibration requirements of the system which is an important criterion especially when the BCI is intended to be used by patients with disabilities.

## 9.5 Conclusion

In this chapter, aiming at reducing the calibration requirements as well as improving the BCI performance, we propose a transfer learning approach that identifies the top similar datasets to the current BCI user and combines the trials from these datasets as well as few training trials from the current user to train a classifier that can predict the test trials of that user with high accuracy. To achieve such aim, EEG and fTCD feature vectors of each trial were projected into two scalar SVM scores. EEG and fTCD class conditional distributions were learnt separately using the scores of each class. Bhattacharyya distance was used to identify similarities between class conditional distributions obtained using training trials of the current BCI user and those obtained using trials of previous BCI users. Experimental results showed that the performance obtained using the proposed transfer learning approach outperforms the performance obtained without transfer learning for both the MI and flickering MR/WG paradigms. However, comparing the performance improvement achieved for both paradigms, it can be noted that the proposed transfer learning algorithm is more efficient when used with the MI paradigm. In particular, average accuracies and ITRs of 80.58%, 75.29%, and 69.16% and 2.34, 2.13, and 2.98 bits/min can be achieved for right MI versus baseline, left MI versus baseline, and right MI versus left MI using 10% of the available data which corresponds to a calibration length of 100 seconds. Moreover, it was found that the calibration requirements of the MI paradigm can be reduced by at least 60.43% when using the proposed transfer learning approach.

## 10.0 Conclusions

In this dissertation, we investigated the possibility of developing 2-class and 3-class fTCD BCI systems and proved that fTCD is a viable candidate for real-time BCIs as it achieved accuracies of approximately 80% and 60% for binary and 3-class BCIs within 3 and 5 s, respectively. Inspired by these findings, we introduced a novel hybrid BCI system that uses electrical brain activity recorded using EEG as well as cerebral blood flow velocity measured using fTCD. This hybrid BCI was designed using two different paradigms. The first paradigm was based on motor imagery (MI) to induce changes simultaneously in EEG and fTCD, while the other system simultaneously utilized mental rotation (MR) and word generation (WG) as stimuli for fTCD and flickering checkerboards to induce SSVEPs in EEG.

To evaluate the performance of both paradigms, we collected data from 21 healthy participants. As a preliminary analysis, features derived from the power spectrum of EEG and fTCD signals were extracted. Mutual information and linear SVM were employed for feature selection and classification. Using the MI paradigm, the EEG-fTCD combination achieved average accuracies of 88.33%, 89.48%, and 82.38% for right arm MI versus baseline, left arm MI versus baseline, and right arm MI versus left arm MI, respectively. In addition, average information transfer rates (ITR) of 4.17, 5.45, and 10.57 bits/min were achieved. As for the flickering MR/WG paradigm, the EEG-fTCD combination obtained accuracies of 89.11%, 80.88%, and 92.38% for MR versus baseline, WG versus baseline, and MR versus WG, respectively. Average ITRs of 4.39, 3.92, 5.60 bits/min were obtained. Compared to the existing work on hybrid BCI that combines EEG with fNIRS, the proposed hybrid system with both paradigms showed important progress towards making such systems real-world-worthy in terms of speed and accuracy.

However, the system has a limitation since the temporal resolution of fTCD is lower than EEG resulting in longer trial lengths that decrease the speed of the system. Such mismatch between the temporal resolution of these modalities can be minimized by introducing advanced analysis techniques for fTCD data to improve the obtained accuracy within the minimum possible task period. To achieve such aim, wavelet decomposition was employed for fTCD analysis since it was used in a previous study (see chapter 3.0) to prove that fTCD is a viable candidate for real-time BCIs.

In addition, to improve both the accuracy and ITR of this novel hybrid BCI, we proposed an EEG-fTCD feature fusion approach and investigated analysis techniques for EEG data of both paradigms. In particular, we proposed a probabilistic fusion of EEG and fTCD evidences instead of simple concatenation of EEG and fTCD feature vectors. Through such a probabilistic fusion, the contributions of each modality towards the correct decision can be optimized. For the MI paradigm, we used common spatial pattern algorithm and wavelet decomposition to extract EEG and fTCD features, respectively, while for the MR/WG paradigm, we used template matching and wavelet decomposition to extract EEG and fTCD features.

Experimental results showed that 93.85%, 93.71%, and 100% average accuracies and 19.89, 26.55, and 40.83 bits/min average ITRs were achieved for right MI vs baseline, left MI versus baseline, and right MI versus left MI, respectively. As for the MR/WG paradigm, average accuracies of 85.29%, 86.27%, and 98.11%, and average ITRs of 8.34, 8.95, and 21.29 bits/min were achieved for WG versus baseline, MR versus baseline, and WG versus MR, respectively. Considering these results, it can be concluded that MI paradigm outperforms MR/WG one in terms of both accuracy and ITR. Moreover, for both paradigms, the EEG-fTCD BCI with the proposed analysis techniques outperforms all EEG-fNIRS BCIs in comparison in terms of accuracy and ITR.

With the aim of increasing the possible number of commands that can be issued through the proposed BCI, we extended our feature extraction and analysis approaches to solve the 3-class problem of each paradigm. It was found that hybrid combination of the MI paradigm is more efficient than the hybrid combination employing the flickering MR/WG paradigm in terms of both accuracy and ITR. In particular, average accuracy of 96.58% and average ITR of 43.59 bits/min were achieved using the MI paradigm compared to 90.60% average accuracy and 25.70 bits/min average ITR obtained using the flickering MR/WG paradigm.

Finally, the generalization of the system across subjects was explored using a transfer learning approach that we proposed to decrease the calibration requirements of both paradigms. The proposed approach was shown to be more successful with data collected through the MI paradigm. In particular, it was found that the calibration requirements can be reduced by at least 60.43% for the MI paradigm, while at most a reduction of 17.31% can be achieved for the flickering MR/WG paradigm.

Considering the analysis results mentioned above, it can be noted that the MI paradigm outperformed the flickering MR/WG paradigm for both binary and 3-class selection problems. Moreover, data collected through the MI paradigm showed better generalization across subjects, therefore, the proposed transfer learning approach was able to significantly reduce the calibration requirements. Consequently, it can be concluded that the proposed hybrid system using the MI paradigm is a more viable candidate for real-time BCI applications. In addition to these significant results, the proposed system is portable and cost-effective compared to the other multimodal BCIs that exploit multimodal brain activity such as EEG-fMRI, EEG-MEG, and EEG-fNIRS BCIs. Moreover, the proposed system is easier to setup (in terms of number of sensors) and faster (in terms of trial length) compared to hybrid BCIs that utilize EEG and fNIRS simultaneously.

## Appendix

In Tables 30-35, we introduce the detailed performance measures of each individual including maximum accuracy and the corresponding sensitivity, specificity, and time for the 3 classification problems solved using both subject-independent and subject-specific thresholds.

**Table 30 Maximum accuracy (Acc) and the corresponding sensitivity (Se), specificity (Sp), and time for each subject using hybrid system, EEG only, and fTCD only. These measures were obtained for right arm MI vs baseline problem using subject-independent threshold.**

Sub_ID	Time(s)	Se Hybrid	Sp Hybrid	Acc Hybrid	Se EEG	Sp EEG	Acc EEG	Se TCD	Sp fTCD	Acc fTCD
1	10	98.08%	88.64%	<b>93.75%</b>	96.15%	86.36%	91.67%	55.77%	59.09%	57.29%
2	10	82.69%	84.09%	83.33%	82.69%	84.09%	83.33%	67.31%	43.18%	56.26%
3	2	84.62%	84.09%	<b>84.38%</b>	80.77%	77.27%	79.17%	55.77%	34.09%	45.83%
4	9	92.31%	81.82%	<b>87.50%</b>	90.38%	70.45%	81.25%	63.46%	45.45%	55.21%
5	9	92.31%	88.64%	<b>90.63%</b>	90.38%	84.09%	87.50%	63.46%	59.09%	61.46%
6	4	82.69%	81.82%	<b>82.29%</b>	78.85%	65.91%	72.92%	61.54%	50.00%	56.25%
7	6	90.38%	75.00%	<b>83.33%</b>	80.77%	77.27%	79.17%	55.77%	56.82%	56.25%
8	7	92.31%	86.36%	<b>89.58%</b>	84.62%	75.00%	80.21%	69.23%	63.64%	66.67%
9	5	65.38%	79.55%	71.88%	78.85%	68.18%	73.96%	53.85%	70.45%	61.46%
10	10	92.31%	88.64%	<b>90.63%</b>	88.46%	84.09%	86.46%	65.38%	75.00%	69.79%
<b>Mean</b>	7.2	<b>87.31%</b>	<b>83.86%</b>	<b>85.73%</b>	85.19%	77.27%	81.56%	61.15%	55.68%	58.65%

**Table 31 Maximum accuracy (Acc) and the corresponding sensitivity (Se), specificity (Sp), and time for each subject using hybrid system, EEG only, and fTCD only. These measures were obtained for right arm MI vs baseline problem using subject-specific thresholds.**

Sub_ID	Time(s)	Se Hybrid	Sp Hybrid	Acc Hybrid	Se EEG	Sp EEG	Acc EEG	Se fTCD	Sp fTCD	Acc fTCD
1	10	98.08%	90.91%	<b>94.79%</b>	92.31%	90.91%	91.67%	55.77%	63.64%	59.38%
2	7	96.15%	88.64%	<b>92.71%</b>	94.23%	88.64%	91.67%	88.46%	29.55%	61.46%
3	7	84.62%	88.64%	<b>86.46%</b>	78.85%	84.09%	81.25%	48.08%	54.55%	51.04%
4	9	92.31%	81.82%	<b>87.50%</b>	90.38%	70.45%	81.25%	63.46%	45.45%	55.21%
5	9	92.31%	88.64%	<b>90.63%</b>	90.38%	84.09%	87.50%	63.46%	59.09%	61.46%
6	7	88.64%	84.09%	<b>86.46%</b>	86.54%	84.09%	85.42%	67.31%	43.18%	56.25%
7	6	92.31%	79.55%	<b>86.46%</b>	84.62%	75.00%	80.21%	46.15%	50.00%	47.92%
8	7	96.15%	86.36%	<b>91.67%</b>	84.62%	77.27%	81.25%	73.08%	65.91%	69.79%
9	5	76.92%	75.00%	<b>76.04%</b>	78.85%	63.64%	71.88%	48.08%	52.27%	50.00%
10	10	92.31%	88.64%	<b>90.63%</b>	88.46%	84.09%	86.46%	65.38%	75.00%	69.79%
<b>Mean</b>	<b>7.7</b>	<b>90.96%</b>	<b>85.23%</b>	<b>88.33%</b>	<b>86.92%</b>	<b>80.23%</b>	<b>83.85%</b>	<b>61.92%</b>	<b>53.86%</b>	<b>58.23%</b>

**Table 32 Maximum accuracy (Acc) and the corresponding sensitivity (Se), specificity (Sp), and time for each subject using hybrid system, EEG only, and fTCD only. These measures were obtained for left arm MI vs baseline problem using subject-independent threshold.**

Sub_ID	Time(s)	Se	Sp	Acc	Se	Sp	Acc	Se	Sp	Acc
		Hybrid	Hybrid	Hybrid	EEG	EEG	EEG	fTCD	fTCD	fTCD
1	10	92.45%	95.45%	<b>93.81%</b>	86.79%	90.91%	88.66%	77.36%	70.45%	74.23%
2	7	94.34%	90.91%	92.78%	96.23%	90.91%	93.81%	77.36%	36.36%	58.76%
3	8	86.79%	93.18%	<b>89.69%</b>	81.13%	79.55%	80.41%	39.62%	54.55%	46.39%
4	2	73.58%	75.00%	<b>74.23%</b>	75.47%	70.45%	73.32%	58.49%	40.91%	50.52%
5	8	83.02%	77.27%	<b>80.41%</b>	79.25%	75.00%	77.32%	30.19%	59.09%	43.30%
6	2	92.45%	79.55%	<b>86.60%</b>	92.45%	77.27%	85.57%	64.15%	38.64%	52.58%
7	3	90.57%	90.91%	<b>90.72%</b>	88.68%	88.64%	88.66%	58.49%	50.00%	54.64%
8	9	90.57%	86.36%	<b>88.66%</b>	88.68%	84.09%	86.60%	49.06%	63.64%	55.67%
9	5	83.02%	75.00%	<b>79.38%</b>	75.47%	72.73%	74.23%	56.60%	38.64%	48.45%
10	9	88.68%	88.64%	<b>88.66%</b>	86.79%	88.64%	87.63%	52.83%	59.09%	55.67%
<b>Mean</b>	<b>6.3</b>	<b>87.55%</b>	<b>85.23</b>	<b>86.49%</b>	<b>85.09%</b>	<b>81.82%</b>	<b>83.61%</b>	<b>56.42%</b>	<b>51.14%</b>	<b>54.02%</b>

**Table 33 Maximum accuracy (Acc) and the corresponding sensitivity (Se), specificity (Sp), and time for each subject using hybrid system, EEG only, and fTCD only. These measures were obtained for left arm MI vs baseline problem using subject-specific thresholds.**

Sub_ID	Time(s)	Se Hybrid	Sp Hybrid	Acc Hybrid	Se EEG	Sp EEG	Acc EEG	Se fTCD	Sp TCD	Acc fTCD
1	10	100.00%	95.45%	<b>97.94%</b>	88.68%	86.36%	87.63%	64.15%	68.18%	65.98%
2	7	96.23%	90.91%	<b>93.81%</b>	92.45%	90.91%	91.75%	92.45%	34.09%	65.98%
3	4	94.34%	93.18%	<b>93.81%</b>	86.79%	75.00%	81.44%	43.40%	61.36%	51.55%
4	5	86.79%	75.00%	<b>81.44%</b>	84.91%	70.45%	78.35%	69.81%	52.27%	61.86%
5	9	86.79%	88.64%	87.63%	84.91%	90.91%	87.63%	58.49%	47.73%	53.61%
6	3	88.68%	84.09%	<b>86.60%</b>	75.47%	72.73%	74.23%	56.60%	50.00%	53.61%
7	3	90.57%	90.91%	<b>90.72%</b>	88.68%	88.64%	88.66%	58.49%	50.00%	54.64%
8	9	96.23%	88.64%	<b>92.78%</b>	92.45%	77.27%	85.57%	56.60%	43.18%	50.52%
9	5	83.02%	75.00%	<b>79.38%</b>	75.47%	72.73%	74.23%	56.60%	38.64%	48.45%
10	6	96.23%	84.09%	90.72%	94.34%	88.64%	91.75%	45.28%	50.00%	47.42%
<b>Mean</b>	<b>6.1</b>	<b>91.89%</b>	<b>86.59%</b>	<b>89.48%</b>	<b>86.42%</b>	<b>81.36%</b>	<b>84.12%</b>	<b>60.19%</b>	<b>49.55%</b>	<b>55.36%</b>

**Table 34 Maximum accuracy (Acc) and the corresponding right arm and left arm sensitivities (SeR, and SeL), and time for each subject using hybrid system, EEG only, and fTCD only. These measures were obtained for right arm MI vs left arm MI problem using subject-independent threshold.**

Sub_ID	Time(s)	SeR Hybrid	SeL Hybrid	Acc Hybrid	SeR EEG	SeL EEG	Acc EEG	SeR fTCD	SeL fTCD	Acc fTCD
1	1	88.46%	84.91%	86.67%	88.46%	84.91%	86.67%	40.38%	49.06%	44.76%
2	5	73.08%	77.36%	75.24%	75.00%	75.47%	75.24%	50.00%	26.42%	38.10%
3	10	78.85%	71.70%	<b>75.24%</b>	76.92%	69.81%	73.33%	59.62%	33.96%	46.67%
4	1	86.54%	81.13%	<b>83.81%</b>	82.69%	83.02%	82.86%	59.62%	32.08%	45.71%
5	1	78.85%	84.91%	<b>81.90%</b>	76.92%	79.25%	78.10%	34.62%	66.04%	50.48%
6	3	82.69%	84.91%	83.81%	84.62%	86.79%	85.71%	46.15%	39.62%	42.86%
7	4	71.15%	71.70%	71.43%	73.08%	77.36%	75.24%	46.15%	43.40%	44.76%
8	7	94.23%	90.57%	<b>92.38%</b>	88.46%	90.57%	89.52%	51.92%	39.62%	45.71%
9	1	71.15%	71.70%	<b>71.43%</b>	76.92%	64.15%	70.48%	44.23%	45.28%	44.76%
10	1	65.38%	71.70%	<b>68.57%</b>	57.69%	73.58%	65.71%	73.08%	52.83%	62.86%
<b>Mean</b>	<b>3.4</b>	<b>79.04%</b>	<b>79.06%</b>	<b>79.05%</b>	<b>78.08%</b>	<b>78.49%</b>	<b>78.29%</b>	<b>50.58%</b>	<b>42.83%</b>	<b>46.67%</b>

**Table 35 Maximum accuracy (Acc) and the corresponding right arm and left arm sensitivities (SeR, and SeL), and time for each subject using hybrid system, EEG only, and fTCD only. These measures were obtained for right arm MI vs left arm MI problem using subject-specific thresholds.**

Sub_ID	Time(s)	SeR	SeL	Acc	SeR	SeL	Acc	SeR	SeL	Acc
		Hybrid	Hybrid	Hybrid	EEG	EEG	EEG	fTCD	fTCD	fTCD
1	1	94.23%	92.45%	<b>93.33%</b>	82.69%	83.02%	82.86%	55.77%	47.17%	51.43%
2	5	73.08%	77.36%	75.24%	75.00%	75.47%	75.24%	50.00%	26.42%	38.10%
3	6	78.85%	84.91%	<b>81.90%</b>	71.15%	71.70%	71.43%	67.31%	71.70%	69.52%
4	2	86.54%	84.91%	<b>85.71%</b>	84.62%	79.25%	81.90%	63.46%	43.40%	53.33%
5	1	78.85%	84.91%	<b>81.90%</b>	76.92%	79.25%	78.10%	34.62%	66.04%	50.48%
6	3	82.69%	84.91%	83.81%	84.62%	86.79%	85.71%	46.15%	39.62%	42.86%
7	4	84.62%	73.58%	<b>79.05%</b>	71.15%	71.70%	71.43%	36.54%	50.94%	43.81%
8	9	98.08%	96.23%	<b>97.14%</b>	98.08%	94.34%	96.19%	50.00%	50.00%	50.00%
9	1	71.15%	71.70%	<b>71.43%</b>	76.92%	64.15%	70.48%	44.23%	45.28%	44.76%
10	2	73.08%	75.47%	<b>74.29%</b>	65.38%	60.38%	62.86%	76.92%	56.60%	66.67%
<b>Mean</b>	<b>3.4</b>	<b>82.12%</b>	<b>82.64%</b>	<b>82.38%</b>	<b>78.65%</b>	<b>76.60%</b>	<b>77.62%</b>	<b>52.50%</b>	<b>49.72%</b>	<b>51.10%</b>

## Bibliography

- [1] L. F. Nicolas-Alonso and J. Gomez-Gil, "Brain computer interfaces, a review.," *Sensors (Basel)*, vol. 12, no. 2, pp. 1211–79, 2012.
- [2] T. S. Davis, H. A. C. Wark, D. T. Hutchinson, D. J. Warren, K. O'Neill, T. Scheinblum, G. A. Clark, R. A. Normann, and B. Greger, "Restoring motor control and sensory feedback in people with upper extremity amputations using arrays of 96 microelectrodes implanted in the median and ulnar nerves," *J. Neural Eng.*, vol. 13, no. 3, p. 036001, Jun. 2016.
- [3] R. Zhang, Y. Li, Y. Yan, H. Zhang, S. Wu, T. Yu, and Z. Gu, "Control of a Wheelchair in an Indoor Environment Based on a Brain&#x2013;Computer Interface and Automated Navigation," *IEEE Trans. Neural Syst. Rehabil. Eng.*, vol. 24, no. 1, pp. 128–139, Jan. 2016.
- [4] A. A. Blank, J. A. French, A. U. Pehlivan, and M. K. O'Malley, "Current Trends in Robot-Assisted Upper-Limb Stroke Rehabilitation: Promoting Patient Engagement in Therapy," *Curr. Phys. Med. Rehabil. Reports*, vol. 2, no. 3, pp. 184–195, Sep. 2014.
- [5] S. Qiu, Z. Li, W. He, L. Zhang, C. Yang, and C.-Y. Su, "Brain–Machine Interface and Visual Compressive Sensing-Based Teleoperation Control of an Exoskeleton Robot," *IEEE Trans. Fuzzy Syst.*, vol. 25, no. 1, pp. 58–69, Feb. 2017.
- [6] M. Kryger, B. Wester, E. A. Pohlmeier, M. Rich, B. John, J. Beaty, M. McLoughlin, M. Boninger, and E. C. Tyler-Kabara, "Flight simulation using a Brain-Computer Interface: A pilot, pilot study," *Exp. Neurol.*, vol. 287, pp. 473–478, Jan. 2017.
- [7] J. Faller, B. Z. Allison, C. Brunner, R. Scherer, D. Schmalstieg, G. Pfurtscheller, and C. Neuper, "A feasibility study on SSVEP-based interaction with motivating and immersive virtual and augmented reality," Jan. 2017.
- [8] T. Zander and C. Kothe, "Towards passive brain–computer interfaces: applying brain–computer interface technology to human–machine systems in general," *J. Neural Eng.*, vol. 8, no. 2, p. 025005, Apr. 2011.
- [9] S. D. Power, T. H. Falk, and T. Chau, "Classification of prefrontal activity due to mental arithmetic and music imagery using hidden Markov models and frequency domain near-infrared spectroscopy," *J. Neural Eng.*, vol. 7, no. 2, p. 026002, Apr. 2010.
- [10] K.-S. Hong and M. J. Khan, "Hybrid Brain–Computer Interface Techniques for Improved Classification Accuracy and Increased Number of Commands: A Review," *Front. Neurobot.*, vol. 11, p. 35, Jul. 2017.
- [11] M. J. Khan and K.-S. Hong, "Passive BCI based on drowsiness detection: an fNIRS study.," *Biomed. Opt. Express*, vol. 6, no. 10, pp. 4063–78, Oct. 2015.

- [12] S. Fager, D. R. Beukelman, M. Fried-Oken, T. Jakobs, and J. Baker, "Access interface strategies.," *Assist. Technol.*, vol. 24, no. 1, pp. 25–33, 2011.
- [13] N. Naseer and K.-S. Hong, "fNIRS-based brain-computer interfaces: a review," *Front. Hum. Neurosci.*, vol. 9, p. 3, Jan. 2015.
- [14] M. O. Sokunbi, D. E. J. Linden, I. Habes, S. Johnston, and N. Ihssen, "Real-time fMRI brain-computer interface: development of a "emotivational feedback" subsystem for the regulation of visual cue reactivity," *Front. Behav. Neurosci.*, vol. 8, p. 392, Nov. 2014.
- [15] T. N. Lal, N. Birbaumer, B. Schölkopf, M. Schröder, N. J. Hill, H. Preissl, T. Hinterberger, J. Mellinger, M. Bogdan, W. Rosenstiel, and T. Hofmann, "A brain computer interface with online feedback based on magnetoencephalography," in *Proceedings of the 22nd international conference on Machine learning - ICML '05*, 2005, pp. 465–472.
- [16] B. Z. Allison, E. W. Wolpaw, and J. R. Wolpaw, "Brain-computer interface systems: progress and prospects.," *Expert Rev. Med. Devices*, vol. 4, no. 4, pp. 463–74, Jul. 2007.
- [17] P. V. Zephaniah and J. G. Kim, "Recent functional near infrared spectroscopy based brain computer interface systems: Developments, applications and challenges," *Biomed. Eng. Lett.*, vol. 4, no. 3, pp. 223–230, Sep. 2014.
- [18] J. R. Wolpaw, N. Birbaumer, D. J. McFarland, G. Pfurtscheller, and T. M. Vaughan, "Brain-computer interfaces for communication and control.," *Clin. Neurophysiol.*, vol. 113, no. 6, pp. 767–91, Jun. 2002.
- [19] L. A. Farwell and E. Donchin, "Talking off the top of your head: toward a mental prosthesis utilizing event-related brain potentials.," *Electroencephalogr. Clin. Neurophysiol.*, vol. 70, no. 6, pp. 510–23, Dec. 1988.
- [20] F. Lotte, M. Congedo, A. Lécuyer, F. Lamarche, and B. Arnaldi, "A review of classification algorithms for EEG-based brain–computer interfaces," *J. Neural Eng.*, vol. 4, no. 2, pp. R1–R13, Jun. 2007.
- [21] G. Bin, X. Gao, Z. Yan, B. Hong, and S. Gao, "An online multi-channel SSVEP-based brain–computer interface using a canonical correlation analysis method," *J. Neural Eng.*, vol. 6, no. 4, p. 046002, Aug. 2009.
- [22] D. Lesenfants, D. Habbal, Z. Lugo, M. Lebeau, P. Horki, E. Amico, C. Pokorny, F. Gómez, A. Soddu, G. Müller-Putz, S. Laureys, and Q. Noirhomme, "An independent SSVEP-based brain–computer interface in locked-in syndrome," *J. Neural Eng.*, vol. 11, no. 3, p. 035002, Jun. 2014.
- [23] M. Nakanishi, Y. Wang, X. Chen, Y.-T. Wang, X. Gao, and T.-P. Jung, "Enhancing Detection of SSVEPs for a High-Speed Brain Speller Using Task-Related Component Analysis," *IEEE Trans. Biomed. Eng.*, vol. 65, no. 1, pp. 104–112, Jan. 2018.

- [24] M. Wang, I. Daly, B. Z. Allison, J. Jin, Y. Zhang, L. Chen, and X. Wang, “A new hybrid BCI paradigm based on P300 and SSVEP,” *J. Neurosci. Methods*, vol. 244, pp. 16–25, Apr. 2015.
- [25] Y. Jeon, C. S. Nam, Y.-J. Kim, and M. C. Whang, “Event-related (De)synchronization (ERD/ERS) during motor imagery tasks: Implications for brain–computer interfaces,” *Int. J. Ind. Ergon.*, vol. 41, no. 5, pp. 428–436, Sep. 2011.
- [26] L. E. H. van Dokkum, T. Ward, and I. Laffont, “Brain computer interfaces for neurorehabilitation – its current status as a rehabilitation strategy post-stroke,” *Ann. Phys. Rehabil. Med.*, vol. 58, no. 1, pp. 3–8, Feb. 2015.
- [27] A. Schlögl, F. Lee, H. Bischof, and G. Pfurtscheller, “Characterization of four-class motor imagery EEG data for the BCI-competition 2005,” *J. Neural Eng.*, vol. 2, no. 4, pp. L14–L22, Dec. 2005.
- [28] K. K. Kai Keng Ang, C. Cuntai Guan, K. S. G. Chua, B. T. Beng Ti Ang, C. Kuah, C. Chuanchu Wang, K. S. Kok Soon Phua, Z. Y. Zheng Yang Chin, and H. Haihong Zhang, “Clinical study of neurorehabilitation in stroke using EEG-based motor imagery brain-computer interface with robotic feedback,” in *2010 Annual International Conference of the IEEE Engineering in Medicine and Biology*, 2010, vol. 2010, pp. 5549–5552.
- [29] K. K. Ang and C. Guan, “EEG-Based Strategies to Detect Motor Imagery for Control and Rehabilitation,” *IEEE Trans. Neural Syst. Rehabil. Eng.*, vol. 25, no. 4, pp. 392–401, Apr. 2017.
- [30] K. LaFleur, K. Cassady, A. Doud, K. Shades, E. Rogin, and B. He, “Quadcopter control in three-dimensional space using a noninvasive motor imagery-based brain–computer interface,” *J. Neural Eng.*, vol. 10, no. 4, p. 046003, Aug. 2013.
- [31] R. Fazel-Rezai, B. Z. Allison, C. Guger, E. W. Sellers, S. C. Kleih, and A. Kübler, “P300 brain computer interface: current challenges and emerging trends.,” *Front. Neuroeng.*, vol. 5, p. 14, 2012.
- [32] J. N. Mak, Y. Arbel, J. W. Minett, L. M. McCane, B. Yuksel, D. Ryan, D. Thompson, L. Bianchi, and D. Erdogmus, “Optimizing the P300-based brain–computer interface: current status, limitations and future directions,” *J. Neural Eng.*, vol. 8, no. 2, p. 025003, Apr. 2011.
- [33] L. F. Nicolas-Alonso and J. Gomez-Gil, “Brain computer interfaces, a review.,” *Sensors (Basel)*, vol. 12, no. 2, pp. 1211–79, 2012.
- [34] T. Hinterberger, S. Schmidt, N. Neumann, J. Mellinger, B. Blankertz, G. Curio, and N. Birbaumer, “Brain-Computer Communication and Slow Cortical Potentials,” *IEEE Trans. Biomed. Eng.*, vol. 51, no. 6, pp. 1011–1018, Jun. 2004.

- [35] A. Y. Kaplan, A. A. Fingelkurts, A. A. Fingelkurts, S. V. Borisov, and B. S. Darkhovsky, "Nonstationary nature of the brain activity as revealed by EEG/MEG: Methodological, practical and conceptual challenges," *Signal Processing*, vol. 85, no. 11, pp. 2190–2212, Nov. 2005.
- [36] S. Brandl, J. Hohne, K.-R. Muller, and W. Samek, "Bringing BCI into everyday life: Motor imagery in a pseudo realistic environment," in *2015 7th International IEEE/EMBS Conference on Neural Engineering (NER)*, 2015, pp. 224–227.
- [37] M. Fatourehchi, A. Bashashati, R. K. Ward, and G. E. Birch, "EMG and EOG artifacts in brain computer interface systems: A survey," *Clin. Neurophysiol.*, vol. 118, no. 3, pp. 480–494, Mar. 2007.
- [38] N. Neumann and A. Kubler, "Training locked-in patients: a challenge for the use of brain-computer interfaces," *IEEE Trans. Neural Syst. Rehabil. Eng.*, vol. 11, no. 2, pp. 169–172, Jun. 2003.
- [39] S. Fazli, S. Dahne, W. Samek, F. Bieszmann, and K.-R. Muller, "Learning From More Than One Data Source: Data Fusion Techniques for Sensorimotor Rhythm-Based Brain-Computer Interfaces," *Proc. IEEE*, vol. 103, no. 6, pp. 891–906, Jun. 2015.
- [40] G. Muller-Putz, R. Leeb, M. Tangermann, J. Hohne, A. Kubler, F. Cincotti, D. Mattia, R. Rupp, K.-R. Muller, and J. del R. Millan, "Towards Noninvasive Hybrid Brain-Computer Interfaces: Framework, Practice, Clinical Application, and Beyond," *Proc. IEEE*, vol. 103, no. 6, pp. 926–943, Jun. 2015.
- [41] H. Morioka, A. Kanemura, S. Morimoto, T. Yoshioka, S. Oba, M. Kawanabe, and S. Ishii, "Decoding spatial attention by using cortical currents estimated from electroencephalography with near-infrared spectroscopy prior information," *Neuroimage*, vol. 90, pp. 128–139, Apr. 2014.
- [42] B.-K. Min, M. J. Marzelli, and S.-S. Yoo, "Neuroimaging-based approaches in the brain-computer interface," *Trends Biotechnol.*, vol. 28, no. 11, pp. 552–560, Nov. 2010.
- [43] L. Holper and M. Wolf, "Single-trial classification of motor imagery differing in task complexity: a functional near-infrared spectroscopy study," *J. Neuroeng. Rehabil.*, vol. 8, no. 1, p. 34, Jun. 2011.
- [44] G. Bauernfeind, R. Scherer, G. Pfurtscheller, and C. Neuper, "Single-trial classification of antagonistic oxyhemoglobin responses during mental arithmetic," *Med. Biol. Eng. Comput.*, vol. 49, no. 9, pp. 979–984, Sep. 2011.
- [45] A. V. Alexandrov, M. A. Sloan, L. K. S. Wong, C. Douville, A. Y. Razumovsky, W. J. Koroshetz, M. Kaps, and C. H. Tegeler, "Practice Standards for Transcranial Doppler Ultrasound: Part I-Test Performance," *J. Neuroimaging*, vol. 17, no. 1, pp. 11–18, Jan. 2007.

- [46] A. J. B. Myrden, A. Kushki, E. Sejdić, A.-M. Guerguerian, and T. Chau, “A Brain-Computer Interface Based on Bilateral Transcranial Doppler Ultrasound,” *PLoS One*, vol. 6, no. 9, p. e24170, Sep. 2011.
- [47] I. Aleem and T. Chau, “Towards a hemodynamic BCI using transcranial Doppler without user-specific training data,” *J. Neural Eng.*, vol. 10, no. 1, p. 016005, Feb. 2013.
- [48] J. Lu, K. A. Mamun, and T. Chau, “Pattern classification to optimize the performance of Transcranial Doppler Ultrasonography-based brain machine interface,” 2015.
- [49] A. Khalaf, M. Sybeldon, E. Sejdic, and M. Akcakaya, “A brain-computer interface based on functional transcranial doppler ultrasound using wavelet transform and support vector machines,” *J. Neurosci. Methods*, vol. 293, pp. 174–182, Jan. 2018.
- [50] M. Matteis, F. Federico, E. Troisi, P. Pasqualetti, F. Vernieri, C. Caltagirone, L. Petrosini, and M. Silvestrini, “Cerebral blood flow velocity changes during meaningful and meaningless gestures - a functional transcranial Doppler study,” *Eur. J. Neurol.*, vol. 13, no. 1, pp. 24–29, Jan. 2006.
- [51] S. Amiri, R. Fazel-Rezai, and V. Asadpour, “A Review of Hybrid Brain-Computer Interface Systems,” *Adv. Human-Computer Interact.*, vol. 2013, pp. 1–8, Feb. 2013.
- [52] I. Choi, I. Rhiu, Y. Lee, M. H. Yun, and C. S. Nam, “A systematic review of hybrid brain-computer interfaces: Taxonomy and usability perspectives.,” *PLoS One*, vol. 12, no. 4, p. e0176674, 2017.
- [53] L. F. Nicolas-Alonso and J. Gomez-Gil, “Brain computer interfaces, a review.,” *Sensors (Basel)*, vol. 12, no. 2, pp. 1211–79, 2012.
- [54] A. Nourmohammadi, M. Jafari, and T. O. Zander, “A Survey on Unmanned Aerial Vehicle Remote Control Using Brain–Computer Interface,” *IEEE Trans. Human-Machine Syst.*, pp. 1–12, 2018.
- [55] G. Pfurtscheller, B. Z. Allison, G. Bauernfeind, C. Brunner, T. Solis Escalante, R. Scherer, T. O. Zander, G. Mueller-Putz, C. Neuper, and N. Birbaumer, “The hybrid BCI,” *Front. Neurosci.*, vol. 4, p. 3, Apr. 2010.
- [56] M. Fatourechi, A. Bashashati, R. K. Ward, and G. E. Birch, “EMG and EOG artifacts in brain computer interface systems: A survey,” *Clin. Neurophysiol.*, vol. 118, no. 3, pp. 480–494, Mar. 2007.
- [57] Á. Costa, R. Salazar-Varas, A. Úbeda, and J. M. Azorín, “Characterization of Artifacts Produced by Gel Displacement on Non-invasive Brain-Machine Interfaces during Ambulation,” *Front. Neurosci.*, vol. 10, p. 60, Feb. 2016.
- [58] M. M. N. Mannan, S. Kim, M. Y. Jeong, and M. A. Kamran, “Hybrid EEG--Eye Tracker: Automatic Identification and Removal of Eye Movement and Blink Artifacts from Electroencephalographic Signal.,” *Sensors (Basel)*, vol. 16, no. 2, p. 241, Feb. 2016.

- [59] X. Yin, B. Xu, C. Jiang, Y. Fu, Z. Wang, H. Li, and G. Shi, "A hybrid BCI based on EEG and fNIRS signals improves the performance of decoding motor imagery of both force and speed of hand clenching," *J. Neural Eng.*, vol. 12, no. 3, p. 036004, Jun. 2015.
- [60] B. Koo, H.-G. Lee, Y. Nam, H. Kang, C. S. Koh, H.-C. Shin, and S. Choi, "A hybrid NIRS-EEG system for self-paced brain computer interface with online motor imagery," *J. Neurosci. Methods*, vol. 244, pp. 26–32, Apr. 2015.
- [61] H. Wang, Y. Li, J. Long, T. Yu, and Z. Gu, "An asynchronous wheelchair control by hybrid EEG–EOG brain–computer interface," *Cogn. Neurodyn.*, vol. 8, no. 5, pp. 399–409, Oct. 2014.
- [62] J. Jiang, Z. Zhou, E. Yin, Y. Yu, and D. Hu, "Hybrid Brain-Computer Interface (BCI) based on the EEG and EOG signals.," *Biomed. Mater. Eng.*, vol. 24, no. 6, pp. 2919–25, 2014.
- [63] X. Dong, H. Wang, Z. Chen, and B. E. Shi, "Hybrid Brain Computer Interface via Bayesian integration of EEG and eye gaze," in *2015 7th International IEEE/EMBS Conference on Neural Engineering (NER)*, 2015, pp. 150–153.
- [64] F. Putze, S. Hesslinger, C.-Y. Tse, Y. Huang, C. Herff, C. Guan, and T. Schultz, "Hybrid fNIRS-EEG based classification of auditory and visual perception processes.," *Front. Neurosci.*, vol. 8, p. 373, 2014.
- [65] R. Ramli, H. Arof, F. Ibrahim, N. Mokhtar, and M. Y. I. Idris, "Using finite state machine and a hybrid of EEG signal and EOG artifacts for an asynchronous wheelchair navigation," *Expert Syst. Appl.*, vol. 42, no. 5, pp. 2451–2463, Apr. 2015.
- [66] S. R. Soekadar, M. Witkowski, N. Vitiello, and N. Birbaumer, "An EEG/EOG-based hybrid brain-neural computer interaction (BNCI) system to control an exoskeleton for the paralyzed hand," *Biomed. Eng. / Biomed. Tech.*, vol. 60, no. 3, pp. 199–205, Jan. 2015.
- [67] S. R. Soekadar, M. Witkowski, C. Gómez, E. Opisso, J. Medina, M. Cortese, M. Cempini, M. C. Carrozza, L. G. Cohen, N. Birbaumer, and N. Vitiello, "Hybrid EEG/EOG-based brain/neural hand exoskeleton restores fully independent daily living activities after quadriplegia," *Sci. Robot.*, vol. 1, no. 1, p. eaag3296, Dec. 2016.
- [68] W.-L. Zheng and B.-L. Lu, "A multimodal approach to estimating vigilance using EEG and forehead EOG," *J. Neural Eng.*, vol. 14, no. 2, p. 026017, Apr. 2017.
- [69] M.-H. Lee, J. Williamson, D.-O. Won, S. Fazli, and S.-W. Lee, "A High Performance Spelling System based on EEG-EOG Signals With Visual Feedback," *IEEE Trans. Neural Syst. Rehabil. Eng.*, vol. 26, no. 7, pp. 1443–1459, Jul. 2018.
- [70] C.-C. Postelnicu and D. Talaba, "P300-Based Brain-Neuronal Computer Interaction for Spelling Applications," *IEEE Trans. Biomed. Eng.*, vol. 60, no. 2, pp. 534–543, Feb. 2013.
- [71] E. Loopez-Larraz, N. Birbaumer, and A. Ramos-Murguialday, "A hybrid EEG-EMG BMI improves the detection of movement intention in cortical stroke patients with complete hand

- paralysis,” in *2018 40th Annual International Conference of the IEEE Engineering in Medicine and Biology Society (EMBC)*, 2018, vol. 2018, pp. 2000–2003.
- [72] T. Kawase, T. Sakurada, Y. Koike, and K. Kansaku, “A hybrid BMI-based exoskeleton for paresis: EMG control for assisting arm movements,” *J. Neural Eng.*, vol. 14, no. 1, p. 016015, Feb. 2017.
- [73] A. Sarasola-Sanz, N. Irastorza-Landa, E. Lopez-Larraz, C. Bibian, F. Helmhold, D. Broetz, N. Birbaumer, and A. Ramos-Murguialday, “A hybrid brain-machine interface based on EEG and EMG activity for the motor rehabilitation of stroke patients,” in *2017 International Conference on Rehabilitation Robotics (ICORR)*, 2017, vol. 2017, pp. 895–900.
- [74] L. Minati, N. Yoshimura, and Y. Koike, “Hybrid Control of a Vision-Guided Robot Arm by EOG, EMG, EEG Biosignals and Head Movement Acquired via a Consumer-Grade Wearable Device,” *IEEE Access*, vol. 4, pp. 9528–9541, 2016.
- [75] S. Shahid, G. Prasad, and R. K. Sinha, “On fusion of heart and brain signals for hybrid BCI,” in *2011 5th International IEEE/EMBS Conference on Neural Engineering*, 2011, pp. 48–52.
- [76] R. Scherer, G. R. Müller-Putz, and G. Pfurtscheller, “Self-initiation of EEG-based brain–computer communication using the heart rate response,” *J. Neural Eng.*, vol. 4, no. 4, pp. L23–L29, Dec. 2007.
- [77] S. Ahn, T. Nguyen, H. Jang, J. G. Kim, and S. C. Jun, “Exploring Neuro-Physiological Correlates of Drivers’ Mental Fatigue Caused by Sleep Deprivation Using Simultaneous EEG, ECG, and fNIRS Data.,” *Front. Hum. Neurosci.*, vol. 10, p. 219, 2016.
- [78] A. P. Buccino, H. O. Keles, and A. Omurtag, “Hybrid EEG-fNIRS Asynchronous Brain-Computer Interface for Multiple Motor Tasks,” *PLoS One*, vol. 11, no. 1, p. e0146610, Jan. 2016.
- [79] M. J. Khan, M. J. Hong, and K.-S. Hong, “Decoding of four movement directions using hybrid NIRS-EEG brain-computer interface,” *Front. Hum. Neurosci.*, vol. 8, p. 244, Apr. 2014.
- [80] J. Shin, K.-R. Müller, C. H. Schmitz, D.-W. Kim, and H.-J. Hwang, “Evaluation of a Compact Hybrid Brain-Computer Interface System,” *Biomed Res. Int.*, vol. 2017, pp. 1–11, Mar. 2017.
- [81] S. Fazli, J. Mehnert, J. Steinbrink, G. Curio, A. Villringer, K.-R. Müller, and B. Blankertz, “Enhanced performance by a hybrid NIRS–EEG brain computer interface,” *Neuroimage*, vol. 59, no. 1, pp. 519–529, 2012.
- [82] B. Blankertz, R. Tomioka, S. Lemm, M. Kawanabe, and K. Muller, “Optimizing Spatial filters for Robust EEG Single-Trial Analysis,” *IEEE Signal Process. Mag.*, vol. 25, no. 1, pp. 41–56, 2008.

- [83] Y. Blokland, L. Spyrou, D. Thijssen, T. Eijsvogels, W. Colier, M. Floor-Westerdijk, R. Vlek, J. Bruhn, and J. Farquhar, “Combined EEG-fNIRS Decoding of Motor Attempt and Imagery for Brain Switch Control: An Offline Study in Patients With Tetraplegia,” *IEEE Trans. Neural Syst. Rehabil. Eng.*, vol. 22, no. 2, pp. 222–229, Mar. 2014.
- [84] A. Faress and T. Chau, “Towards a multimodal brain-computer interface: combining fNIRS and fTCD measurements to enable higher classification accuracy,” *Neuroimage*, vol. 77, pp. 186–94, Aug. 2013.
- [85] A. Khalaf, E. Sejdic, and M. Akcakaya, “EEG-ftCD hybrid brain–computer interface using template matching and wavelet decomposition,” *J. Neural Eng.*, vol. 16, no. 3, p. 036014, Jun. 2019.
- [86] A. Khalaf, E. Sejdic, and M. Akcakaya, “Common spatial pattern and wavelet decomposition for motor imagery EEG- fTCD brain-computer interface,” *J. Neurosci. Methods*, vol. 320, pp. 98–106, May 2019.
- [87] J. Ma, Y. Zhang, A. Cichocki, and F. Matsuno, “A Novel EOG/EEG Hybrid Human–Machine Interface Adopting Eye Movements and ERPs: Application to Robot Control,” *IEEE Trans. Biomed. Eng.*, vol. 62, no. 3, pp. 876–889, Mar. 2015.
- [88] K. Lin, A. Cinetto, Y. Wang, X. Chen, S. Gao, and X. Gao, “An online hybrid BCI system based on SSVEP and EMG,” *J. Neural Eng.*, vol. 13, no. 2, p. 026020, Apr. 2016.
- [89] A. Chowdhury, H. Raza, Y. K. Meena, A. Dutta, and G. Prasad, “An EEG-EMG correlation-based brain-computer interface for hand orthosis supported neuro-rehabilitation,” *J. Neurosci. Methods*, vol. 312, pp. 1–11, Jan. 2019.
- [90] R. Chowdhury, M. Reaz, M. Ali, A. Bakar, K. Chellappan, and T. Chang, “Surface Electromyography Signal Processing and Classification Techniques,” *Sensors*, vol. 13, no. 9, pp. 12431–12466, Sep. 2013.
- [91] X. Chai, Z. Zhang, Y. Lu, G. Liu, T. Zhang, and H. Niu, “A Hybrid BCI-Based Environmental Control System Using SSVEP and EMG Signals,” Springer, Singapore, 2019, pp. 59–63.
- [92] S. L. Shishkin, Y. O. Nuzhdin, E. P. Svirin, A. G. Trofimov, A. A. Fedorova, B. L. Kozyrskiy, and B. M. Velichkovsky, “EEG Negativity in Fixations Used for Gaze-Based Control: Toward Converting Intentions into Actions with an Eye-Brain-Computer Interface,” *Front. Neurosci.*, vol. 10, p. 528, Nov. 2016.
- [93] A. Riccio, E. M. Holz, P. Aricò, F. Leotta, F. Aloise, L. Desideri, M. Rimondini, A. Kübler, D. Mattia, and F. Cincotti, “Hybrid P300-Based Brain-Computer Interface to Improve Usability for People With Severe Motor Disability: Electromyographic Signals for Error Correction During a Spelling Task,” *Arch. Phys. Med. Rehabil.*, vol. 96, no. 3, pp. S54–S61, Mar. 2015.

- [94] Y. Punsawad, Y. Wongsawat, and M. Parnichkun, "Hybrid EEG-EOG brain-computer interface system for practical machine control," in *2010 Annual International Conference of the IEEE Engineering in Medicine and Biology*, 2010, vol. 2010, pp. 1360–1363.
- [95] R. N. Khushaba, S. Kodagoda, S. Lal, and G. Dissanayake, "Driver Drowsiness Classification Using Fuzzy Wavelet-Packet-Based Feature-Extraction Algorithm," *IEEE Trans. Biomed. Eng.*, vol. 58, no. 1, pp. 121–131, Jan. 2011.
- [96] A. Sassaroli and S. Fantini, "Comment on the modified Beer–Lambert law for scattering media," *Phys. Med. Biol.*, vol. 49, no. 14, pp. N255–N257, Jul. 2004.
- [97] A. Khalaf, E. Sejdic, and M. Akcakaya, "Towards optimal visual presentation design for hybrid EEG—fTCD brain–computer interfaces," *J. Neural Eng.*, vol. 15, no. 5, p. 056019, Oct. 2018.
- [98] A. Khalaf, E. Sejdic, and M. Akcakaya, "A novel motor imagery hybrid brain computer interface using EEG and functional transcranial Doppler ultrasound," *J. Neurosci. Methods*, vol. 313, pp. 44–53, Feb. 2019.
- [99] C.-C. Postelnicu, F. Girbacia, and D. Talaba, "EOG-based visual navigation interface development," *Expert Syst. Appl.*, vol. 39, no. 12, pp. 10857–10866, Sep. 2012.
- [100] F. Lotte, L. Bougrain, A. Cichocki, M. Clerc, M. Congedo, A. Rakotomamonjy, and F. Yger, "A review of classification algorithms for EEG-based brain–computer interfaces: a 10 year update," *J. Neural Eng.*, vol. 15, no. 3, p. 031005, Jun. 2018.
- [101] G. Vingerhoets and N. Stroobant, "Lateralization of Cerebral Blood Flow Velocity Changes During Cognitive Tasks," *Stroke*, vol. 30, no. 10, 1999.
- [102] A. J. B. Myrden, A. Kushki, E. Sejdic, A.-M. Guerguerian, and T. Chau, "A Brain-Computer Interface Based on Bilateral Transcranial Doppler Ultrasound," *PLoS One*, vol. 6, no. 9, 2011.
- [103] M. Li, H. Huang, M. L. Boninger, and E. Sejdic, "An analysis of cerebral blood flow from middle cerebral arteries during cognitive tasks via functional transcranial Doppler recordings," *Neurosci. Res.*, vol. 84, pp. 19–26, 2014.
- [104] R. C. Oldfield, "The assessment and analysis of handedness: the Edinburgh inventory.," *Neuropsychologia*, vol. 9, no. 1, pp. 97–113, Mar. 1971.
- [105] L. H. Monsein, A. Y. Razumovsky, S. J. Ackerman, H. J. W. Nauta, and D. F. Hanley, "Validation of transcranial Doppler ultrasound with a stereotactic neurosurgical technique," *J. Neurosurg.*, vol. 82, no. 6, pp. 972–975, Jun. 1995.
- [106] K. Nakagawa, T. Ishibashi, M. Matsushima, Y. Tanifuji, Y. Amaki, and H. Furuhata, "Does Long-Term Continuous Transcranial Doppler Monitoring Require a Pause for Safer Use?," *Cerebrovasc. Dis.*, vol. 24, no. 1, pp. 27–34, May 2007.

- [107] M. Peters and C. Battista, “Applications of mental rotation figures of the Shepard and Metzler type and description of a mental rotation stimulus library,” *Brain Cogn.*, vol. 66, no. 3, pp. 260–264, 2008.
- [108] M. H. R.R. Diehl, M. Sitzer, “Changes of cerebral blood flow velocity during cognitive activity,” *Stroke*, vol. 21, no. 8, pp. 1236–1237, 1990.
- [109] D. Valencia, “Discrete Wavelet Transform Filter Bank Implementation,” 2010. [Online]. Available: <https://www.dsprelated.com/showarticle/115.php>.
- [110] L. T. Decarlo, “On the meaning and use of kurtosis,” *Psychol. Methods*, vol. 2, no. 3, pp. 292–307, 1997.
- [111] H. L. MacGillivray, “The Mean, Median, Mode Inequality and Skewness for a Class of Densities,” *Aust. J. Stat.*, vol. 23, no. 2, pp. 247–250, Jun. 1981.
- [112] Sidney Siegel, *Nonparametric statistics for the behavioral sciences ebook « Mara’s life*. New York: McGraw-Hill, 1956.
- [113] R. C. Blair and J. J. Higgins, “A Comparison of the Power of Wilcoxon’s Rank-Sum Statistic to That of Student’s t Statistic under Various Nonnormal Distributions,” *J. Educ. Stat.*, vol. 5, no. 4, p. 309, 1980.
- [114] C.-W. Chih-Wei Hsu and C.-J. Chih-Jen Lin, “A comparison of methods for multiclass support vector machines,” *IEEE Trans. Neural Networks*, vol. 13, no. 2, pp. 415–425, Mar. 2002.
- [115] J. Shin, K.-R. Müller, and H.-J. Hwang, “Near-infrared spectroscopy (NIRS)-based eyes-closed brain-computer interface (BCI) using prefrontal cortex activation due to mental arithmetic,” *Sci. Rep.*, vol. 6, p. 36203, Nov. 2016.
- [116] A. Goyal, A.-A. Samadani, A.-M. Guerguerian, and T. Chau, “An online three-class Transcranial Doppler ultrasound brain computer interface,” *Neurosci. Res.*, vol. 107, pp. 47–56, 2016.
- [117] A. Myrden, A. Kushki, E. Sejdíć, and T. Chau, “Towards increased data transmission rate for a three-class metabolic brain-computer interface based on transcranial Doppler ultrasound,” *Neurosci. Lett.*, 2012.
- [118] J. N. Mak and J. R. Wolpaw, “Clinical Applications of Brain-Computer Interfaces: Current State and Future Prospects,” *IEEE Rev. Biomed. Eng.*, vol. 2, pp. 187–199, 2009.
- [119] F. Cincotti, D. Mattia, F. Aloise, S. Bufalari, G. Schalk, G. Oriolo, A. Cherubini, M. G. Marciani, and F. Babiloni, “Non-invasive brain–computer interface system: Towards its application as assistive technology,” *Brain Res. Bull.*, vol. 75, no. 6, pp. 796–803, Apr. 2008.

- [120] A. Kübler, V. K. Mushahwar, L. R. Hochberg, and J. P. Donoghue, “BCI Meeting 2005--workshop on clinical issues and applications,” *IEEE Trans. Neural Syst. Rehabil. Eng.*, vol. 14, no. 2, pp. 131–4, Jun. 2006.
- [121] A. Ramos-Murguialday, D. Broetz, M. Rea, L. Läer, O. Yilmaz, F. L. Brasil, G. Liberati, M. R. Curado, E. Garcia-Cossio, A. Vyziotis, W. Cho, M. Agostini, E. Soares, S. Soekadar, A. Caria, L. G. Cohen, and N. Birbaumer, “Brain-machine interface in chronic stroke rehabilitation: a controlled study.,” *Ann. Neurol.*, vol. 74, no. 1, pp. 100–8, Jul. 2013.
- [122] N. Stroobant and G. Vingerhoets, “Transcranial Doppler ultrasonography monitoring of cerebral hemodynamics during performance of cognitive tasks: a review.,” *Neuropsychol. Rev.*, vol. 10, no. 4, pp. 213–31, Dec. 2000.
- [123] P. D. Welch and P. D., “The Use of Fast Fourier Transform for the Estimation of Power Spectra: A Method Based on Time Averaging Over Short, Modified Periodograms,” *IEEE Trans. Audio Electroacoust.*, Vol. AU-15, p. 70-73, vol. 15, pp. 70–73, 1967.
- [124] Y. Saeys, I. Inza, and P. Larranaga, “A review of feature selection techniques in bioinformatics,” *Bioinformatics*, vol. 23, no. 19, pp. 2507–2517, Oct. 2007.
- [125] Hanchuan Peng, Fuhui Long, and C. Ding, “Feature selection based on mutual information criteria of max-dependency, max-relevance, and min-redundancy,” *IEEE Trans. Pattern Anal. Mach. Intell.*, vol. 27, no. 8, pp. 1226–1238, Aug. 2005.
- [126] J. Pohjalainen, O. Räsänen, and S. Kadioglu, “Feature selection methods and their combinations in high-dimensional classification of speaker likability, intelligibility and personality traits,” *Comput. Speech Lang.*, vol. 29, no. 1, pp. 145–171, Jan. 2015.
- [127] S. Fazli, J. Mehnert, J. Steinbrink, G. Curio, A. Villringer, K.-R. Müller, and B. Blankertz, “Enhanced performance by a hybrid NIRS–EEG brain computer interface,” *Neuroimage*, vol. 59, no. 1, pp. 519–529, Jan. 2012.
- [128] J. Mueller, W. Legon, A. Opitz, T. F. Sato, and W. J. Tyler, “Transcranial Focused Ultrasound Modulates Intrinsic and Evoked EEG Dynamics,” *Brain Stimul.*, vol. 7, no. 6, pp. 900–908, Nov. 2014.
- [129] A. Khalaf, M. Sybeldon, E. Sejdic, and M. Akcakaya, “An EEG and fTCD based BCI for control,” in *Conference Record - Asilomar Conference on Signals, Systems and Computers*, 2017.
- [130] M. I. Vanegas, A. Blangero, and S. P. Kelly, “Exploiting individual primary visual cortex geometry to boost steady state visual evoked potentials.,” *J. Neural Eng.*, vol. 10, no. 3, p. 036003, Jun. 2013.
- [131] H. Ramoser, J. Muller-Gerking, and G. Pfurtscheller, “Optimal spatial filtering of single trial EEG during imagined hand movement,” *IEEE Trans. Rehabil. Eng.*, vol. 8, no. 4, pp. 441–446, 2000.

- [132] D. Devlaminck, B. Wyns, M. Grosse-Wentrup, G. Otte, and P. Santens, “Multisubject learning for common spatial patterns in motor-imagery BCI,” *Comput. Intell. Neurosci.*, vol. 2011, p. 217987, Oct. 2011.
- [133] Yijun Wang, Shangkai Gao, and Xiaornog Gao, “Common Spatial Pattern Method for Channel Selection in Motor Imagery Based Brain-computer Interface,” in *2005 IEEE Engineering in Medicine and Biology 27th Annual Conference*, 2005, pp. 5392–5395.
- [134] B. Blankertz, R. Tomioka, S. Lemm, M. Kawanabe, and K. Muller, “Optimizing Spatial filters for Robust EEG Single-Trial Analysis,” *IEEE Signal Process. Mag.*, vol. 25, no. 1, pp. 41–56, 2008.
- [135] M. Grosse-Wentrup, C. Liefhold, K. Gramann, and M. Buss, “Beamforming in Noninvasive Brain–Computer Interfaces,” *IEEE Trans. Biomed. Eng.*, vol. 56, no. 4, pp. 1209–1219, Apr. 2009.
- [136] Haiping Lu, How-Lung Eng, Cuntai Guan, K. N. Plataniotis, and A. N. Venetsanopoulos, “Regularized Common Spatial Pattern With Aggregation for EEG Classification in Small-Sample Setting,” *IEEE Trans. Biomed. Eng.*, vol. 57, no. 12, pp. 2936–2946, Dec. 2010.
- [137] A. Khalaf, M. Sybeldon, E. Sejdic, and M. Akcakaya, “A brain-computer interface based on functional transcranial doppler ultrasound using wavelet transform and support vector machines,” *J. Neurosci. Methods*, vol. 293, 2018.
- [138] B. W. Silverman, *Density estimation for statistics and data analysis*. Chapman and Hall, 1986.
- [139] B. Thompson, Thompson, and Bruce, “Canonical Correlation Analysis,” in *Encyclopedia of Statistics in Behavioral Science*, Chichester, UK: John Wiley & Sons, Ltd, 2005.
- [140] M. Nakanishi, Y. Wang, Y.-T. Wang, and T.-P. Jung, “A Comparison Study of Canonical Correlation Analysis Based Methods for Detecting Steady-State Visual Evoked Potentials,” *PLoS One*, vol. 10, no. 10, p. e0140703, Oct. 2015.
- [141] M. NAKANISHI, Y. WANG, Y.-T. WANG, Y. MITSUKURA, and T.-P. JUNG, “A HIGH-SPEED BRAIN SPELLER USING STEADY-STATE VISUAL EVOKED POTENTIALS,” *Int. J. Neural Syst.*, vol. 24, no. 06, p. 1450019, Sep. 2014.
- [142] M. Nakanishi, Y. Wang, S.-H. Hsu, Y.-T. Wang, and T.-P. Jung, “Independent component analysis-based spatial filtering improves template-based SSVEP detection,” in *2017 39th Annual International Conference of the IEEE Engineering in Medicine and Biology Society (EMBC)*, 2017, pp. 3620–3623.
- [143] B. Obermaier, C. Neuper, C. Guger, and G. Pfurtscheller, “Information transfer rate in a five-classes brain-computer interface,” *IEEE Trans. Neural Syst. Rehabil. Eng.*, vol. 9, no. 3, pp. 283–288, 2001.

- [144] M. Labecki, R. Kus, A. Brzozowska, T. Stacewicz, B. S. Bhattacharya, and P. Suffczynski, “Nonlinear Origin of SSVEP Spectra-A Combined Experimental and Modeling Study.,” *Front. Comput. Neurosci.*, vol. 10, p. 129, 2016.
- [145] R. Chellappa, A. Veeraraghavan, N. Ramanathan, C.-Y. Yam, M. S. Nixon, A. Elgammal, J. E. Boyd, J. J. Little, N. Lynnerup, P. K. Larsen, and D. Reynolds, “Gaussian Mixture Models,” in *Encyclopedia of Biometrics*, Boston, MA: Springer US, 2009, pp. 659–663.
- [146] V. Jayaram, M. Alamgir, Y. Altun, B. Scholkopf, and M. Grosse-Wentrup, “Transfer Learning in Brain-Computer Interfaces Abstract\uFFFFDThe performance of brain-computer interfaces (BCIs) improves with the amount of avail,” *IEEE Comput. Intell. Mag.*, vol. 11, no. 1, pp. 20–31, Feb. 2016.
- [147] S. J. Pan and Q. Yang, “A Survey on Transfer Learning,” *IEEE Trans. Knowl. Data Eng.*, vol. 22, no. 10, pp. 1345–1359, Oct. 2010.
- [148] M. Sybeldon, L. Schmit, E. Sejdic, and M. Akcakaya, “Transfer learning for EEG based BCI using LEARN++.NSE and mutual information,” in *2017 IEEE International Conference on Acoustics, Speech and Signal Processing (ICASSP)*, 2017, pp. 2632–2636.
- [149] Sung-Hyuk Cha, “Comprehensive Survey on Distance/Similarity Measures between Probability Density Functions,” *Int. J. Math. Model. METHODS Appl. Sci.*, vol. 1, no. 4, pp. 1–8, 2007.
- [150] P. Stoica and Y. Selen, “Model-order selection,” *IEEE Signal Process. Mag.*, vol. 21, no. 4, pp. 36–47, Jul. 2004.